

Investigations on the Adhesion of Polyurethane Foams on Thermoplastic Material Systems



Dissertation
zur Erlangung des akademischen Grades
Doktor-Ingenieur (Dr. -Ing.)
genehmigt durch

Mathematisch-Naturwissenschaftlich-Technische Fakultät
(Ingenieurwissenschaftlicher Bereich)
der Martin-Luther-Universität Halle-Wittenberg

von Herrn M.Phil. Nasir Mahmood
geb. am 07.05.1974 in Bahawalpur (Pakistan)

Gutachter:

1. Prof. Dr. J. Kressler
2. Prof. Dr. H. Roggendorf
3. Prof. Dr. G. Heinrich

Merseburg, den 28-01-2005

urn:nbn:de:gbv:3-000007920

[<http://nbn-resolving.de/urn/resolver.pl?urn=nbn%3Ade%3Agbv%3A3-000007920>]

*Dedicated to My Wife
and Daughter*

List of publications

- 1 Nasir Mahmood, Karsten Busse, Joerg Kressler, “Neutron reflection measurements on polyurethane foam/thermoplastics interfaces”, *Polym. Mat. Sci. and Eng.* 2004, 90, 831.
- 2 Nasir Mahmood, Joerg Kressler, Karsten Busse, “Structure Analysis in Polyurethane Foams at Interfaces.” (in press).
- 3 Nasir Mahmood, Joerg Kressler, Karsten Busse, “Surface and interface studies on polyurethane foam/thermoplastic systems” Poster accepted in *Polymeric Materials*, Martin Luther University Halle-Wittenberg Halle (Saale) Germany Sep. 29-30th 2004.
- 4 Karsten Busse, Nasir Mahmood, Joerg Kressler, “Adhesion behavior of polyurethane foam on thermoplastics” Poster presented at the *Frühjahrstagung 2004 Fachverband Chemische Physik und Polymerphysik, Deutsche Physikalische Gesellschaft e. V.*, Regensburg, Germany, March. 8-12th, 2004.
- 5 Nasir Mahmood, Karsten Busse, Joerg Kressler, “Nano structured polyurethane foams” Poster presented at the *Innovations forum Nano strukturierte Materialien* Halle (Saale) Germany, Nov. 24-25th, 2003.
- 6 Nasir Mahmood, Jürgen Vogel, Andre Wutzler, Joerg Kressler, “In-situ FTIR-ATR Studies of Structure Development in Polyurethane Foam Systems” Poster presented at the *Polymeric Materials*, MLU Halle-Wittenberg Halle (Saale) Germany Sep. 25-27th, 2002.
- 7 Nasir Mahmood, Karsten Busse, Joerg Kressler, “Surface and Interface Studies on Polyurethane Foam/Thermoplastic Systems”.(to be submitted)
- 8 Nasir Mahmood, Karsten Busse, Joerg Kressler, “Adhesion behavior of Polyurethane Foams with Thermoplastics”. (to be submitted)

Contents

List of publications	III
Abbreviations and symbols	VII
1. Adhesion of polyurethane foams with thermoplastics	1
1.1. Introduction	1
1.1.1. Adhesive joint durability	2
1.1.2. Testing of adhesive joints	3
1.1.3. Adhesion theories	5
1.2. Polyurethane foams	9
1.2.1. Manufacturing of PU foams	9
1.2.2. Foam chemistry and morphology	12
1.3. Thermoplastic materials	15
1.4. Objectives and summary of this work	15
2. Experimental	18
2.1. Materials	18
2.2. Adhesion behavior of PU foams with thermoplastic material systems	18
2.2.1. Preparation of test samples	18
2.2.2. Aging of test samples	19
2.2.3. Peel test	21
2.3. Contact angle studies on thermoplastics and PU foam systems	22
2.3.1. Contact angle measurements	22
2.3.2. Tensiometry	23
2.4. Microscopic studies	24
2.4.1. Atomic force microscopy	24
2.4.2. Optical microscopy	24

2.5.	ToF-SIMS and XPS studies	25
2.5.1.	Time of flight secondary ion mass spectrometry	25
2.5.2.	X-ray photoelectron spectroscopy	25
2.6.	Structure analysis in polyurethane foams at the interface	26
2.6.1.	FTIR spectroscopy	26
2.6.2.	Small angle X-ray scattering	26
2.6.3.	Transmission electron microscopy	26
2.6.4.	Neutron reflection	26
2.7.	Diffusion coefficient studies of MDI in thermoplastics	27
2.7.1.	Gravimetric analysis	27
2.7.2.	FTIR microscopy	27
2.7.3.	Optical microscopy	28
3.	Results and discussion	29
3.1.	Adhesion behavior of PU foams with thermoplastic material systems	29
3.1.1.	Analysis of the peel test results	29
3.1.2.	Adhesion performance before climate treatments	32
3.1.3.	Adhesion performance after climate treatments	34
3.1.3.1.	Testing of samples under modified climate cycles	35
3.1.4.	Short summary of adhesion test results	39
3.2.	Contact angle studies on thermoplastics and PU foam systems	40
3.2.1.	Contact angle results of neat TP materials	41
3.2.2.	Behavior of samples from PU foam/TP material interface	42
3.2.3.	Contact angle results of PU foam samples	44
3.2.4.	Contact angle hysteresis	44
3.2.5.	Short summary of contact angle results	46
3.3.	Microscopic studies	47
3.3.1.	Atomic force microscopy	48

3.3.2.	Optical microscopy	53
3.3.3.	Short summary of microscopic results	54
3.4.	ToF-SIMS and XPS studies	55
3.4.1.	Time of flight secondary ion mass spectrometry	55
3.4.2.	X-ray photoelectron spectroscopy	60
3.4.3.	Short summary of ToF-SIMS and XPS results	62
3.5.	Structure analysis in polyurethane foams at the interface	63
3.5.1.	FTIR spectroscopy	64
3.5.2.	Small angle X-ray scattering	69
3.5.3.	Transmission electron microscopy	71
3.5.4.	Neutron reflection	73
3.5.5.	Short summary of structure analysis results	77
3.6.	Diffusion coefficient studies of MDI in thermoplastics	78
3.6.1.	MDI mass uptake by thermoplastics	79
3.6.2.	Determination of type of diffusion	81
3.6.3.	Optical microscopy	82
3.6.4.	Determination of diffusion coefficient	84
3.6.5.	FTIR microscopy	84
3.6.6.	Short summary of diffusion coefficient results	88
4.	Summary	89
5.	Zusammenfassung	94
6.	Future work	98
7.	Literature	99
	Appendixes	107
	Acknowledgement	115
	Resume	116

Abbreviations and symbols

ABS	acrylonitrile-butadiene-styrene polymer
AFM	atomic force microscopy
ATR	attenuated total reflectance
ASTM	American Society for Testing and Materials
a.u.	arbitrary unit
α	diffusion exponent
BE	binding energy
CFCs	chlorofluorocarbons
CFHCs	chlorofluorohydrocarbons
CD	compact disc
D	diffusion coefficient
d	diffusion length, interdomain spacing
DMF	dimethyl formamide
DABCO	diazabicyclooctane
eV	electron volt
FTIR	Fourier transform infra-red spectroscopy
F	force
ϕ	work function
γ	surface tension
G	adhesion energy or fracture energy
GF	glass fiber
$h\nu$	photon energy
HDI	hexamethylene diisocyanate
IC	isocyanates
IMFP	inelastic mean free path
IPDI	isophorone diisocyanate
IRE	internal reflection element
λ	wavelength

lv	liquid vapour
<i>M</i>	mass
MA	maleic anhydride
MDI	4,4'-diphenylmethane diisocyanate
mrad	milliradian
NDI	naphthalene diisocyanate
NR	neutron reflection
PB	polybutadiene
PC	polycarbonate
PEO	polyethylene oxide
PG	propylene glycol
pK _a	negative logarithm of dissociation constant of acid
PU	polyurethane
PO	polyol
PPO	polypropylene oxide
PS	polystyrene
ρ	density
<i>q</i>	scattering vector
Ra and Rz	surface roughness factors
RH	relative humidity
RMM	relative molecular mass
RMS	root mean square
RPM	revolution per minute
RT	room temperature
RuO ₄	Ruthenium tetraoxide
SAR	Silicone acrylate rubber
SAN	styrene-acrylonitrile
SAXS	Small angle X-ray scattering
sl	Solid liquid
SMA	poly (styrene-co-maleic anhydride)
sv	solid vapour

<i>t</i>	time
TDI	toluene diisocyanate
TEA	tertiary amine
TMP	trimethylolpropane
ToF-SIMS	time of flight secondary ion mass spectrometry
TP	thermoplastic
TEM	transmission electron microscopy
θ_a	advancing contact angle
θ_r	receding contact angle
<i>V</i>	volume
<i>W</i>	width
WA	work of adhesion
wt	weight
XPS	X-ray photoelectron spectroscopy

Chapter 1

Adhesion of polyurethane foams with thermoplastics

1.1. Introduction

The process that allows the adhesive to transfer a load from the adherend to the adhesive joint is known as the adhesion. In general the adhesive can be a complex polymer, which intimately interact, either through chemical/physical forces, to the adherend surface to which it is being applied. The chemical interactions result from atomic scale attractions between specific functional groups of the adhesive and the adherend surface. During the early phase of the curing process the viscous adhesive material will flow to enable contact with the adherend and penetration of the surface asperities. As curing proceeds, the viscous mixture becomes a rigid solid as the compounds react and cohesively link the adhesive, often referred to as crosslinking. This process enables strength to be established between the joined adherends.

There are a large number of areas where adhesives are used to join materials. The wide range of industries using the technology indicates the diversity of application. In the automotive industry, examples of the use of adhesive bonding include the manufacture of doors, engines and car bodies. Other industrial examples include bridge construction and electronic component manufacture.¹

Polyurethanes (PU) today account for the largest percentage (by weight or volume) of any plastic materials used in automotive industry and their growth rate is also faster than that of other plastics.^{2,3} PU have influenced automotive developments over the past two decades. Their modest beginning was in the late 1950s when cut slabstock foam was used to soften hard metal spring seats in combination or in competition with horse hair, cotton wadding, etc. Nowadays, an estimated 20 kg of various PU are used per automobile, ranging from all foam seat cushions and backs to crash pads, bumpers, fenders, etc.⁴ The developments in adhesives technology, particularly the discovery of PU adhesives,⁵ have lead to the recommendation to use adhesive bonding technology in many industrial applications.⁶

PU adhesives are normally defined as those adhesives that contain a number of urethane groups in the molecular backbone or which are formed during use, regardless of the chemical composition of the rest of the chain. Thus a typical urethane adhesive may contain, in addition to urethane linkages, aliphatic and aromatic hydrocarbons, esters, ethers, amides, urea and allophanate groups. An isocyanate group reacts with the hydroxyl groups of a polyol to form the repeating urethane linkage. Isocyanates react with water to form a urea linkage and carbon dioxide as a by-product. Urethane adhesives have some advantages due to the following reasons: (1) they effectively wet the surface of most substrates, (2) they readily form hydrogen bonds to the substrates, (3) small molecular size allows them to permeate porous substrates, and (4) they form covalent bonds with substrates that have active hydrogen. One of the primary mechanisms of bonding by urethane adhesive is believed to be through isocyanate (-NCO) to the active hydrogen containing surfaces,⁷ and the through polar, (-NH and C=O) groups. These polar groups are capable of forming strong chemical/physical interactions with the polar surfaces (functional group having active hydrogen). Acceptance of PU in a wide variety of different automobile end uses can be attributed to the versatility of the urethane polymer. This enables it to fulfil a number of important functions, such as providing comfort, safety and structural strength to the various automotive parts as needed.

1.1.1. Adhesive joint durability

The reliability of adhesion technology is often considered in terms of the ability of an adhesive joint/bond to maintain its initial strength despite long-term exposure to testing conditions. This property is often referred to as joint durability. Although obtaining high initial strength is relatively easy, but obtaining good durability in extreme environmental conditions is comparatively more difficult. The most important factor leading to joint degradation is moisture.⁸ Moisture is responsible for the vast majority of bond failures, either in the field during service or in the laboratory during research. The rate of bond degradation mainly depends on environment, materials and stress. The environment is dominated by temperature and moisture and that affects the adhesive bond durability in a number of ways: (1) reversibly altering the adhesive (e.g. plasticization, hydrolysis), (2) swelling the adhesive and inducing concomitant stresses, (3) disrupting secondary bonds

across the adherend-adhesive interface (e.g. hydrogen bonding), and (4) hydrating or corroding the adherend surface. However, to obtain a durable bond between adhesive and adherend much attention should be given to material selection and also to the preparation methods.

The formation of strong and durable adhesive joints depends on complex physical and chemical phenomena in relevance to the material properties. Both these discourage material manufacturers to adopt the technology.⁹ In addition, the manufacturing process also involves complicated procedures. From a technical point of view, adhesive bonding offers several advantages compared with other conventional joining methods, including the possibility of joining dissimilar materials, ability to join thin sheets effectively and improved appearance of the finished structure. However, to attain a long service life under demanding conditions, it is necessary to have materials with good surface and mechanical properties.

1.1.2. Testing of adhesive joints

The mechanical performance of the adhesive bond can be measured in a variety of ways. There are over 30 standards¹⁰ such as peel test, wedge test etc and many more non-standard tests¹¹ used to measure the mechanical properties of an adhesive bond. The peel test is the method to access the bond energy for such a joint in which one of the adhering sheets is either much stiffer than the other or is firmly attached to a rigid support. Figure 1.1 describes the three commonly used peel test configurations, i.e. 90°-peel test (L-peel test), the 180°-peel test (U-peel test), and T-peel test. Usually the peel angle θ is kept constant during the test. For testing the materials, various mixed (modes II and I) loading can be obtained at different peel angles. Figure 1.2 highlights the difference in mode I and II. Mode I opening or tensile mode is a process when the crack surface move directly apart. Mode II is sliding or in plane shear mode where the crack surfaces slides over one another in a direction perpendicular to the leading edge of the crack. An ASTM D3167 standard floating roller peel test arrangement for the 90°-peel¹² is shown in Figure 1.3. In the following Figure 1.3 the peel test is demonstrated, to show that the load is applied in a mode I direction. In mode I, opening or peel is the most severe loading that a bonded joint can tolerate. In this case, the joint only face load in the vicinity of its

application and the resulting bond strength attained is reduced due to the diminished load sharing capacity of the joint.

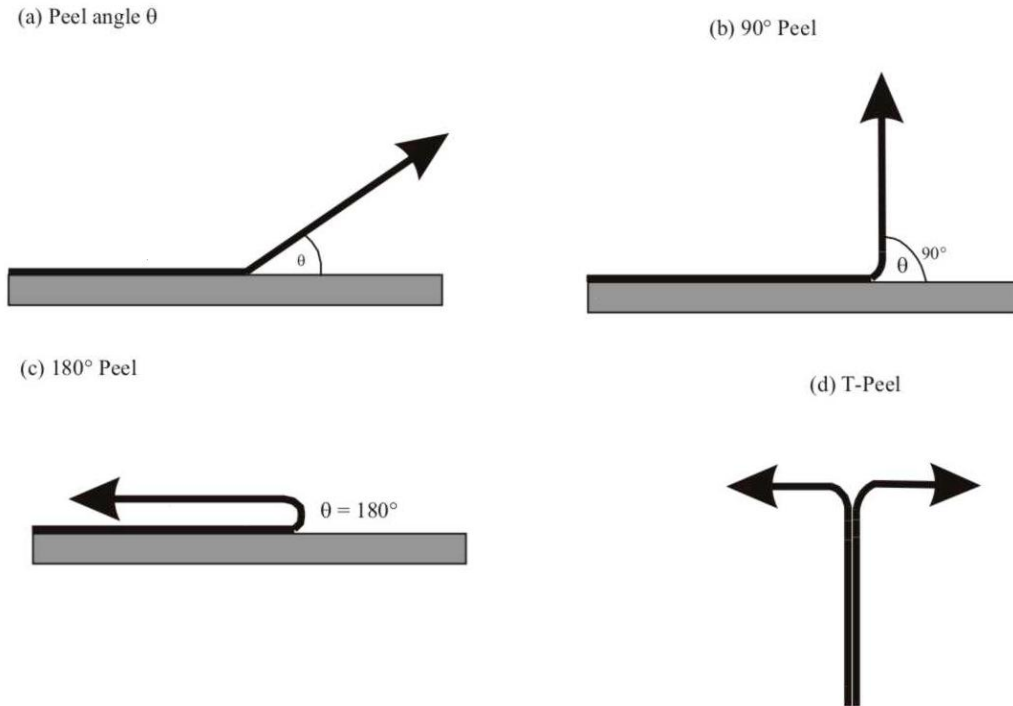


Figure 1.1: Several typical peel test configurations: (a) representation of peel angle, (b) 90° peel test, (c) 180° peel test, (d) T-peel test.

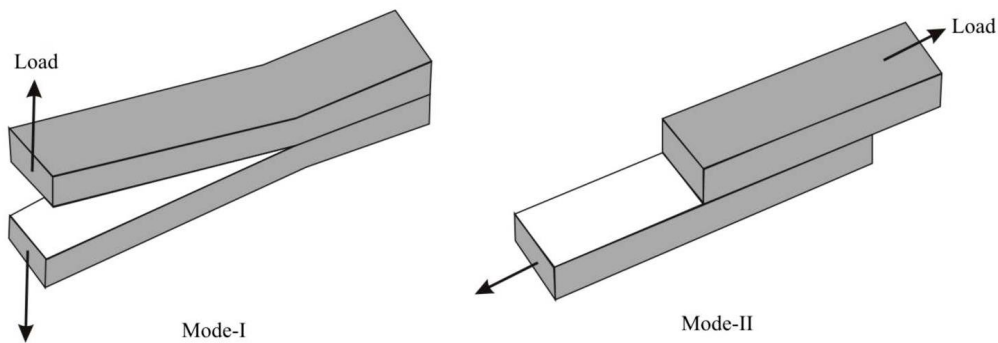


Figure 1.2: Basic modes of loading during fracture mechanics.

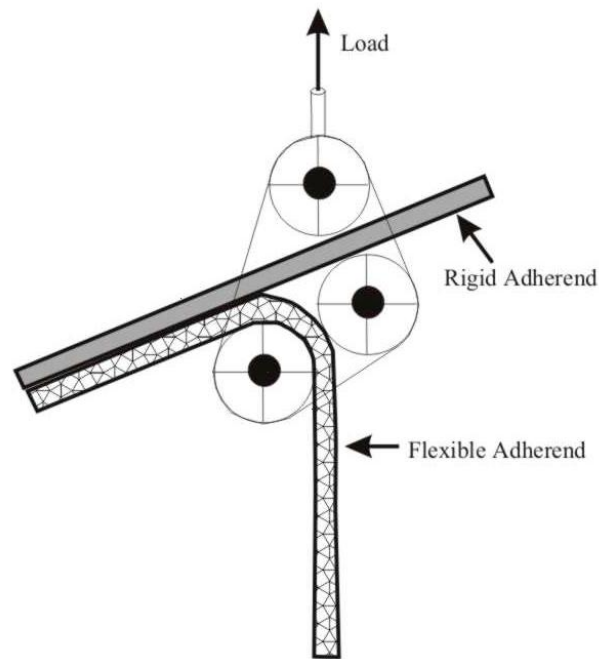


Figure 1.3: Schematic representation of floating roller (90°-peel) peel test arrangement.¹²

The test described in Figure 1.3 highlights the method used to study the mechanical properties of adhesive bonds. A modified form of this testing arrangement was used to measure the PU foam/thermoplastic (TP) material joint strength in the present work (see also Figure 2.2 Chapter 2).

1.1.3. Adhesion theories

In the past thirty years, the level of basic adhesion research has outnumbered the growing use of the technological applications. Despite this, a single unifying theory that adequately describes all adhesion phenomena is yet to be proposed. However, several basic models have been established. The adhesion theories can be classified into four areas: mechanical interlocking, diffusion, electronic, and adsorption.¹³

Mechanical interlocking theory

Packham¹⁴ reviewed the mechanical interlocking theory where the mechanism of this theory suggests that the adhesive mechanically interlock with the irregularities of a roughened surface. The mechanical interlocking is believed to be the primary adhesion mechanism when an adhesive penetrated and set in a porous material.¹⁵ Later, this theory

was discounted by providing examples where the adhesion of resin to wood increased as the surface roughness of the wood decreased.¹⁶ In this case chemical bonding was believed to be the primary mechanism. However, work by Bright et al.¹⁷ and Arrowsmith¹⁸ suggested that the number of pores penetrated by the adhesive is linked with adhesion strength. These findings revived the mechanical adhesion theory. Finally, Venables¹⁹ work of examining the phosphoric acid anodise (PAA) process indicated a link with surface micro-porosity and bond strength. The presence of long needle-like protrusions on the PAA aluminium surface was also believed to be critical in the mechanical keying mechanisms. This work has contributed in making this mechanism an often-quoted reason for the observed bonding performance. Evans et al.²⁰ and Wang et al.²¹ have studied the anodizing process on metal surface where they found that the surface roughness contribute to increase the energy dissipation processes in the zone of interface separation.

Diffusion theory

The diffusion theory of adhesion states that the adhesion strength of polymers to themselves (autohesion) or to each other is due to mutual diffusion²² (interdiffusion) of macromolecules across the interface. Voyutskii²³ believes that the adhesion between two polymers is a result of interfacial interdiffusion of polymer chains. This occurs when the polymers are mutually soluble and the macromolecules from the respective polymers are sufficiently mobile. Critics of the theory believe if the interdiffusion process is involved, the joint strength should depend on the type of the material, enhanced wetting, temperature, molecular weight, and formation of primary and secondary interfacial forces.²⁴ The diffusion mechanisms in polymer-polymer junctions contribute greatly to the adhesion strength. The interdiffusion mechanism mainly depends upon the dynamics of polymer chains in the interfacial region. The fundamental understanding of the molecular dynamics of entangled polymers has advanced due to the theoretical approach proposed by a number of authors.²⁵⁻²⁷ This new approach stems from the idea that polymers cannot pass each other in concentrated solution or melt or solid form. Therefore, a chain with a random coil conformation is trapped in an environment of fixed obstacles.

De Gennes has assumed a wormlike motion of confined chains and gave it the name ‘reptation’. The most important and useful application of reptation concept is the crack healing.²⁸ The problem of healing is to correlate the macroscopic strength measurements to the microscopic description of motion. The difference between self-diffusion phenomena in the bulk polymer and healing is that the polymer chains in the former case move over distances larger than their gyration radii, whereas in the other case, healing is essentially complete in terms of joint strength. Several authors reported that the healing is controlled by different factors, such as (I) the number of bridges across the interface, (II) the crossing density of molecular contacts²⁹ (III), the center of mass Fickian interdiffusion distance³⁰ (IV), and the monomer segment interpenetrating distance.²⁸ The resulting scaling laws for the fracture energy versus time during healing are the following.

$$G \sim \begin{cases} t^{1/2} M^{-3/2} & \text{for (I) and (II)} & (1.1) \\ t^{1/2} M^{-1} & \text{for (III)} & (1.2) \\ t^{1/2} M^{-1/2} & \text{for (IV)} & (1.3) \end{cases}$$

Where G , t , and M , represents the fracture energy, time of diffusion, and the mass of diffusing materials, respectively.

Electronic theory

This theory states that the work of adhesion is due to the formation of an electrical double layer between the adhesive and substrate. According to Deryaguin³¹ the high joint strength results from the electrostatic interactions between the adhesive and the adherend. As the distance between the charges increases so does the electrostatic potential. When the bonds break, the discharge energy provides a measure of the interfacial adhesion forces present. Evidence for the theory provided by Deryaguin³¹ and Weaver³² suggested the interfacial charge was an important parameter in determining the adhesive strength. However, work by Skinner et al.³³ and Chapman³⁴ indicated that these forces were small relative to the forces of molecular attraction, i.e. van der Waals interactions. The

electrostatic theory tends to be more appropriate where particles are interacting with substrate surface and less applicable to interactions between plane surfaces.^{1,35}

Adsorption theory

According to the adsorption theory of adhesion, the interatomic and intermolecular interactions between adhesive and substrate are responsible for adhesive forces. These interactions are classified into primary (chemical bonding) and secondary forces

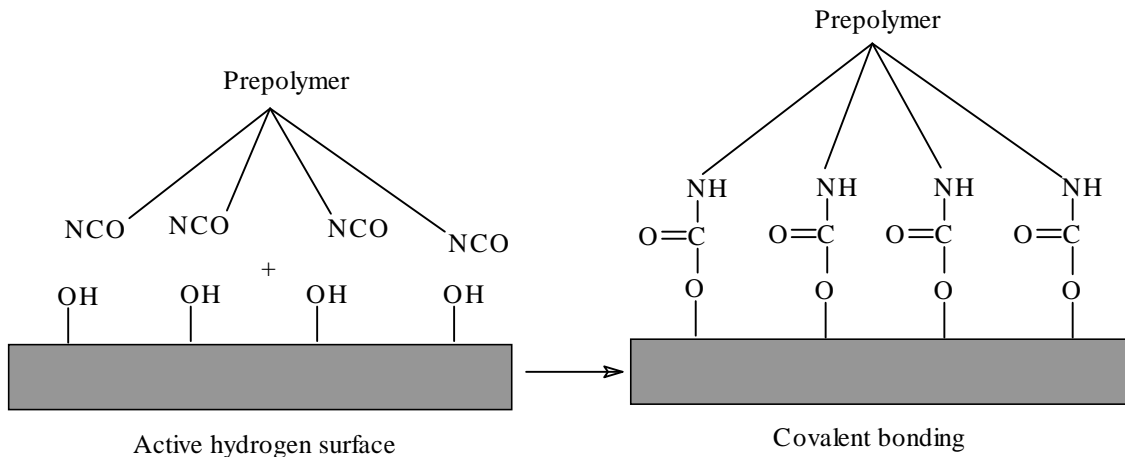


Figure 1.4: Schematic representation for covalent bonding of urethane adhesive with polar surface.⁷

(physical interactions, e.g. hydrogen bonding). The primary bonds are the strongest with energies in the range of 1000-100 kJ/mol as compared with 40-20 kJ/mol of secondary forces. In case of urethane adhesives bonded to active hydrogen containing substrates, a primary bond is believed to exist^{7,36} as explained in Figure 1.4.

Thermodynamic measurements of the adhesive and substrate are often employed to determine the adhesive forces acting across the interface.³⁷ The work of adhesion, (WA), is the energy required for separating a unit area of two phases. This is determined by adding the surface free energy of the two phases and subtracting their interfacial energy. Several examples in the literature describe the correlation between WA and adhesive bond strength.³⁸⁻⁴¹ Andrews et al.⁴² and Gent et al.⁴³ have shown that if the energy dissipation processes involved in bond fracture are accounted, and failure is interfacial, then WA may be determined directly. Other workers also support this

view.^{44,45} As discussed before that the interactions occurring at the interface produce adhesive bonds of different strengths. Fowkes⁴⁶ and Owens et al.⁴⁷ classified two types of bond interactions and the way in which the adhesive and adherend surfaces could be related. Fowkes established that the weaker dispersion forces interacting at the interface could be related by their geometric mean. Owens developed the relationship to include a polar interaction term for the stronger adhesion forces. However, according to Fowkes the acid-base interactions are the dominant adhesive force. Bolger⁴⁸ also estimated acid-base interactions by measuring the isoelectric point of the oxide surface and the pK_a (negative logarithm of dissociation constant of acid) of the adhesive bonding to the surface. Watts et al.⁴⁹ have applied these principles to examine polymer interactions with inorganic substrates.

1.2. Polyurethane foams

The PU foams are cellular or expanded materials synthesized by the reaction of diisocyanate with polyol in the presence of a blowing agent. Depending upon the mechanical properties of PU foam, it is either categorized as flexible, rigid or semirigid material. The first PU foams obtained (which were of rigid kind) were described by Bayer in 1947⁵⁰ and the first flexible soft foams by Hoechstlen in 1952.⁵¹

1.2.1. Manufacturing of PU foams

The raw materials used for preparing PU foams are:

1. Isocyanates
2. Polyols
3. Chain extenders or branching agents
4. Blowing agents
5. Surfactants
6. Catalysts
7. Fillers, pigments, or dyes

The isocyanates (IC) are major components of PU foam, they may be aliphatic like hexamethylene diisocyanate (HDI), isophorone diisocyanate (IPDI), or aromatic like toluene diisocyanate (TDI), 4,4'-diphenylmethane diisocyanate (MDI), and naphthalene

diisocyanate (NDI). TDI is used for soft PU foams, rigid foams are made from prepolymer based on MDI, whereas semirigid foams contain both TDI and MDI. Microcellular elastomers are made from MDI.

The polyols are either polyether, such as propylene glycol (PG) and trimethylolpropane (TMP) combined with sucrose or polyester, such as ethylene glycol, 1,2-propanediol, 1,4-butanediol, and diethylene glycol combined with glycerol. Polyethers are used to produce flexible and rigid foams and polyesters are used to produce elastomers, flexible foams and coatings.

Chain extending agents are the diols and diamines of small molar mass. They increase the size of the rigid segments as well as the hydrogen bonding density and the relative molar mass (RMM) of the PU foam. The corresponding tri- or more highly functional compounds act as branching or crosslinking agents. Among the chain extenders are ethylene glycol, diethylene glycol, propylene glycol, dipropylene glycol, 1,4-butanediol, 1,4-cyclohexandiol, N,N'-di(hydroxyethyl) piperazine, aminoalcohols, hexamethylenediamine, hydrazine, etc.

The blowing agents for the PU foams are water or low boiling inert solvents⁵² usually halogen derivatives. Water reacts with isocyanate groups to produce carbon dioxide, which acts as the foaming agent. Whereas the low boiling solvents include chlorofluorocarbons (CFCs), chlorofluorohydrocarbons (CFHCs), e.g. trichlorofluoro carbon CFCl_3 (CFC-11), dichlorodifluoro carbon CF_2Cl_2 (CFC-12), CHClF_2 (HCFC-22), CHCl_2CF_3 (HCFC-123), and $\text{CH}_3\text{CCl}_2\text{F}$ (HCFC-141b).

Pentane or isopentane (b.p.27.9°C) are other alternatives to the PU foam blowing agents. In order to protect the ozone layer, CFCs can be easily eliminated in the manufacture of flexible PU foams by water (which evolves CO_2). The replacement of physical blowing agent in a PU foam formulation by water, however increases the:

1. viscosity (by elimination of the solvent and the appearance of an increased number of urea linkages),
2. reactivity of the reaction mixture (the additional exothermic reaction of the isocyanate group with water).

Surfactants are indispensable in PU foam manufacture⁵³ especially for the low- density varieties. They reduce the work required to increase the interfacial area, allow reduction

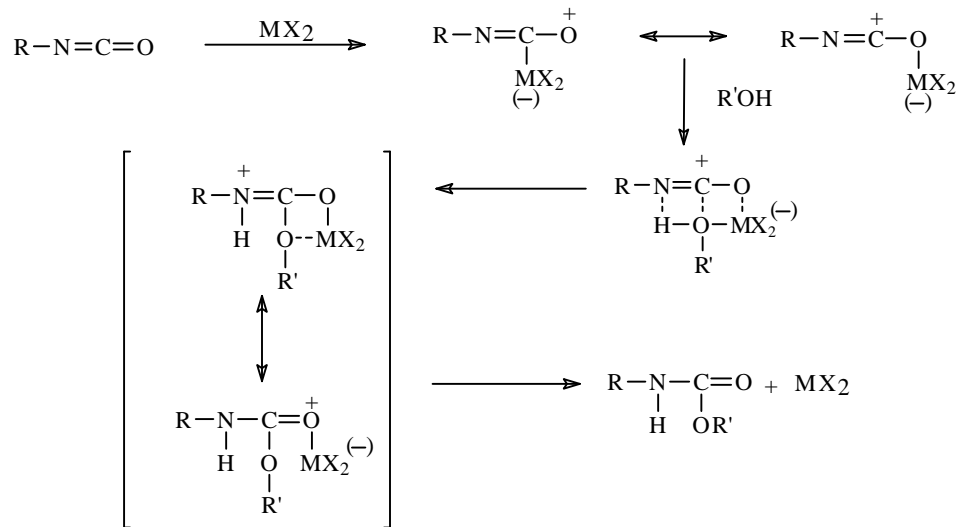
of the bubble size and control of the structure and enhancement of the foam stability. Surfactants play a significant role at each stage of PU foam formation by:

1. facilitating the thorough mixing of the PU foam mixture components,
2. stabilizing the bubble nuclei in a liquid reaction mixture, preventing the bubbles from coalescing to form large size bubbles,
3. facilitating the control over the fluidity of the polymerizing liquid mixture in the expansion process as a result of bubble growth,
4. allowing tight control of the time and degree of opening of the cell structure of the foams produced.

A wide variety of ionic compounds were originally used as surfactants in PU foam manufacture e.g. sulphonated hydrocarbons, fatty acids or sodium salts of alkoxyglycols, as well as some non-ionic compounds, such as oxyethylenated alkylphenols, or alkylene oxide block copolymers. The majority of PU foams are currently manufactured by using non-ionic organosilicon-polyether copolymer.⁵⁴

The catalysis of isocyanate reactions is of great significance in foam manufacture. It affects not only the overall rate of polymer formation but also affects the relative rates of individual reactions and enables the structure and properties of the end product to be controlled. The catalysts control the foaming and curing rates and enable manufacture of PU foam at an economical rate. The presence of the catalysts accounts, however, not only for the synthesis but also for the PU decomposition process. The isocyanate reaction catalysts are divided into two major groups, tertiary amines and organometallic compounds, especially tin derivatives. Tertiary amine catalyze reactions of isocyanate group with both water and hydroxyl groups. The most active amine catalyst of convenient steric structure is diazabicyclooctane (DABCO).⁵⁵

The organo tin catalysts are more active than the amine catalysts.⁵⁶ Both di- and tetravalent tin compounds act as the catalysts. Tin (IV) compounds are somewhat more active and they have a negative effect on PU foam aging. The commonly used organotin catalysts are dimethyltin dichloride, dibutyltin dilaurylmercaptide, dibutyltin maleate, and tin caprylate. The mechanism of catalysis by organometallic compounds is illustrated in scheme 1.1



R and R', are alkyl chains
M, is a metal or alkylmetal
X, is an acid residue

Scheme 1.1: Schematic representation of mechanism of catalysis of urethane formation.⁵⁷

Fillers may be classified as the particulate, flaky and fibrous fillers. Usually particulate fillers increase the density and hardness of PU foams. They also reduce their ignitability and increase their absorption of mechanical energy. Typically, calcium carbonate and barium sulphates are used for this purpose. Flaky fillers include mica, talc, and glass flakes. They reinforce the polymer. The fibrous fillers include, natural and synthetic, organic and inorganic fibers, e.g. carbon fibers, glass fiber etc.^{58,59} Fibrous fillers are used to increase the rigidity and elastic modulus.

1.2.2. Foam chemistry and morphology

Chemistry

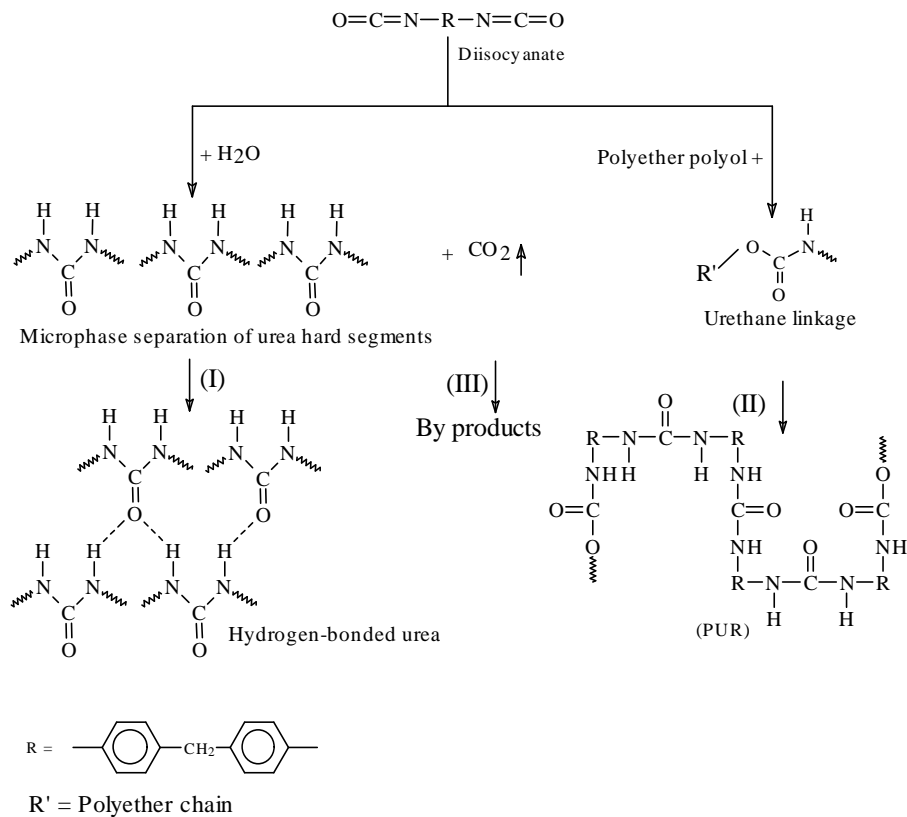
The following four stages can be distinguished in the foam production process:

1. A latent stage, lasting up to 30 s, starts as soon as the reactants have been mixed, and ends when the mixture starts increasing in volume. At this stage two sub stages are apparent: The period in which the evolving blowing gas dissolves in the reactant

mixture until saturation. The period in which once gas saturation has been achieved, with the participation of the dissolved air, micronuclei of bubbles emerge and the mixture starts to look like a cream.

2. The foam growth stage, which begins with a visible increase in volume of the reactant mixture and ends when the mixture attains the highest possible volume.
3. The foam stabilization stage, which corresponds to a stage of increasing mixture viscosity. The liquid components of the reactant mixture turn into a solid polymer.
4. The maturation stage in which the foam becomes crosslinked and acquires an acceptable strength.

Furthermore, the schematic illustration of all these four stages during foaming process is shown in reaction scheme 1.2.



Scheme 1.2: Schematic representation of foaming process of polyurethanes.⁶⁰

Morphology

PU foams are made up of long polyol chains that are linked together by shorter hard segments formed by diisocyanate and chain extenders. The resulting structure of urethane network is depicted schematically in Figure 1.5. Polyol chains (referred as soft segment) exhibit low-temperature flexibility and room temperature elastomeric properties to polymer morphology. Typically, low molar mass polyols give the best adhesive properties. Generally, the higher the soft segment concentration, the lower will be modulus, tensile strength, hardness and tear strength, while elongation will increase.

The short chain diols and diamines act as chain extenders. Diisocyanate molecules link to the chain extenders forming the hard segment structures. The hard segments impart the higher glass transition temperature. The long hard segment structures aggregate together due to similarities in polarity and hydrogen bonding to form a pseudo crosslinked network structure.⁷ The hard domains effect modulus, hardness and tear strength and also serve to increase resistance to compression and extension.

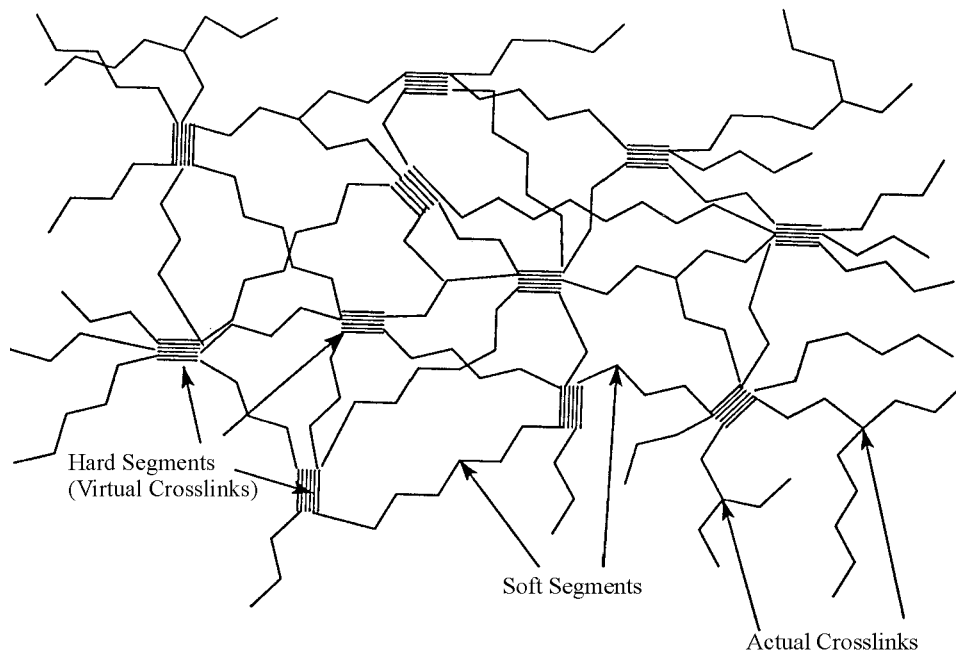


Figure 1.5: Schematic representation of PU foam morphology.⁷

The presence of both soft and hard segments in PU foam structures gives rise to different glass transition temperatures in the range of -30°C to 150°C . The lower glass

transition temperature is usually due to the soft segment and the higher for hard segments. In order to get a product with high performance characteristics, one needs the proper choice of materials with desired properties.

1.3. Thermoplastic materials

TP materials are a very large polymer class and this allows one to find a suitable polymer for nearly every application. Among the TP polymers polycarbonate (PC) is an important engineering polymer that is widely used since its development in 1953 and first production in 1960.⁶¹ Its main features are transparency, toughness and high temperature stability. It is applied in car parts (e.g. dash boards, headlights) glazing, lighting, housing for electrical equipment, packaging (e.g. milk bottles) or as compact disc (CD). Apart of these uses, this material has some drawbacks which limits its applications.⁶²⁻⁶⁵ In order to overcome the limitations, PC is often blended with an engineering polymer, like acrylonitrile-butadiene-styrene (ABS).⁶⁶ PC/ABS is one of the most successful commercial polymer blend since the first patent date from 1964.⁶⁷ This blend combines the good mechanical and thermal properties of PC and the ease of processability. PC/ABS actually is a ternary blend, since ABS itself usually consists of styrene-acrylonitrile random copolymers (SAN) and dispersion of grafted polybutadiene (PB). The properties of such a ternary blend will depend on the structure properties of the components. Sometimes a reinforcing material like glass fiber is added to the blending mixture in order to increase the impact strength. Also glass fibers increase the surface roughness, which aid in adhesion. Poly (styrene-co-maleic anhydride) (SMA) polymer is another engineering material that has wide range of utilities. But this material is often brittle at temperatures as low as -30°C ⁶⁸ and may not meet the ductility requirements demanded by the end users like in car industry.

1.4. Objectives and summary of this work

The adhesion between PU foams and TP materials is a broad area requiring consideration of numerous controlling parameters.⁶⁹⁻⁷² The large difference in the mechanical properties between PU foam and TP material systems makes it necessary to consider different mechanisms of adhesion in these two groups of materials.

The objective of this study is to:

Systematically investigate the factors, which influence the work of adhesion of PU foam and TP material joints.

The peel test is used to assess the bond strength of contact surface before and after different climate treatments. The bond durability is described in terms of the change in work of adhesion of the PU foam/TP materials joint upon exposure to -40 to 80°C and 80% relative humidity (RH) environment, relative to the adhesion strength of untreated samples. The 80°C and 80% RH environment provides an extreme climate exposure and is used to simulate the aging of the PU foam/TP material joint over a period of several days. Apart of standard climate test cycle, the influence of high humidity and low temperature was also investigated separately.

The contact angle studies were carried out with respect to surface properties of materials. The surface properties of materials play a vital role in adhesive bond strength and durability.

The optical microscope image analysis was also carried out on peel test samples to get some information on interaction behavior of materials at interface.

The diffusion process of MDI (one of the foam components) has been investigated in detail. These studies were carried out using FTIR microscopy, light microscopy and gravimetric analysis.

The importance of foaming reaction for adhesion (or cohesion) was investigated by Fourier transform infrared attenuated total reflectance (FTIR-ATR) spectroscopy. Such type of investigations gives information about the chemical structure and also about the foaming process. The foam structures in intimate contact with TP material have some significant influence on the peel strength of the adhesive joint.

The use of surface analytical tools like X-ray photoelectron spectroscopy (XPS), time of flight secondary ion mass spectrometry (ToF-SIMS) and atomic force microscopy (AFM) also aids in elucidating the mechanisms involved in the failure of the adhesive joint and contributes to the development of the materials. The nature of the interface of PU foam/TP material was examined by using AFM, XPS, and ToF-SIMS after climate treatments. These experiments help to understand the interface chemistry and morphology of materials.

Neutron reflection (NR) and transmission electron microscopy (TEM) studies have been carried out on PU foam flat surfaces separated from TP material. These experiments were carried out on deuterated and non-deuterated samples before and after climate treatments. The NR experiments were carried out on all three PU foam formulations. While the TEM measurements were done on thin PU film formed at the interface between PU foam and TP material. Nearly 260 to 400 nm thick elongated structures were observed in PU film at interface. Small angle X-ray scattering (SAXS) experiments were carried out on bulk PU foam and PU film samples. These experiments were performed to study the hard segments in deuterated and non-deuterated PU foam film at interface.

The knowledge established after all these experiments is important in understanding the PU foam/TP material joint durability and strength. This work establishes the parameters associated with adhesion strength of PU foam/TP material system joints. The experience gained from this work can be used to evaluate the performance of more complex systems based on a thorough characterization of the TP material and foam surface chemistry and topography. The work also indicates that the climate treatment has severe effect on the adhesion performance. The overall adhesion performance is linked to both of the properties of PU foam and TP material systems. The major findings presented in these investigations are summarized as the direct correlation of adhesion of PU foam with TP material system mainly depends upon the type of TP material and PU foam systems. The joint durability is strongly affected by climate treatments. This information can be used to develop a material system, which has the capacity to withstand the extreme climate conditions. The significant conclusions drawn from these investigations are summarized Chapter 4.

Chapter 2

Experimental

2.1. Materials

The reagents for PU foams and TP material plates were used as obtained from supplier. Three PU foam formulations and five different TP material systems have been part of these investigations. The TP material plates were the blends of different copolymers and in some cases glass fiber was used as reinforcing material (see Table 2.1). The PU foam formulations were based on MDI, polyether polyol [a mixture of poly(propylene oxide) “PPO” and poly(ethylene oxide) “PEO” 80:20 wt.-%, and a dispersion of SAN in PPO (2:98 wt.-%)], and water or deuterium oxide as blowing agent. An isocyanate index (isocyanate index is the molar ratio of isocyanate versus active hydrogen bearing groups, i.e. hydroxyl and amino groups) of 88 was used through out the work.

Table 2.1: Details about TP material plates.

Thermoplastic material systems	Names used
Polycarbonate/Acrylonitrile butadiene styrene-Styrene maleic anhydride	PC/ABS-SMA
Styrene maleic anhydride copolymer	SMA
Polycarbonate/Silicone acrylate rubber-Glass fiber	PC/SAR-GF
Polycarbonate/Acrylonitrile butadiene styrene	PC/ABS
Polycarbonate/Acrylonitrile butadiene styrene-Glass fiber	PC/ABS-GF

2.2. Adhesion behavior of PU foams with thermoplastic material systems

2.2.1. Preparation of test samples

Three different PU formulation were used (PU-a, PU-b, and PU-c), and their details are reported in Table 2.2. To differentiate between the use of H₂O and D₂O as blowing agents, either an ‘h’ or a ‘d’ will be used in the naming scheme (e.g. h-PU-a for non-

deuterated PU foam sample of formulation ‘a’). When also a climate treatment was performed, that will be indicated by an additional ‘-T’ in the name (e.g. h-PU-a-T).

In order to prepare the samples with PU foam adhered to TP material plates, an appropriate amount of polyol was mixed with MDI (for formulation details see Table 2.2) and mechanically stirred for 10 s at 1400 rpm. Finally the reacting mixture was transferred to a foaming tool (the volume of foaming tool was 800 cm³), which already contains a TP material plate. The tool was then closed to allow the process to progress for 10 min at 40°C. After 10 min the foamed plate was removed from the foaming tool. The density (ρ) of all the foamed materials was calculated $\sim 0.16 \pm 0.02$ g/cm³ from the weight and the dimensions of the foamed plates using Equation 2.1.

$$\rho_{\text{Foam}} = \frac{m_{\text{Foamed plate}} - m_{\text{TP Substrate}}}{V_{\text{Foamed plate}} - V_{\text{TP Substrate}}} \quad (2.1)$$

$m_{\text{Foamed plate}}$ Mass of foam plate $V_{\text{Foamed plate}}$ Volume of foamed plate
 $m_{\text{TP Substrate}}$ Mass of TP substrate $V_{\text{TP Substrate}}$ Volume TP substrate

Table 2.2: Formulation details of PU foam systems.

Foaming system	Polyol [g]	Isocyanate (MDI) [g]	H₂O or D₂O [g]	Additives / Catalysts*
PU-a	100 (PO-a)	45	2.6	I
PU-b	100 (PO-b)	44	2.8	II
PU-c	100 (PO-c)	54	3.1	III

*Additives/catalysts were used to enhance the reaction rate in three PU foam formulations, by adding additive II the reaction rate was doubled in PU-b foam system compared to PU-a system with additive I, and the additive III in PU-c foam accelerate foam formation compared to the other two PU foams (PU-a and PU-b).

2.2.2. Aging of test samples

The test samples were stored at room temperature for one week before any climate treatment. Then the samples were transferred to the climate chamber (Climates/Sapratin Model: Excal 2221 HA, France) and treated under four different climate cycles:

1. **Standard climate treatment:** It is a standard climate treatment which involves heating of samples from room temperature (RT) to 80°C and then cooling to -40°C with 80% relative humidity (RH) for 24 cycles (11 days) treatment (Figure 2.1a).
2. **case 1:** Includes heating of samples from RT to 80°C with 80% humidity (in 1 h), stored for 4h under this condition, cooled down in 1 h to RT and then immediately reheated to 80°C (Figure 2.1b). The whole cycle was repeated 24 times.
3. **case 2:** Includes a cooling down of samples from RT to -40°C (in 1 h), stored for 72 h at this temperature condition and then heating to RT (Figure 2.1c).
4. **case 3:** This treatment is the standard climate cycle test but without defined amount of humidity (no humidity was supplied from external source).

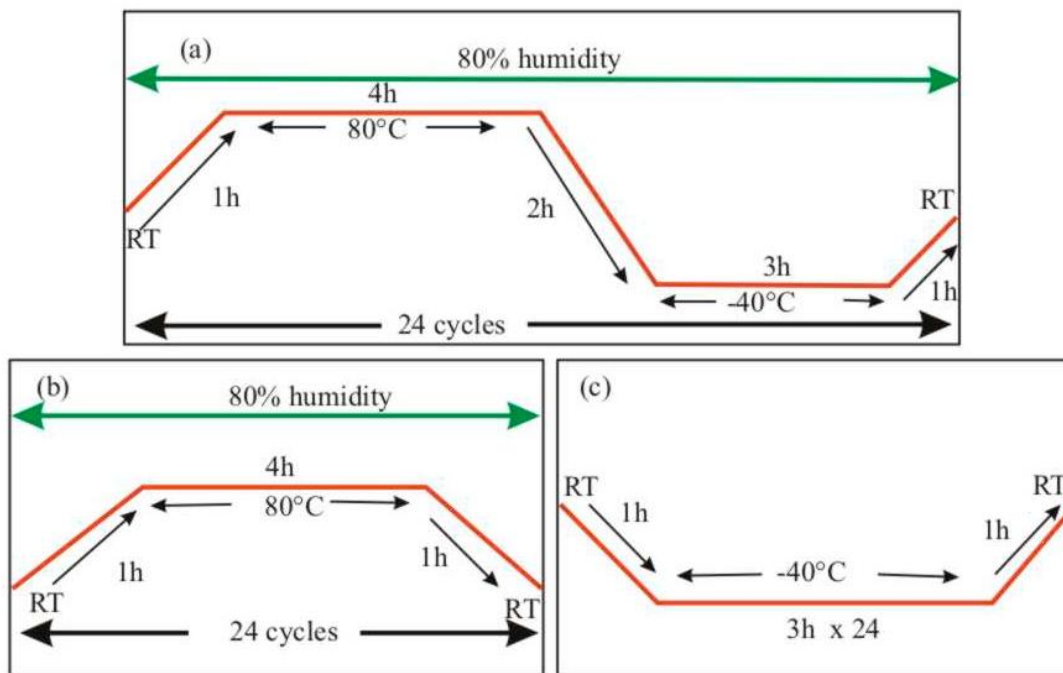


Figure 2.1: Schematic representation of climate cycles: (a) standard climate treatment, (b) case 1 climate treatment (a treatment of samples in a cycle with 80% humidity and RT to 80 °C conditions) and (c) case 2 climate treatment (involves cooling down of samples from RT to -40 °C (for 72 h at -40 °C) and then heating the samples to RT conditions).

2.2.3. Peel test

The peel test samples were prepared by cutting into rectangular strips of dimensions of $120 \times 18 \times 5$ mm. The peel test was carried out by peeling the PU foam layer from TP material surface at a peel angle of 90° and at room temperature conditions. The schematic drawing of peel test arrangement is shown in Figure 2.2. The test uses the peel test fixture and computerized Zwick 1120 Werkstoffprüfmaschine. The testing machine provides a constant rate of peel and continuously measures the force of detachment during the test. The peel fixture consists of a moving base and a holding point fixed to the testing machine. The peeling rate used was 10 mm/min. The peel force (N/mm) required for separating the PU foam layer from the TP material substrate was recorded and taken as a measure of the adhesion strength. The force (F) per unit width of peeled strip was calculated by dividing the measured force (P) by the width (W) of sample strip (Equation 2.2). For each TP material system five sample strips were measured in order to calculate the error value.

$$F = \frac{P}{W} \quad (2.2)$$

F is the force per unit width of sample strip, P measured force, W width of sample strip

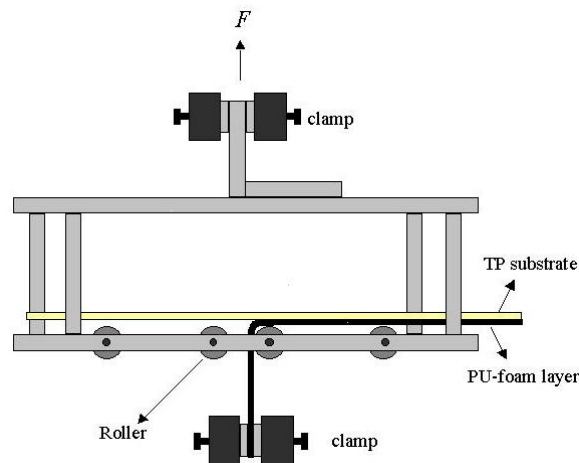


Figure 2.2: Schematic representation of peel test arrangement. A flexible PU foam layer was peeled from rigid TP material plate at a peel angle of 90° . The peel rate supplied from the instrument was 10 mm/min.

2.3. Contact angle studies on thermoplastics and PU foam systems

2.3.1. Contact angle measurements

The testing liquids used to characterize the polymer surfaces through contact angle measurements were double distilled water, ethylene glycol, diiodomethane, α -bromonaphthalene (fresh distilled prior to use), glycerol and formamide. The characteristic properties of these liquids are given in Table 2.3.

Table 2.3: Characteristic data of the test liquids used for the sessile drop studies.

Test liquids	Source	γ_{lv} [mN/m]	polarity	γ_{lv}^d [mN/m] ^a	γ_{lv}^p [mN/m] ^b	$(\gamma_{lv}^p / \gamma_{lv}^d)^{1/2}$
α -bromonaphthalene ⁷³	Aldrich	46.60	0.0000	44.60	0.00	0.00
Diiodomethane ⁷⁴	Merck	50.80	0.0453	48.50	2.30	0.22
Ethyleneglycol ⁷³	Merck	47.70	0.3522	30.90	16.80	0.74
Glycerol ⁷³	Merck	63.40	0.4146	37.00	26.40	0.84
Formamide ⁷⁵	Merck	58.20	0.5070	28.69	29.51	1.01
EG/W=30/70 ⁴⁴	Merck	61.59	0.6672	20.50	41.09	1.42
Bidistilled water ⁷³		72.80	0.7005	21.80	51.00	1.53

^a γ_{lv}^d is calculated by $\gamma_{lv}^d = \gamma_{lv} - \gamma_{lv} \times \text{polarity}$, ^b γ_{lv}^p is calculated by $\gamma_{lv}^p = \gamma_{lv} \times \text{polarity}$

For contact angle measurement the TP material plates were cut into small plates with dimensions 20 mm in width and 80 mm in length. Using sandpaper their edges were cleaned. The plates were washed with distilled water and finally cleaned by ultrasonic treatment, dried in oven at 50°C for 36 h. Plates were stored in a desiccator prior to measurements. The foam samples with flat and clean surface were prepared by using polyethylene sheet in foaming tool. The contact angle was measured on both sides of the drop with a Krüss G40 instrument at a temperature of 20°C. For every solvent eight measurements were carried out and the mean value was calculated. Surface tensions were calculated using the geometric mean method of Owens, Wendt, and Rabel.^{46,76} Furthermore, the contact angle data analysis is explained in detail in Appendix.

The advancing and receding contact angles on TP materials were measured with a OCA contact angle system model TBU 90E from data physics GMBH Germany using liquid foam components (MDI and polyols) and water. These measurements were carried out by tilt plate method.⁷⁷ The plates were inclined to a fixed angle of 45°. In each series and for each liquid the contact angles were measured for at least 8 to 10 droplets with drop volume of 30 μl at $20 \pm 1^\circ\text{C}$.

2.3.2. Tensiometry

The surface tension of liquid foam components was measured by using the Wilhelmy plate method. These measurements were carried out on Krüss K8 Tensiometer (Hamburg). The principle of this technique is shown in Figure 2.3 The sample container was cleaned with chromic acid and water and then dried in oven. The test fluid was filled

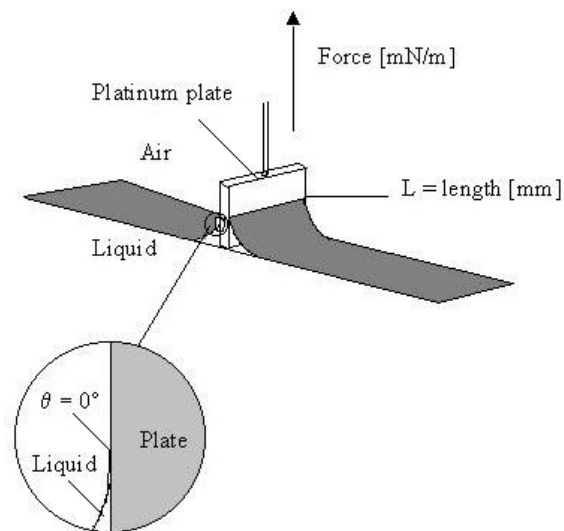


Figure 2.3: Schematic representation of working principle of tensiometry.

into the container. The temperature of the test liquid was maintained at 20°C before each measurement. When it was assured that the required temperature has been attained the platinum plate was brought in contact to surface of test liquid and the resulting value was recorded from the instrument. After each measurement the platinum plate was cleaned in propane flame. The surface tension (γ_{lv}) value was obtained by using Equation 2.3.

$$\gamma_{lv} = F / L \cos \theta \quad (2.3)$$

In this Equation γ_{lv} is the liquid vapour surface tension, F is the force measured from the instrument, L , is the wetted length, θ is the contact angle formed between the plate and liquid surface.

2.4. Microscopic studies

2.4.1. Atomic force microscopy

The AFM topographic images were acquired from neat TP material plates and materials from interface using a digital instruments industries (Santa Barbara) multimode atomic force microscope equipped with a nanoscope III controller. These images were acquired in tapping mode with a resonant oscillating frequency of 300 kHz and a microfabricated silicone cantilevers of spring constant 15 N/m at ambient pressure, room temperature and relative humidity conditions. The mean surface roughness (R_a), which is the average vertical deviation of the surface relative to the surface plane and the root-mean-square (RMS) were calculated by an software provided with the instrument based on Equation (2.4):

$$R_a = \frac{1}{L_x L_y} \int_0^{d_x} \int_0^{d_y} |f(x, y)| dx dy \quad (2.4)$$

where $f(x,y)$ is the surface relative to the center plane and L_x, L_y are the dimensions of the surface.

2.4.2. Optical microscopy

PU foam layer separated from TP material after peel test was used to acquire the optical micrographs. The images were obtained from flat PU foam sample surface by using Axioplan 2 imaging and Axiophot 2 universal microscopy from Carl Zeiss equipped with an AxioCam Mrc digital camera. The images were recorded with a 10x lens in reflection mode.

2.5. ToF-SIMS and XPS studies

2.5.1. Time of flight secondary ion mass spectrometry

The samples for ToF-SIMS studies were also prepared in the same way like peel test and carefully separated from interface before experiments. The ToF-SIMS spectra were acquired on an Ion ToF-IV, Reflectron analyzer instrument using an Ar⁺ (10 keV) ion source with a 45° polar angle of source axis. In this system, the secondary ions were accelerated up to 2 keV energy. A 100 × 100 μm² sample surface area was rastered for 105 s. The spectra were acquired for 100 s with an ion flux of 6.28 × 10⁸ ions. A mass resolution m/Δm of ~7500 was used. To enhance the sensitivity for high-mass ions, a 10 keV post-acceleration was applied. The mass scale was normalized to a particular PC fragment ion peak at 211 a.m.u. in all the samples.

2.5.2. X-ray photoelectron spectroscopy

Samples for XPS studies were prepared in the same way like peel test samples and carefully separated from interface before any investigation. The surface chemical composition was determined from the neat TP material and also from PU foam/TP interface by XPS using an ESCALAB iXL 220 spectrometer from Thermo-VG scientific operating at a pressure in 1 × 10⁻⁸ to 1 × 10⁻¹⁰ mbar range, equipped with an AlK_α and a MgK_α X-ray source and a monochromator. Spectra were recorded at a takeoff angle of 30° (angle between the plan of the sample surface and the entrance lens of the analyzer) and with a pass energy of 100 eV. The theoretical analyzer resolution expected with that setting is 0.5 eV. For each sample, a detailed scan of the O1s, C1s, N1s, and Si2p lines was performed with a step width of 0.1 eV and pass energy of 20 eV. The calibration of the binding energy (BE) scale was made by setting the C1s BE of the neutral carbon (C-C and C-H bonds) peak at 284.6 eV. The C1s and O1s were resolved into individual Gaussian peaks using origin software (originLab, Massachusetts, USA).

2.6. Structure analysis in polyurethane foams at the interface

2.6.1. FTIR spectroscopy

The FTIR measurements were carried out on a FTIR spectrometer Perkin-Elmer S2000, equipped with a diamond single ATR cell Golden Gate heatable up to 200°C of LOT Oriel (Darmstadt, Germany). A small portion of PU foam reaction mixture was placed on preheated (40°C) ATR cell and spectra were recorded using 50 s intervals. The change in intensity of isocyanate band was used to calculate the reaction time for each reacting foam mixture.

2.6.2. Small angle X-ray scattering

The compact PU film was powdered after cooling in liquid nitrogen. The powdered samples were filled in glass capillaries for measurements. SAXS measurements were performed with an RIGAKU rotating anode RU-3HR equipped with a Siemens Hi-Star 2 D area detector and in an evacuated Kratky compact camera (Anton Paar KG) with a scintillation counter in a step-scanning mode. CuK_α radiation with a wavelength of $\lambda = 0.154$ nm was used, monochromatized by a 10 μm thin nickel (Ni) filter. The obtained scattering profiles were corrected for background scattering and (if necessary) desmeared.⁷⁸ The scattering vector q is defined by $q = (4\pi/\lambda)\sin\theta$.

2.6.3. Transmission electron microscopy

The TEM images were obtained on a LEO 912, transmission electron microscope (LEO Electron Microscopy Ltd., Cambridge, United Kingdom), using an accelerating voltage of 120 kV. The compact PU film from interface was microtomed perpendicular to the surface after cooling in liquid nitrogen. TEM micrographs were acquired from thin samples after staining in RuO_4 .

2.6.4. Neutron reflection

The PU foam samples were separated from the interface as schematically shown in Figure 2.4 and the flat PU foam surface was exposed to the neutron reflection instrument

(HADAS) at Jülich research center, Germany. These experiments were carried out using a 2 D position sensitive detector and neutrons with a wavelength of 4.52 Å.

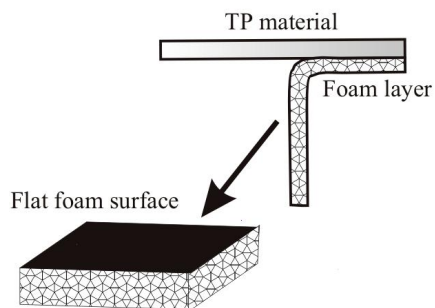


Figure 2.4: Schematic representation of separation of PU foam/TP material interface: a flexible PU foam layer was removed from TP material in similar way like peel test. The flat PU foam surface was exposed to NR reflection studies.

2.7. Diffusion coefficient studies of MDI in thermoplastics

2.7.1. Gravimetric analysis

This technique was used to calculate the weight gain of TP materials in MDI after diffusion process. The diffusion process of MDI, one of the foam components, was studied using five different TP material systems at 40°C. Small TP strips having approximate dimensions of 2 × 5 × 10 mm were cut from each TP material plate. Each strip was weighed and then dipped into isocyanate, removed after certain intervals of time (5, 21, 45, 70, and 100 h, respectively), dried with tissue paper and weighed. The final weight gain was obtained by weighing the samples after 100 h.

2.7.2. FTIR microscopy

These studies were carried out on Bruker IF55 FTIR spectrometer equipped with Bruker microscope. Liquid nitrogen cooled samples (samples from section 2.7.1) were microtomed using HM360 microtome from Microm. Thickness of the samples was maintained to 10 micron. The microtomed samples were fixed on a sample holder with the help of cellophane tape. First spectrum was taken from pure TP material and later

spot was moved over MDI diffused area (see Figure 2.5). The spot size used was $50 \times 50 \mu\text{m}$ and the spectra were recorded by moving the spot by $16.5 \mu\text{m}$ after every scan.

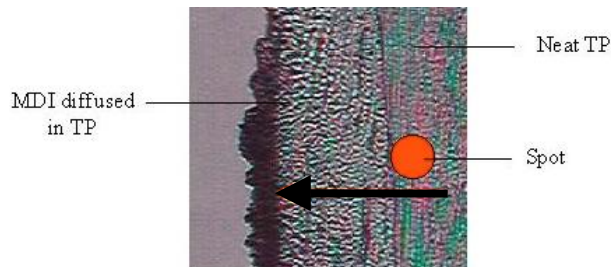


Figure 2.5: Schematic representation of an investigated sample. The first spectra was taken from sample area without diffused layer of MDI and later spot was moved on sample area with MDI. The scanning direction is indicated by arrow.

2.7.3. Optical microscopy

The microtomed samples prepared for FTIR microscopy studies in section 2.7.2 were also used for image analysis. The samples were fixed on glass slides by using silicone oil and then the images were acquired using DM RX research light microscope, with a magnification power of $16\times$ up to $500\times$. All the images were acquired by using $16\times$ lens.

Chapter 3

Results and discussion

3.1. Adhesion behavior of PU foams with thermoplastic material systems

The study of adhesion can be broadly divided into the areas of “Surface Science”⁷⁹, “Mechanistic Studies” and “Material Properties”^{80,81}. Each of these aspects is extremely important and focuses on different but interrelated concepts in addressing the general phenomenon of adhesion.^{82,83} Without going into the details of each of these sciences, the work in this chapter will address the specific topics that are directly relevant to this research work. In this regard, the important features of the TP material adherents and PU foams will be discussed. For adhesion strength measurements, the most widely used test, the “peel test”^{84,85} will be discussed with reference to the mechanics involved in this test. The effects of climate treatment on adhesion performance will also be discussed in detail.

Regarding adhesion performance studies three PU foam systems and five different TP materials were evaluated by using the peel test method, as described in Chapter 2 section 2.2.3. The apparent difference in three foaming systems was water content. The PU foam formulations also differ from each other on the basis of added additives and the additives were used to enhance the reaction rate. The PU-a and PU-b have shown good adhesion (cohesive failure) with all the TP material systems before climate treatment whereas poor adhesion (adhesive failure) performance was observed for PU-c foam system. The adhesion performance of PU-a and PU-b foam on exposure to different climate condition was also tested.

3.1.1. Analysis of the peel test results

The adhesion force measured in peel test is demonstrated in Figure 3.1.1a. The *force* axis represents the force required to peel and deform PU foam from TP material and the *elongation* axis represents the maximum peeled length of PU foam from TP material. The

peel force shown in Figure 3.1.1a also represents an example of cohesive peeling, whereas an example of adhesive peeling is shown in Figure 3.1.1b. The adhesion strength per unit width of sample strips was calculated by dividing the measured force by width of each sample. The force due to the stretching and breaking of foam (region I and III in Figure 3.1.1a) was excluded in order to minimize the error value. Normally the force measured due to the breaking of foam was higher when compared to the peeling force. For each TP material plate, five samples were tested and an average value is reported as interfacial adhesion strength of a particular PU foam/TP material system.

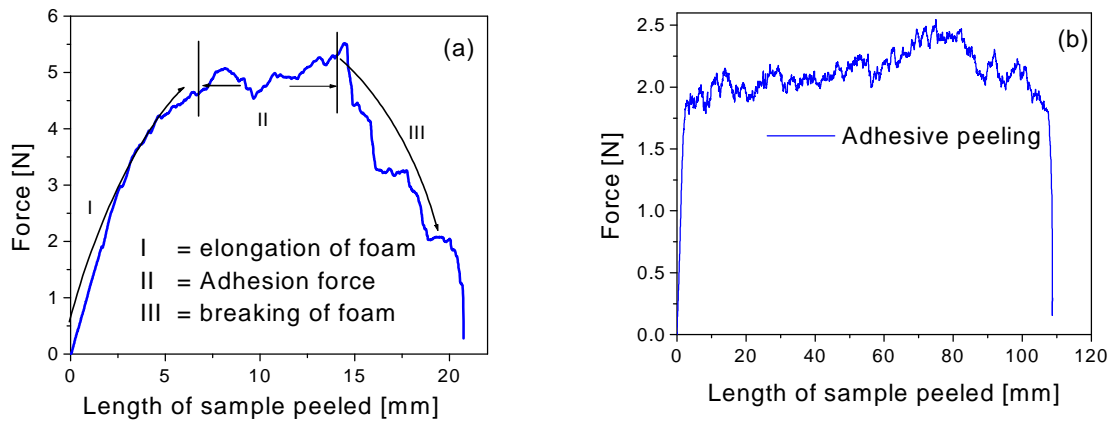


Figure 3.1.1: Plots of “peel test” data obtained when an 18 mm wide sample with a 2 mm PU-a foam layer thickness was peeled at a peel rate of 10 mm/min from PC/ABS-SMA TP material using Zwick testing machine (a) before climate test and (b) after climate treatment. The adhesion force was calculated by excluding the force due to foam elongation and foam breaking. In Figure (a), the area indicated by I-III positions represents the elongation of foam, adhesion force at interface, and breaking of foam respectively.

The investigated PU foam systems have shown very strong adhesion to TP materials before any climate treatment and the peel forces were as high as 5-6 N/mm (depending on the nature of the TP material). In case, where the adhesion of the PU foam to the TP material substrate is stronger than the peel force, it often happens that instead of the expected interfacial failure between the PU foam and TP material substrate, a cohesive failure within PU foam occurs. It should be noted that the adhesion of PU foam to the TP material is not the limiting factor, but simply the relative low cohesive strength of PU foam bulk, which is lower than the adhesion strength for a particular PU foam/TP material joint. In order to differentiate the different types of peeling behavior of PU foam some observed modes of failure during peel test experiments are shown in Figure 3.1.2.

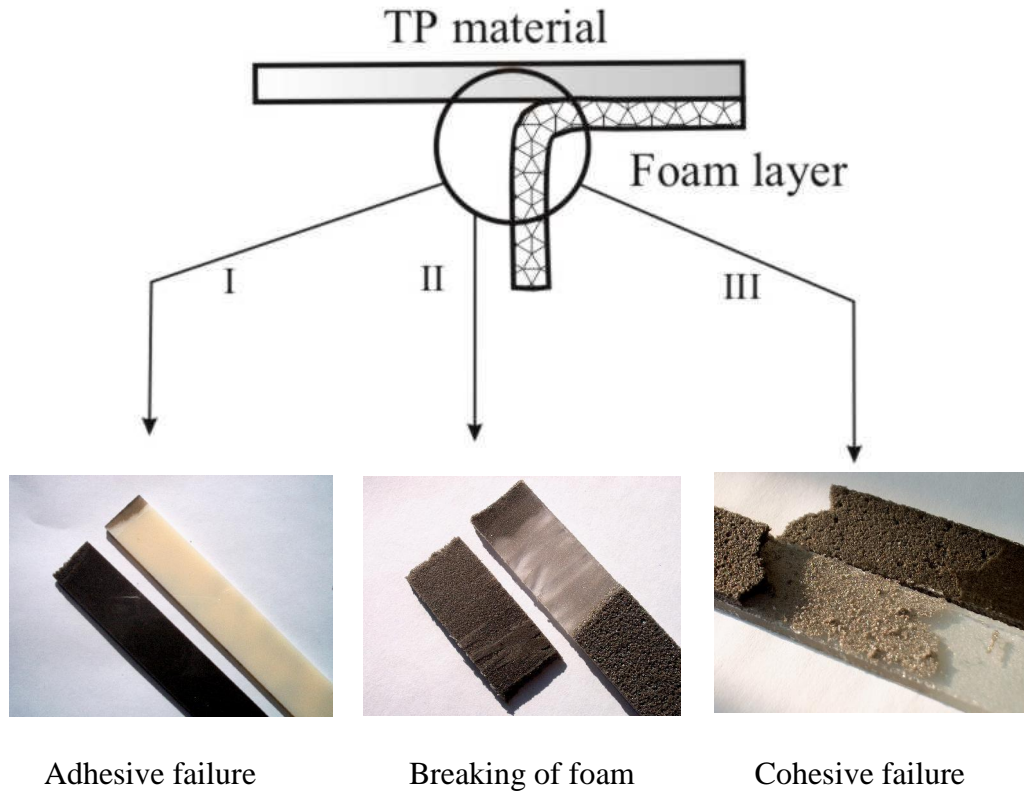


Figure 3.1.2: Schematic representation of modes of failure during “peel test”. In the Figure I-III represents adhesive failure, breaking and cohesive failure of PU foam from TP material plates, respectively.

The adhesive peeling occurs when both materials separate from interface, whereas cohesive failure is followed by the failure from inside the foam material leaving behind a thin PU film on TP material surface. But in some cases only after small peeling of PU foam, the foam breaks and this is designated as breaking of foam in the Figure 3.1.2. Before climate treatment the cohesive breaking was observed in case of PU-a and PU-b foam systems with different TP materials and after climate treatments it has changed to adhesive failure.

3.1.2. Adhesion performance before climate treatments

In the following section the peel test results of PU-a, PU-b and PU-c foam systems with five different TP material samples are explained. The results for PU-a and PU-b foam systems are plotted in Figure 3.1.3a and 3.1.3b. The PU foam adhesion strength with TP material samples was calculated by dividing the measured peel force by the width of each sample strip. The untreated samples have shown nearly the same behavior during peeling test, i.e. cohesive failure.

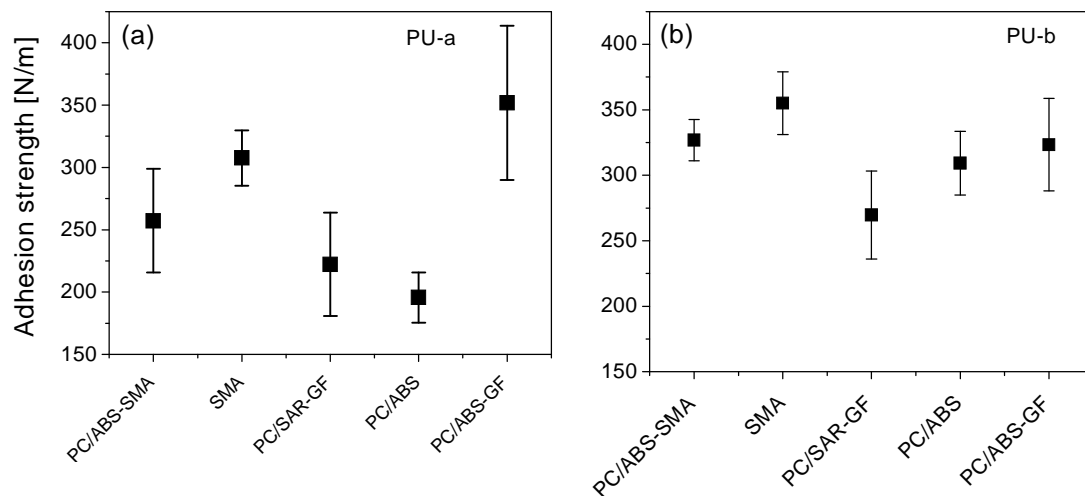


Figure 3.1.3: Adhesion strength of PU-a (a) and PU-b (b) foam systems with five different TP materials as measured by “peel test” method before climate treatment.

In case of PU-a foam system PC/ABS-GF has shown the higher peel strength compared to the other TP materials. The reason for this may be the surface roughness and

also the higher PC⁶⁰ content compared to the other samples. Higher surface roughness means mechanical interlocking at the interface. Keisler et al.⁷⁹ and Sancaktar et al.⁸⁶ have indicated the importance of surface roughness towards adhesion strength of materials, where they have found the higher joint strength for samples with high surface roughness. The hydroxyl group from PC gives reaction with isocyanate group and that could also contribute to the interfacial strength.

On the other hand in case of PU-b foam system the higher peeling force was observed for SMA TP material compared to the other samples. Whereas the lowest peel strength was for the PC/SAR-GF samples. The other three TP materials have shown comparable peel strength.

The PU-c foam system has shown weak adhesion performance in comparison to PU-a and PU-b foam systems. The results for PU-c foam system are depicted in Figure 3.1.4. The PU-c foam system has shown better adhesion performance with SMA TP

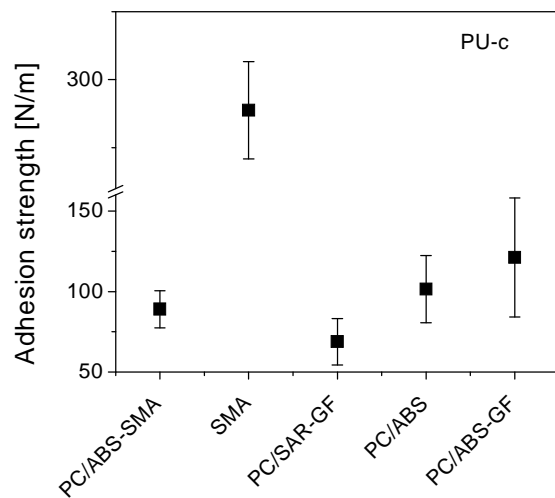


Figure 3.1.4: Adhesion strength of PU-c foam system with five different TP materials as measured by “peel test” method before climate treatment.

material out of five TP materials. The possible reason for this is the interfacial reaction of maleic anhydride (component of SMA TP material) with MDI during the foaming process.⁸⁷ The observed mode of peeling for PU-c foam system from SMA was cohesive and from PC containing TP materials it was adhesive peeling. So due to the worse

adhesion properties of PU-c foam system with PC containing TP materials, it was not proceeded for further adhesion durability studies like climate change experiments.

As PU-a and PU-b foam systems have shown cohesive failure in untreated form, so it was necessary to check the joint durability under hostile treatment conditions. For this purpose, samples from these two foam systems were tested under different climate conditions, in order to compare adhesion strength of these two foam systems with different TP materials.

3.1.3. Adhesion performance after climate treatments

The bond durability (adhesion strength) of PU-a and PU-b foam systems with five different TP samples was evaluated after different climate treatments and the results are depicted in Figure 3.1.5a and 3.1.5b. Details about climate cycles are given in Chapter 2

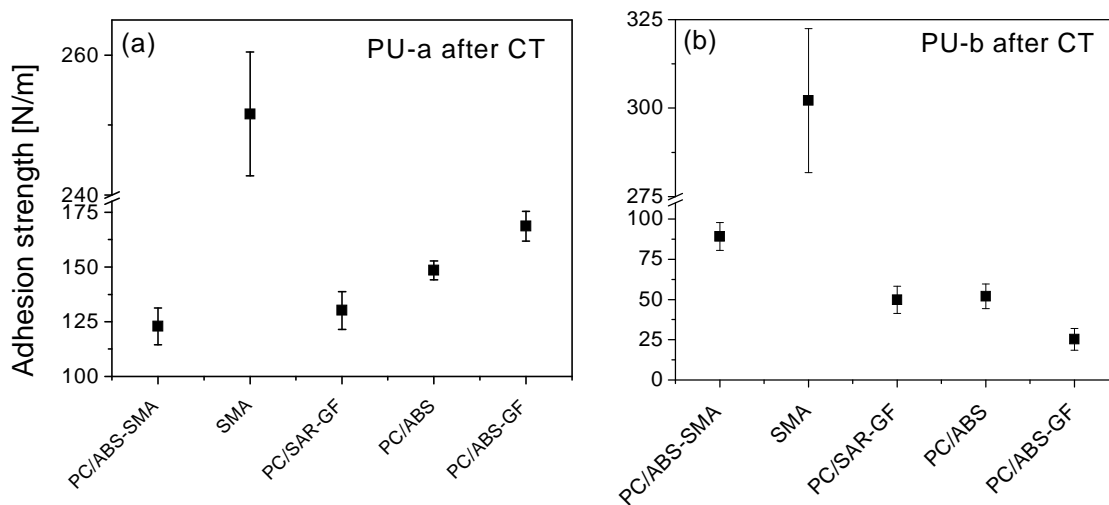


Figure 3.1.5: Adhesion strength of PU foam system with five different TP materials as measured by “peel test” method after standard climate treatment (RT to 80°C + 80 % RH to -40°C for 24 cycles): (a) PU-a foam system, (b) PU-b foam system.

section 2.2.2. The adhesion strength was badly reduced after standard climate treatment (CT) in all the samples except SMA TP material. In case of SMA sample only 10-15 % PU foam TP material adhesion was lost but in other TP materials it was more than 50 % as compared to the untreated samples.

In PU-a foam system the severe effect of climate treatment was observed on adhesion of PU foam with PC/ABS-SMA and PC/SAR-GF TP materials. PC/ABS-GF sample has shown some better performance. The PU-a foam system has shown cohesive failure from SMA TP material and from the other four TP materials it was adhesive peeling.

In PU-b foam system more than 70% loss of adhesion strength was recorded with four TP materials in comparison to the untreated samples. However, the better adhesion was observed on SMA TP material similar to PU-a foam system. Furthermore, the severe effect of climate treatment was recorded with PC/ABS-GF sample. On the basis of above discussed results it can be assumed that the bond formed between MA and MDI remain unaffected after climate treatments. But in case of PC containing TP materials the formed interface is only based on physical interactions like hydrogen bonding and that can be highly affected by the diffused water during climate treatments. Also the samples with high surface roughness (GF containing sample) have not shown better adhesion performance, which means that surface roughness is not the limiting factor for adhesion under the influence of climate conditions with high humidity.

3.1.3.1. Testing of samples under modified climate cycles

In order to get information about the influence of different parts of climate cycle towards adhesion, the samples were treated in some modified cycles and the details about these treatments are mentioned in Chapter 2.

The effect of high humidity on interface was evaluated by treating the samples in a climate cycle without humidity (case 3 climate treatment) and the results are plotted for PU-a and PU-b foam systems in Figure 3.1.6a and 3.1.6b. The case 3 climate treatment did not show any observable effect on adhesion. Although the measured force was lower compared to the untreated samples but the observed mode of peeling was cohesive in most of the tested samples. For comparison of peeling mode before and after the case 3 climate treatment, a plot of peel test data is displayed in Figure 3.1.7. One can notice from the Figure that the peeling behavior is quite similar to untreated sample but with lower force.

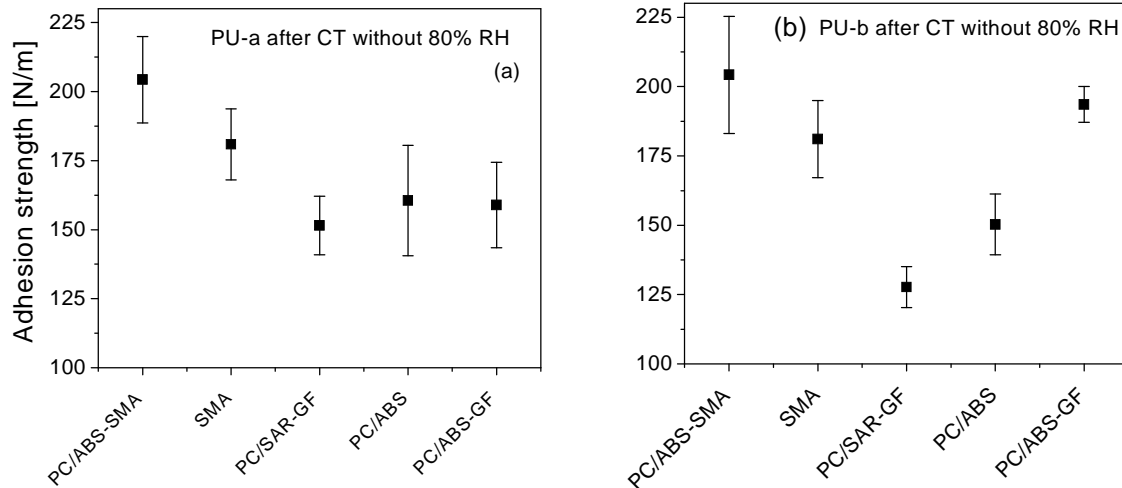


Figure 3.1.6: Adhesion strength for: (a) PU-a and (b) PU-b foam systems with five different TP materials as measured by “peel test” method after case 3 (RT to 80°C to –40 °C without 80% RH cycle) climate treatment.

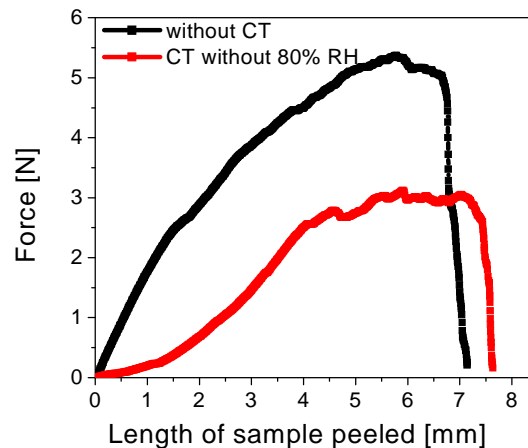


Figure 3.1.7: Plot of “peel test” data obtained when an 18 ± 0.5 mm wide sample with a 2 ± 0.25 mm thick PU-a foam layer was peeled from SMA TP material at a peel rate of 10 mm/min using Zwick testing machine.

In case of PU-b foam system, lower peel strength was observed on PC/ABS and PC/SAR-GF samples as compared to the other three TP materials but the observed mode of failure was cohesive. The reduction in peel strength of these samples may be due to the sample preparation, e.g. incomplete mixing of foam reactants strongly influences the

adhesion properties.⁸⁸ Similar to the untreated samples, in this case also the measured adhesion force does not correspond exactly to the interface separation force.

But after comparison of these results with standard climate test samples it seems that the RH badly reduces the adhesion strength of PU foam with TP material systems.⁸⁹ After determining that the case 3 climate treatment did not show any observable effect on adhesion performance, it can be assumed:

1. that the diffused water strongly reduces the adhesion of PU foam with TP materials.
2. the unreacted MDI had possibility to react with hydrogen active groups present at TP material surface in the absence of water, or diffuse into the TP material and make some contribution in strengthening the interface.⁹⁰ The diffused MDI will react with PC hydroxyl groups in the bulk TP material.

Therefore, when the MDI diffusion process is operating, the chains move mainly along their contour length by the process of reptation because the motion in other directions is limited by entanglement with other chains. When PU foam and TP material were brought into contact there were, of course, no chains crossing the interface. After complete contact of two materials (PU foam and TP material) the interface broaden rapidly with most of the diffusion being caused by the Rouse-like (unentangled) motion of small segments of chains of unreacted isocyanate groups.⁸²

Effect of humidity and temperature on adhesion strength

The effect of high temperature with high RH and low temperature parts was also checked separately on PU-a foam system and the results are shown in Figure 3.1.8. The effect of case 1 climate treatment on adhesion was exactly the same like the standard climate test cycle. The possible reason for this is the diffusion of water that causes the failure of adhesion. The diffused water strongly affects the physical interactions i.e. hydrogen bonding at the interface as well as some chemical interactions at the interface.^{91,92}

The case 2 climate treated samples, showed more or less the same results like untreated samples. It was also noticed that the PU foam samples from case 2 showed the cohesive failure while in case 1 always adhesive failure occurred, except the SMA sample.

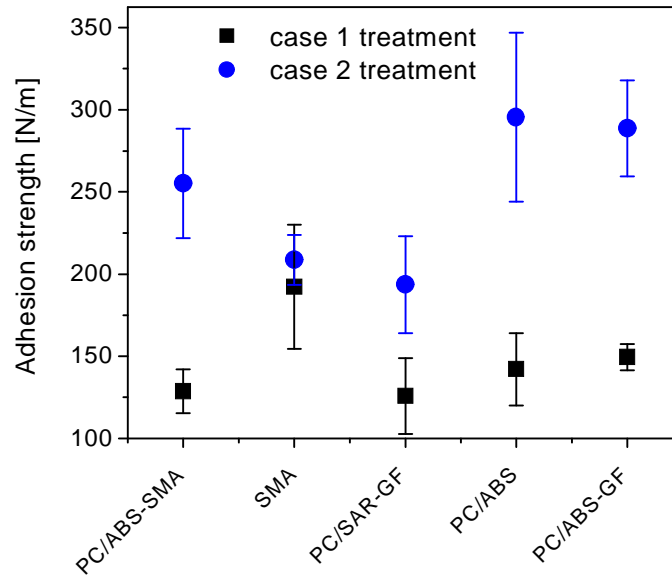


Figure 3.1.8: Adhesion strength of PU-a foam system with five different TP material systems as measured by “peel test” method after case 1 (RT to 80°C + 80 % RH) and case 2 (RT to -40°C) climate treatments.

Adhesion strength and number of climate cycles

The results obtained on four TP material systems with PU-a foam system at different treatment times during climate cycle are displayed in Figure 3.1.9. The experience gained through this experiment shows that the adhesion strength for all the TP materials reduced with increased number of climate cycles. It should be pointed out here that the observed peeling behavior in all samples was adhesive even after one cycle of treatment. But the adhesion between PC/ABS-GF, PC/SAR-GF and PC/ABS-SMA as TP materials and the PU foam was too strong to separate them. As the treatment time was extended to 3-5 cycles, the maximum loss in adhesion was observed in all four samples. Relatively speaking that up to 5 cycles less effect was observed in PC/ABS-GF and PC/ABS sample compared to two other samples. From these results it become obvious that one can get very conclusive information on adhesion durability of PU foam with TP materials even after five cycles of treatment except for keeping the sample in climate chamber for 24 cycles.

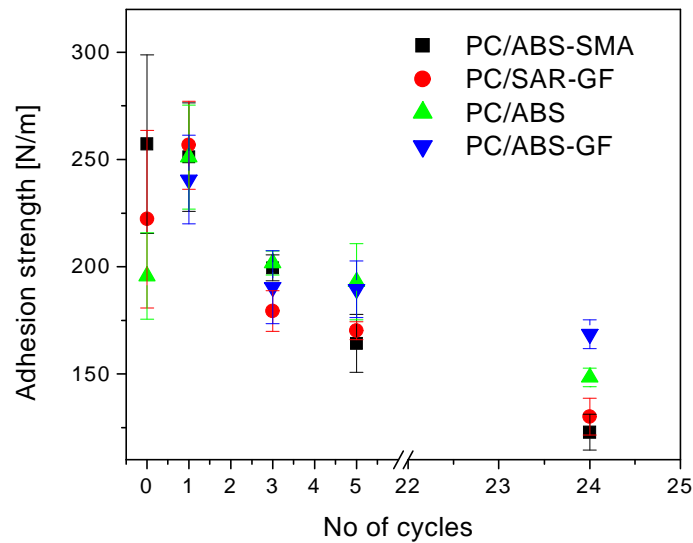


Figure 3.1.9: Adhesion strength of PU-a foam system with four different TP material systems as measured by “peel test” method after: 1, 3, 5 and 24 cycles of treatment involving standard climate cycle (RT to 80°C + 80 % RH to -40°C = 11 h 1 cycle).

3.1.4. Short summary of adhesion test results

The following observations can be drawn on adhesion behavior of PU foam with TP materials:

1. SMA shows the best adhesion with all PU foam formulations compared to the other TP materials.
2. PU-a shows the best adhesion out of all foam materials.
3. PU-a and PU-b shows cohesive failure before climate treatment with all five TP materials.
4. PU-c shows worst adhesion out of all foam materials. Only in contact with SMA cohesive failure was observed.
5. Climate treatments lower the adhesion force for most of the samples. Only adhesion on SMA was not measurably influenced after climate treatments.
6. Climate treatment shows stronger effect on PU-b foam compared to PU-a system.
7. After climate treatment PC/ABS-GF (high PC content, glass fiber) shows better adhesion with PU-a foam systems compared to PC/ABS-SMA, PC/SAR-GF and

PC/ABS. But PC/SAR-GF, the other glass fiber containing sample shows low adhesion.

8. A standard climate treatment with no humidity produces cohesive failure with strongly reduced cohesive strength of PU foam.
9. A cyclic climate treatment at RT and 80°C with 80 % RH shows nearly the same effect, as the standard cycle i.e., the low temperature part is not the limiting factor.
10. The interfacial cohesive strength of PU-a foam with TP materials was changed to adhesive failure after five cycles of treatments in four tested TP materials.

SMA is the best TP material for adhesion. The reason is (probably) a chemical linkage between isocyanate and MA, which gives imide linkage.

PU-a is the best foam system for adhesion. The reason could be the slower foaming process (due to the type of polyol and H₂O content) compared to the other systems.

3.2. Contact angle studies on thermoplastics and PU foam systems

In adhesion studies the wetting of the substrate surface is very important.⁹³⁻⁹⁵ The most common method for investigating the wetting behavior is the contact angle technique. According to the literature⁹⁵ the contact angles on polymer surfaces are not only influenced by the interfacial tensions but also due to the surface properties of materials. In principle these measurements are simple to carry out, but a number of parameters e.g. surface roughness or surface inhomogeneities complicate their interpretation.

Measurement of contact angle on solid surfaces gives information about the surface tension; beside this it is also possible to measure the advancing and receding contact angles on the same solid surface. The advancing and receding contact angles provide useful information on the surface tension and wetting properties of a solid surface. There are at least three different methods for receding contact angle measurements, i.e. Wilhelmy balance, tilted plate, and syringe methods.⁷⁷

In present work the contact angle was measured by sessile drop method and the contact hysteresis were carried out by tilted plate method.

The purpose of the studies presented in this part of thesis was to:

1. investigate the surface free energy of TP material plates and foamed samples surfaces.

- observe the behavior of liquid foam components on TP materials plates and estimation of their surface energies.

3.2.1. Contact angle results of neat TP materials

The contact angle results for neat TP material samples together with the surface tensions and their polar as well as disperse contribution are plotted in Figure 3.2.1. The scattering of the data obtained by sessile drop measurements can be explained by the influence of the chemistry of the samples. One can see that surface tension values calculated by using geometric mean method (calculation method is explained in Appendix) predict higher values for the disperse components and smaller values of the polar component which are independent of the chemical composition of each material.

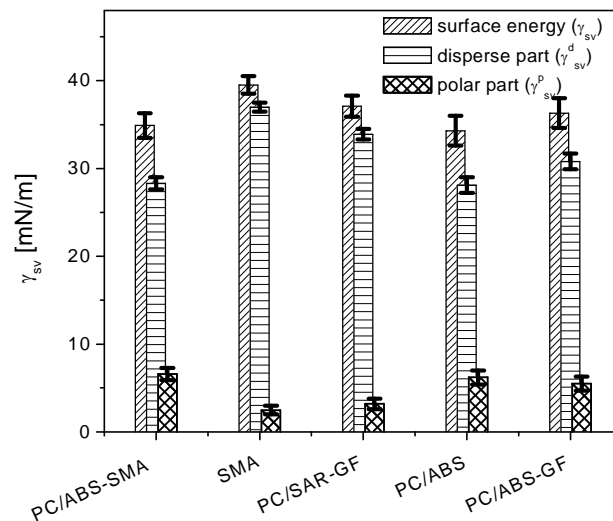


Figure 3.2.1: Surface tension [total (γ_{sv}), polar (γ_{sv}^p), and disperse part (γ_{sv}^d) of surface tension] data plot for five different TP materials.

SMA has the highest overall surface tension compared to the PC containing TP materials. The polar part of surface tension was lower for this sample compared to the other samples and this is assumed to be due to the low MA content (10 wt.-%) in MA-co-PS copolymer. The higher polar component of surface tension was observed for PC containing TP materials except PC/SAR-GF sample. Furthermore, among PC containing samples, the samples with glass fibers like PC/ABS-GF and PC/SAR-GF have higher overall surface tension. Another comparison among these samples can be made on the

basis of PC content in TP materials. The sample with high PC content (PC/ABS-GF) has higher surface tension compared to the sample (PC/ABS) with low PC content. Also the surface tension results on PC/ABS, PC/ABS-GF and SMA samples are quite similar to that obtained previously.⁹⁶

3.2.2. Behavior of samples from PU foam/TP material interface

The PU foam layer was removed from the TP material plates after climate treatment and the contact angle measurements were carried out on TP plate surface using a series of different solvents (see Experimental section for details). Figure 3.2.2 shows the surface tension data of four different TP material plates (PC/ABS-SMA, PC/ABS, PC/ABS-GF, and PC/SAR-GF). It can be seen from the Figure that all the TP materials have quite

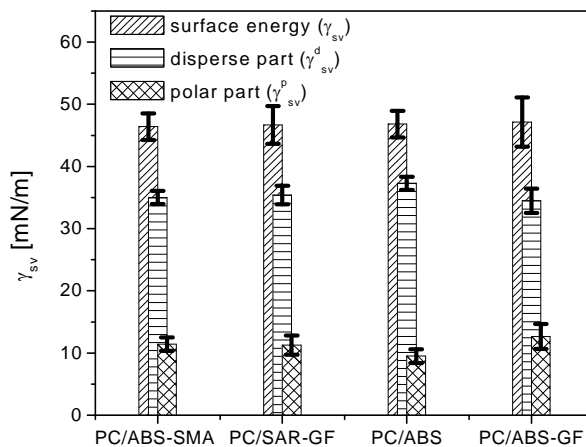


Figure 3.2.2: Surface tension [total (γ_{sv}), polar (γ_{sv}^p), and disperse part (γ_{sv}^d) of surface tension] data plot for four different TP materials separated from PU foam interface after climate treatment.

higher surface tension values compared to the neat plates. The total surface tension for all the samples was $\sim 46.00 \pm 1$ mN/m. Also the polar and disperse components of surface tension are quite similar for all the samples. Such type of change in surface tension of TP materials separated from PU foam interface after climate treatment is suspected due to the following reasons:

1. some part of foam material left on the surface,

2. the surface has become rough after removing from PU foam,
3. or some additives have deposited on the surface (e.g. catalyst),
4. water sorption during climate treatment.

In order to check the influence of these factors on surface tension, the PC/ABS-GF sample taken from PU foam interface was investigated in detail after complete washing procedure (see Experimental section) and the results are shown in Figure 3.2.3. The total surface tension of the sample was not affected with washing and drying, however, the polar and disperse parts were changed significantly. The disperse part was changed from 34.5 to 45.5 mN/m, while the polar part was decreased from 12.7 to 3.5 mN/m for PC/ABS-GF after washing and drying. It shows that the sorbed water during climate

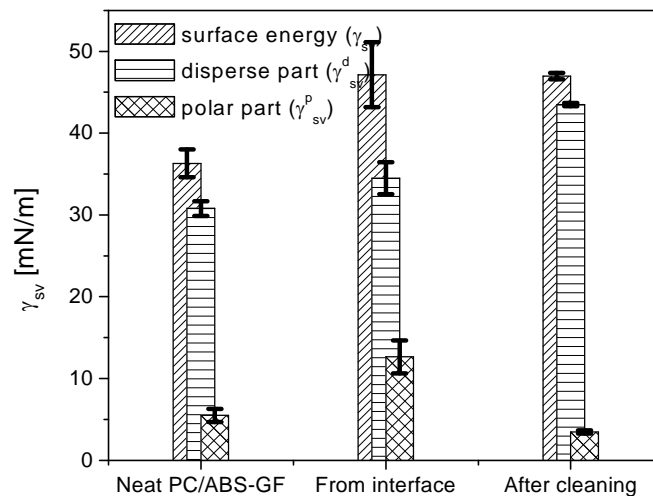


Figure 3.2.3: Surface tension [total (γ_{sv}), polar (γ_{sv}^p), and disperse parts (γ_{sv}^d) of surface tension] data plot for neat TP material (PC/ABS-GF), TP material separated from PU foam interface after climate treatment, and TP material after complete washing.

treatments has been removed after drying the sample. In any case the results for interface sample (PC/ABS-GF) are not similar to that of neat PC/ABS-GF surface. On the basis of these results it can be concluded that the foaming on TP material surface leads to change the surface properties and that can be related to the interfacial reaction.

3.2.3. Contact angle results of PU foam samples

The results obtained on foamed plates are presented in Figure 3.2.4. It can be seen from the Figure, the determined polar and disperse components of surface tension differ markedly for the three foam systems. The PU-b and PU-c foam systems have higher polar component than the PU-a. This means that these foam systems have high surface polarity. Among the three tested samples PU-c foam system has higher disperse parts as

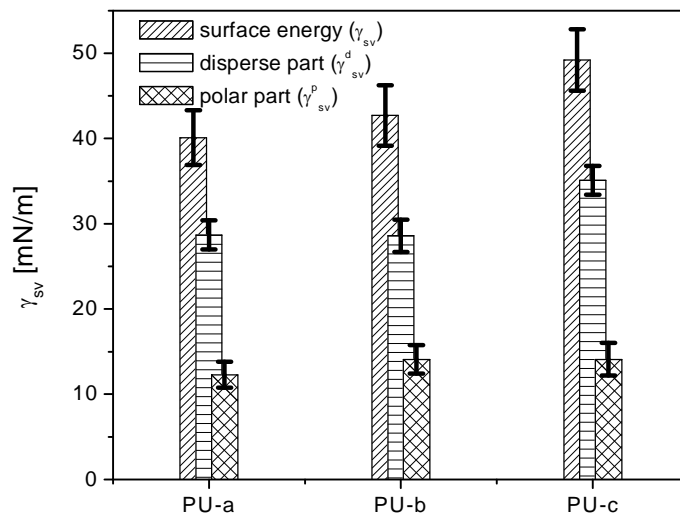


Figure 3.2.4: Surface tension [total (γ_{sv}), polar (γ_{sv}^p), and disperse parts (γ_{sv}^d) of surface tension] data plot for three different PU foam samples.

well as the total surface tension then the other two systems. The total surface tension for these three foam systems is in the order, i.e. PU-c>PU-b>PU-a. The difference in the surface tension values among these three samples may be a result of the differences in surface chemistry.

3.2.4. Contact angle hysteresis

The behavior of foam components (MDI, polyol) and water on TP materials was investigated by contact angle technique. The contact angle hysteresis was measured with water and liquid foam components on different TP materials. The surface tension of TP materials was calculated using Equation (3.2.1).^{97,98}

$$\gamma_{sl} = \gamma_{lv} (\cos \theta_r - \cos \theta_a) \frac{(1 + \cos \theta_a)^2}{(1 + \cos \theta_r)^2 - (1 + \cos \theta_a)^2} \quad (3.2.1)$$

in this Equation γ_{sl} is the solid liquid surface tension, γ_{lv} liquid vapour surface tension, θ_r and θ_a are receding and advancing contact angles respectively.

In order to carry out the contact angle hysteresis measurements it was necessary first to measure the surface tensions of liquid foam components. The Wilhelmy plate method was employed to measure the surface tension of liquid foam components at $20 \pm 0.5^\circ\text{C}$. Higher surface tension (47.6 mN/m) was measured for MDI in comparison to the polyols. The surface tension for polyols was approximately 35 mN/m.

The advancing and receding contact angles measured on different TP materials are given in the Appendix Tables (A1 to A5) for each TP material. The measured contact angles were dependent on the drop volume on substrate surface. SMA and PC/ABS-GF samples had shown water advancing contact angles in the range of $79^\circ \pm 3.5^\circ$ and $78^\circ \pm 4^\circ$, respectively with high degree of hysteresis. Whereas PC/ABS-SMA, PC/SAR-GF and PC/ABS samples produced the higher contact angles. The θ_a was higher in PC/SAR-GF compared to PC/ABS-GF and the possible reasons for high θ_a is due to the surface roughness of these two TP materials. The surface roughness contributes towards different contact angle values in the following ways:⁹⁹

1. when the contact angle is measured on a drop of water placed to the direction of glass fiber then it will advance on the surface (more wetting) and the resulting angle will be smaller.
2. if the contact angle is measured on a drop of water placed perpendicular to the glass fiber, it will pin the motion of drop (less wetting) and the reflected angle will be higher.

However, the advancing and receding contact angles were very low with liquid foam components in comparison to water on all TP materials. The observed θ_a was in the range of 30° to 45° on all TP materials with four different liquid foam components. The contact angle hysteresis was also relatively high as measured with water. Especially the hysteresis was high on PC/SAR-GF sample with all the foam components. In these experiments, our interest was to get information on wetting behavior of TP materials with

liquid foam components as expected. The high degree of wetting of TP materials may happen due to interaction of MDI and polyols with polar TP materials surface. There is a possibility that MDI can interact through isocyanate group whereas the polyol make some H-bonding with TP material surface.

The surface energies were calculated from the advancing and receding contact angles using equation 3.2.1. According to this equation, the solid surface tension must be less than the probe liquid surface tension if a definite contact angle is formed between solid and liquid. The results based on this calculation method have revealed the higher surface tension for all TP materials determined from MDI than that obtained from polyol contact angles (refers to appendix Table A-1.1 to A-1.5). The lower surface tension was calculated for all TP materials with water and polyol contact angles. In fact, there is no clear difference among the surface tension values obtained from three different polyol contact angles. Among the TP materials PC/ABS-GF has the higher surface tension calculated from the contact angles of all four liquids. The similar trend in surface tension was observed for SMA and PC/ABS-GF sample. The surface tension for PC/ABS-SMA, PC/SAR-GF and PC/ABS samples obtained from water and MDI contacts angle was quite low as compared to the PC/ABS-GF and SMA samples. This shows that water and MDI have more affinity towards PC/ABS-GF and SMA samples in comparison to the other TP materials.

3.2.5. Short summary of contact angle results

In all the tested samples, the higher surface tension (39.5 ± 1 mN/m) was found for neat SMA TP material as compared to the PC containing TP materials. The glass fiber containing TP materials have higher surface tension compared to the sample without glass fiber. The sample with high PC content (70 wt.-%), PC/ABS-GF has shown the higher surface tension (36.3 ± 1.7 mN/m) as compared to the sample (PC/ABS) having low PC content (60 wt.-%).

The surface tension of TP materials from PU foam (PU-a) interface after climate treatment has increased significantly as compared to the neat TP materials. After washing and drying the sample (PC/ABS-GF) the total surface tension remained unchanged but the polar part was decreased from 12.7 to 3.5 mN/m. The decrease in polar part of surface

tension can be related to the evaporation of sorbed water (during climate treatment) from TP material. The total surface tension remained unchanged and that could be due to the non-washable PU foam parts linked to TP material.

Among PU foam samples PU-c system has the highest and PU-a foam system has the lowest surface tension. The difference in surface tension of PU foam samples may be a result of chemistry related differences among the samples.

High degree of contact angle hysteresis was observed for water on all TP materials. The liquid foam components have shown the maximum wetting, which is obvious from their smaller contact angles on all TP materials. No direct correlation of surface roughness and contact angle hysteresis was observed in samples with glass fiber. The total surface tension obtained for TP materials from MDI and water contact angles was higher compared to polyols.

3.3. Microscopic studies

The aim of the work presented in this section is to investigate the PU foam/TP materials surface and interface topographic properties, with special emphasis on the adhesion at interface. In this study attempt is made to distinguish between two important aspects, the mechanism by which the two materials interact at molecular level and the deformations that occur in the materials interface after testing. These deformations on the interface are those that dissipate the energy supplied by the interfacial strength. A strong adhesion at interface will produce the defect or deformations and when the adhesion is weak the materials will separate without any defect on the surface and for more details, a schematic illustration of materials from interface is given in Figure 3.3.1.

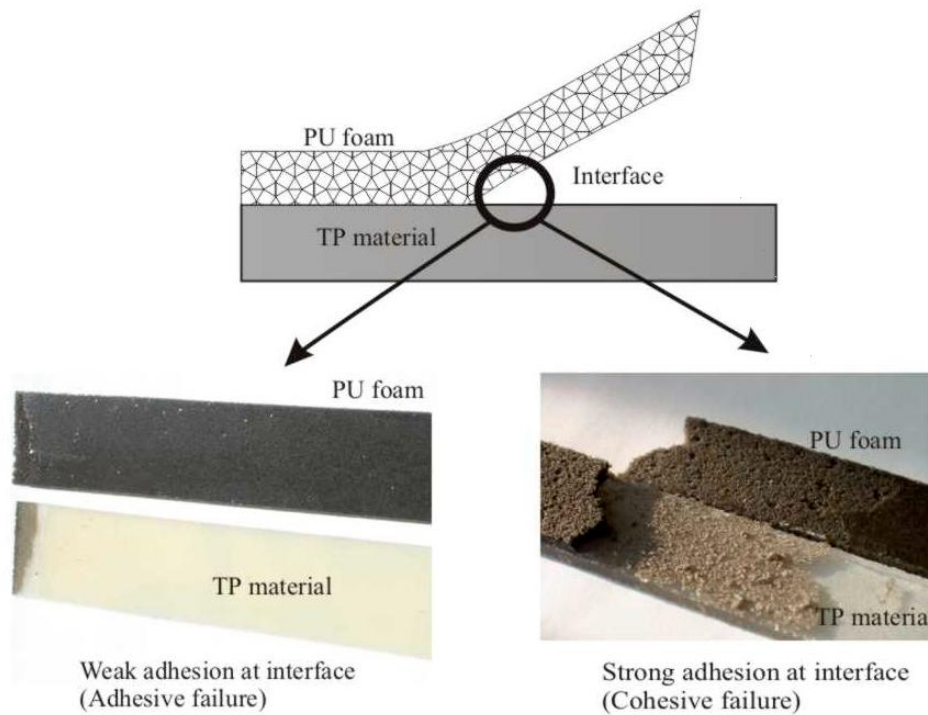


Figure 3.3.1: Schematic representation of PU foam/TP materials at the interface (top) and the pictures of the surfaces formed after separating the components (bottom). The plane surface of two materials represents weak adhesion at the interface (adhesive failure) and the strong adhesion at the interface (cohesive failure) shows a PU foam layer on the surface of materials from interface.

The foam material was separated from TP material interface in the same manner like presented in Figure 3.3.1. Regarding microscopic studies, the neat material and material from the interface after climate treatment were investigated using AFM and optical microscope techniques. For quantitative evaluation of interaction behavior at interface, the surface roughness of PC/ABS-SMA TP material was calculated from AFM height images.

3.3.1. Atomic force microscopy

In AFM height image of neat TP material (PC/ABS-SMA) some spherical structures of ~500 nm in diameter can be seen, (the spherical structures are actually the particles on the surface of TP material). Corresponding to the total composition, these particles might

have been formed by ABS or SMA phase. However, as these uniformly shaped spherical particles resemble the microstructure of classical rubber modified ABS grade,¹⁰⁰ these appear to belong mainly to the rubber phase of ABS. The amount of PC is 55 wt.-% of

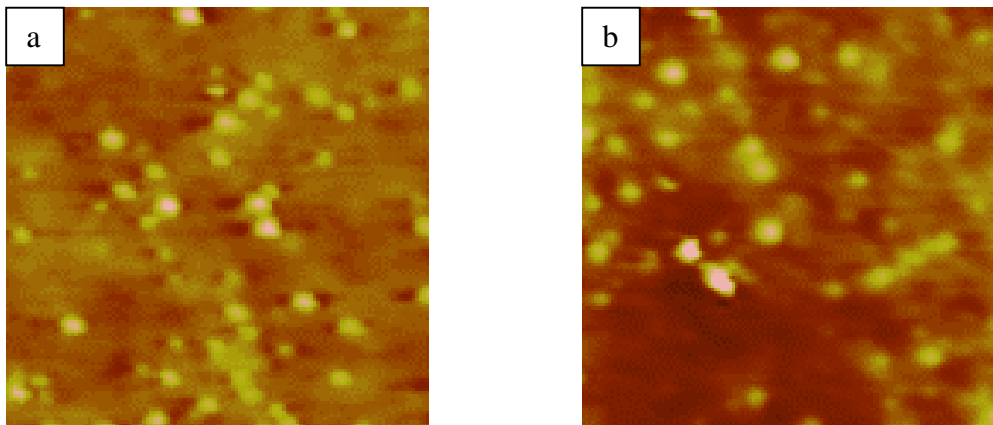


Figure 3.3.2: AFM height image of (a) neat PC/ABS-SMA TP material and (b) PC/ABS-SMA TP material from PU-b foam interface after climate treatment and “peel test”. The image size is $10 \times 10 \mu\text{m}$.

the total composition of TP material. But due to the surface property and polarity of PC component of TP material, the area occupied by PC (see background of Figure 3.3.2a) appears larger than that expected from the overall composition.

Some information on the interaction behavior between PU foam and TP material can be obtained by comparing Figure 3.3.2a and 3.3.2b. With respect to the size and distribution of the spherical particles, these two surfaces seem to be identical. However, the background of the sample surface in these images looks quite different. In Figure b, the ‘background’ has become significantly rougher indicating that there has been some interaction (chemical nature) between the foam materials and the TP material.

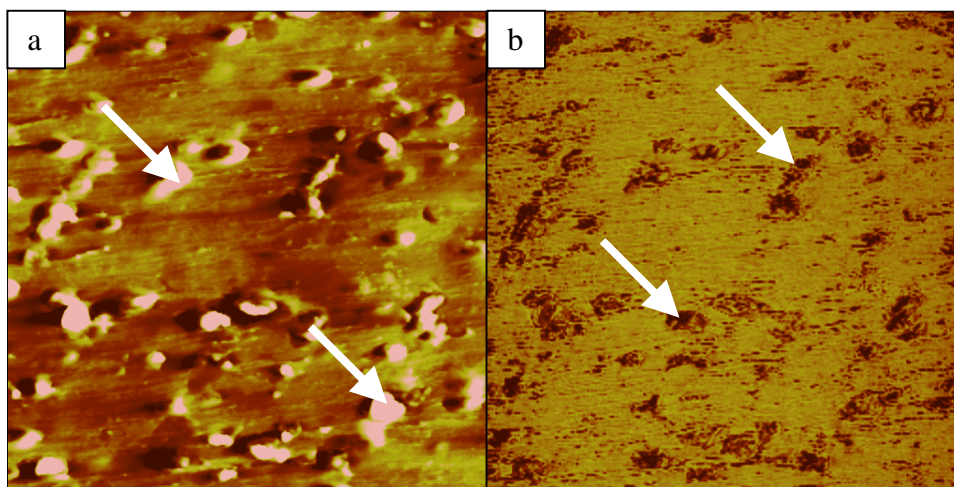


Figure 3.3.3: AFM height (a) and phase (b) images of PU-b foam after removing from PC/ABS-SMA TP material exactly after climate treatment and “peel test”. Arrows in Figure (a) show some deformations on PU foam surface caused during the separation process. The dark spots in Figure (b) are pointed out by arrows. The scan size in both the images is $20 \times 20 \mu\text{m}$.

Observing the foam side in Figure 3.3.3, one can clearly notice dark spots (indicated by arrows in Figure 3.3.3b) in the range of $\sim 500 \text{ nm}$, coming as ‘negative’ from the dispersed particles in TP material. But the separation of PU foam from TP material causes the deformation of PU foam surface, which leads to the formation of raised edges on PU foam surface (in height image pointed out by arrow). The formation of raised edges at foam surface can be related to the chemical interaction of PU foam with TP materials. Kieffer et al.^{101,102} have also observed a similar behavior on interfacial reaction of polyurethanes with hydroxyl groups on cured epoxy. It is also possible that during curing process, the specific groups (unreacted isocyanate groups) from PU foam mixture migrate to the interface region and later they form chemical linkages to the active hydrogen containing groups (e.g. hydroxyl group) on TP material surface.¹⁰³⁻¹⁰⁶

The AFM height image for PC/ABS-SMA TP material obtained after removing from PU-a foam system (foam with good adhesion) is displayed in Figure 3.3.4b. In this image the interaction behavior of PU foam with TP material is more clearly visible compared to previous discussed sample. The areas indicated by arrows in Figure 3.3.4b clearly show that some foam parts (~ 0.5 to $0.25 \mu\text{m}$) are left on TP material surface. The

appearance of particles on TP material from PU foam interface is quite different (become rough) than the neat material (Figure 3.3.4a). So it indicates that the foam system with better adhesion also adhere to the particles on TP material surface.

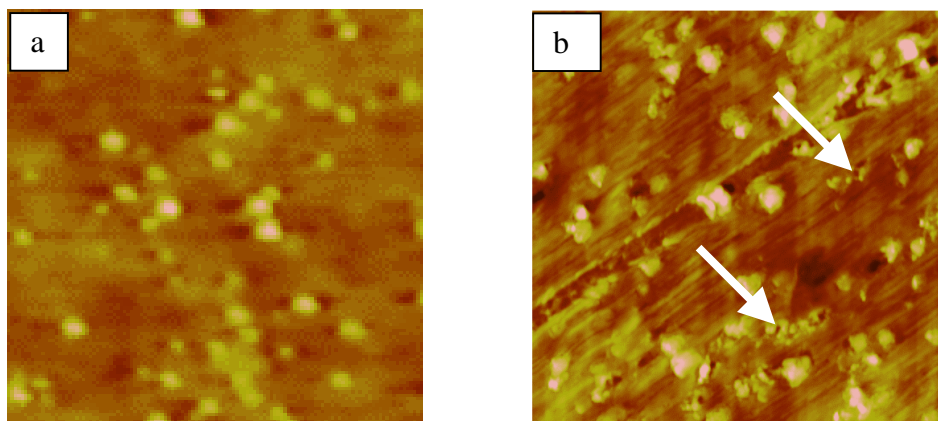


Figure 3.3.4: AFM height images (a) neat PC/ABS-SMA TP material, and (b) PC/ABS-SMA TP material from PU-a foam interface after climate treatment and “peel test”. The PU foam related parts are indicated by arrows in Figure (b). The scan size in both the micrographs is $10 \times 10 \mu\text{m}$.

Additional information on the interaction behavior between PU foam and TP materials can be obtained by quantitatively analyzing the surface roughness of the neat TP material and TP material from interface. The surface roughness of neat PC/ABS-SMA TP material, and the PC/ABS-SMA TP materials from PU foam/TP material interface was calculated from AFM height images by placing a diagonal line in the images and the corresponding section analysis plot for each material are depicted in Figure 3.3.5. It was found that the root mean square (RMS) roughness of neat PC/ABS-SMA TP material was changed from 7.5 to 23.0 nm after removing from PU-b foam surface. Whereas the roughness for the same TP material from PU-a foam system interface is relatively high (28.4 nm) compared to TP material from PU-b foam system. The increase in surface roughness of TP material from PU foam interface is a clear indication of interfacial reaction.^{107,108} Dillingham et al.¹⁰⁹ have studied the adhesion of isocyanate based polymers to steel where they found that the origin of excellent adhesion of polymers to

steel is due to the formation of oxide-cyanate esters (analogous to urethane). So the increase in surface roughness of TP material from PU foam interface is due to the chemical reaction of isocyanate with active hydrogen containing groups such as hydroxyl groups.

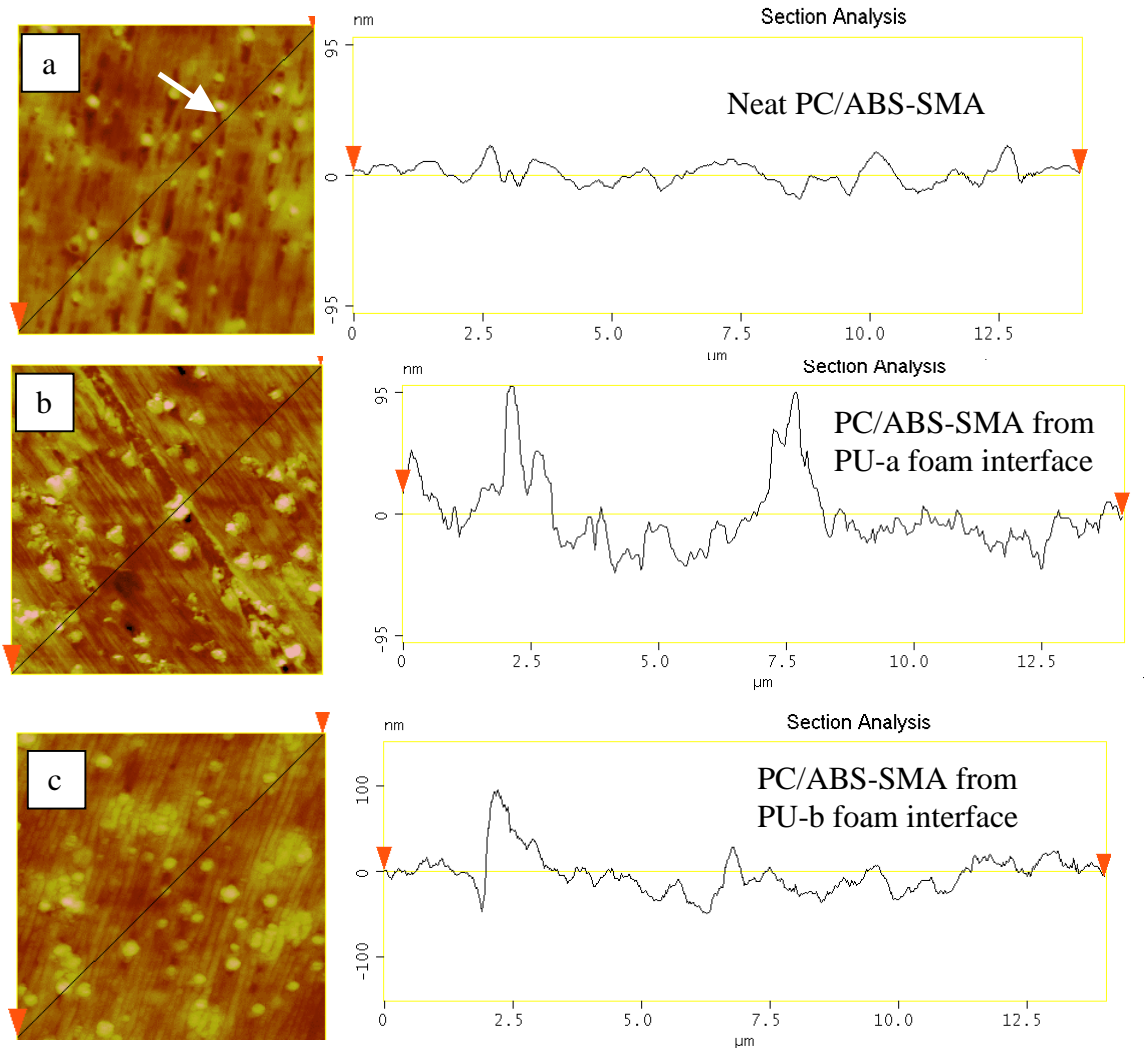


Figure 3.3.5: Cross sectional line profiles of the AFM height images for: (a) neat PC/ABS-SMA, (b) PC/ABS-SMA TP material separated from PU-a and (c) from PU-b foam interface, after climate treatment and “peel test”.

Also the line profile of neat PC/ABS-SMA totally differs for the same sample from PU foam interface. The background in the image of neat PC/ABS-SMA TP material

(Figure 3.3.5a) is quite smooth as compared to the samples from interface (Figure 3.3.5b and 3.3.5c). The roughness of background matrix is also quite high in TP material from PU-a foam interface, as it is clear from section analysis. The particles on the surface of TP material have maximum height in the range of 50-100 nm. The change in the shape of particles is also observable from the line profile, as it is indicative in TP material from PU-a interface (Figure 3.3.5b). All these observations clearly demonstrate the change in surface of TP material from interface is due to the interfacial reaction of TP material with PU foam.

3.3.2. Optical microscopy

In order to understand the interaction behavior at the interface, it was attempted to image the PU foam layer separated from TP materials (after climate treatment) with light microscope. The scanned area (100 μm) from PU foam surface indicates that some spots have appeared on PU foam surface after separating from TP interface (see Figure 3.3.6a). The higher number of such type of spots was observed in case of PU foam sample separated from SMA plate (see to Figure 3.3.6a). These spots on PU foam surface appear after separating from TP material are due to the “collapse of PU foam thinnest parts”. The collapse of PU foam is due to the chemical/physical interactions at the interface.¹¹⁰

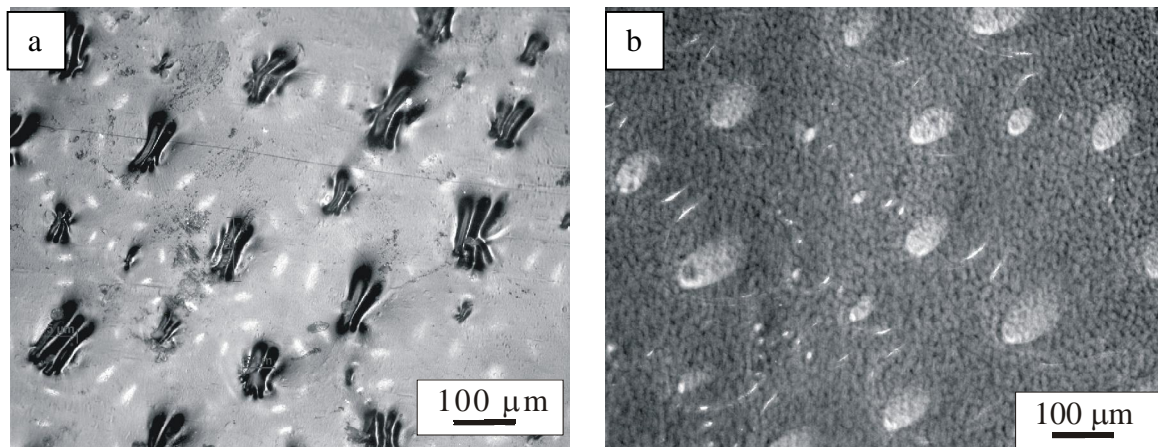


Figure 3.3.6: Optical microscope images acquired from PU foam surface after climate treatment and “peel test”. (a) after separating from SMA TP material, (b) PU foam from PC/ABS surface.

From chemistry point of view, there are different possible ways of interactions at PU foam TP materials interface but following are the significant:

1. chemical reaction of MA with unreacted isocyanate, (product of this reaction is an imide linkage).
2. esterification of MA with –OH groups from reacting PU foam mixture,¹¹¹
3. reaction of MDI with active hydrogen containing functional groups, i.e. hydroxyl group from polycarbonate, (product of this reaction is urethane linkage),
4. hydrogen bonding at the interface and other secondary interaction forces.

Although the possibility of all interactions at interface as mentioned above is likely but the effect of climate treatments is totally different on them. The ester and amide bonds are strongly affected (hydrolysis) by high humidity and temperature conditions.¹¹² But the imide bond is not sensitive towards hydrolysis in an environment with high humidity and temperature conditions.¹¹¹ Therefore, it can be assumed that in case of SMA TP material the interface region is mainly occupied by imide linkages. The increased adhesion of PU foam with SMA TP material is also related to the interface reaction.¹¹³

In case of PC containing samples, the interfacial adhesion between PU foam and TP materials was badly influenced by climate treatment and there were no deformations on PU foam surface after peeling, as observed in previous discussed sample (Figure 3.3.6b). On the basis of this observation it is clear that in case of PC containing samples the interface is mainly kept together by the interaction, which are very sensitive to the climatic conditions with high humidity.

3.3.3. Short summary of microscopic results

The interface between PU foam was studied using AFM and light microscopic techniques. For quantitative evaluation of interaction behavior of TP material at interface the surface roughness was measured from AFM height images. The AFM images have provided a direct evidence of the chemical interaction of some TP material part with PU foam material. As a result of chemical linkage, the PU foam parts (0.5 μm size) were left on TP material surface after climate treatment and peel test measurements. The change in surface roughness of TP material from interface is also related to the interfacial reaction.

In optical light microscopic images, the observed defects on PU foam surface are directly linked to interface behavior of PU foam with TP materials. The highest number of defects was observed on PU foam sample from SMA interface. These defects are related to the interfacial strength of PU foam with TP material. As PU foam from SMA surface has highest number of defects and also it has best adhesion compared to the PC containing TP materials.

3.4. ToF-SIMS and XPS studies

When polymeric materials of different properties are joined together, a variety of interactions can occur at the interface.¹¹⁴ The structure and composition of surface functional groups can play an important role in determining how these interactions proceed. Analysis of the relative surface and interface composition of materials from interface is very important for predicting the durability of bonded joints. Thus, in order to gain a greater understanding of the interaction behavior at interface, a detailed characterization of materials is necessary. XPS has been used to investigate the surface chemical composition, and other properties of polymer blends and copolymers.¹¹⁵⁻¹¹⁷ ToF-SIMS has gained importance over the last decade in the characterization of polymer surfaces due to its high molecular specificity, extreme surface sensitivity, high mass resolution and its ability to provide detailed information on the surface molecular structures.¹¹⁸⁻¹²⁰

The results discussed in this section are mainly related to the study of chemical composition of neat TP material plates (before foaming process) and samples from PU foam/TP material plate interface after climate treatment, by employing ToF-SIMS and XPS techniques.

3.4.1. Time of flight secondary ion mass spectrometry

The ToF-SIMS spectrum of neat PC/ABS-SMA TP material is shown in Figure 3.4.1 and the proposed fragmentation pattern for PC is given in scheme 3.4.1. By considering the total composition of TP materials (blends), it was assumed that the surface is mainly composed of PC and therefore the measured ToF-SIMS data were interpreted through assigning the peaks to PC fragments. The mass scale was calibrated by using the ~211

mass peak of PC. In order to correlate the spectra of TP material from interface, the intensity was normalized to the same PC fragment at $m/z \sim 211$. The negative ion spectrum of neat PC/ABS-SMA (Figure 3.4.1) can be characterized by a series of PC fragment ion peaks at $m/z = 93$ ($C_6H_5O^-$), 117 ($C_8H_5O^-$), 133 ($C_9H_9O^-$), 211 ($C_{14}H_{11}O_2^-$), 227 ($C_{15}H_{15}O_2^-$), 255 ($C_{15}H_{11}O_4^-$). While peaks at $m/z = 75$ ($CH_3SiO_2^-$), 149 ($C_3H_9Si_2O_3^-$), indicates the presence of some surface impurity like silicone oil at TP material surface. In the spectrum some peaks were also in the doublet form (as shown in the Figure 3.4.2), which can only be assigned to the unstable fragments, changing their structure on flight and these double peaks were not observable in neat TP and PU foam samples.

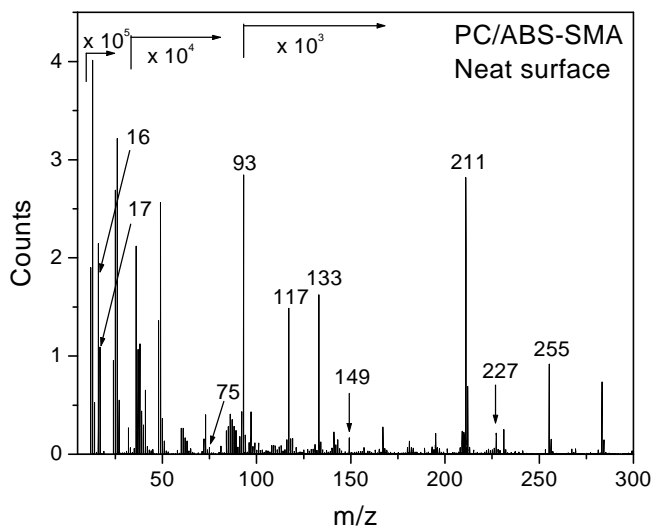


Figure 3.4.1: ToF-SIMS negative ion spectra for neat PC/ABS-SMA sample in the range of 5-300 a.m.u. The PC related mass numbers are labeled in the Figure.

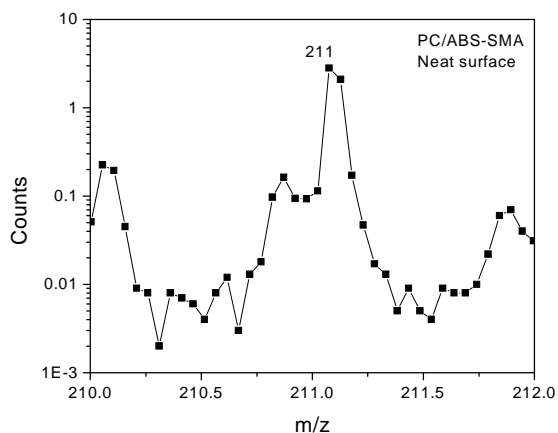
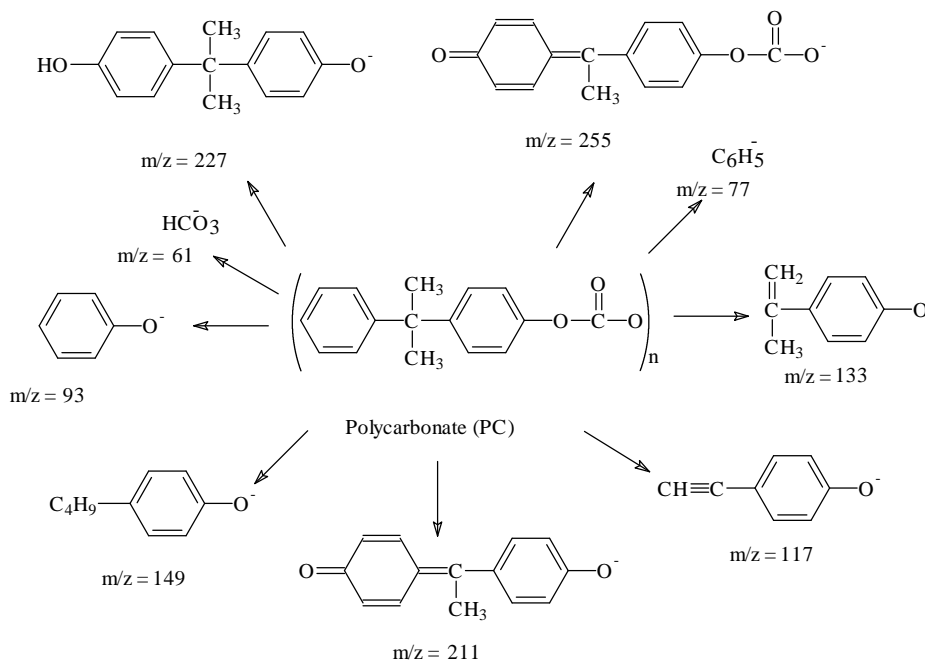


Figure 3.4.2: ToF-SIMS negative ion spectra for neat PC/ABS-SMA sample for one of the doublet peak at m/z 211.



Scheme 3.4.1: Proposed fragment structures for some of the characteristic ions in the negative ion spectra of bis-phenol A based polycarbonate.¹²¹

The negative ion ToF-SIMS spectra for PC/ABS-SMA TP material acquired from PU-foam interface after climate treatment is shown in Figure 3.4.3. The spectra of this sample greatly differ from the spectra of neat PC/ABS-SMA and the significant differences can be distinguished in the spectra of these two samples:

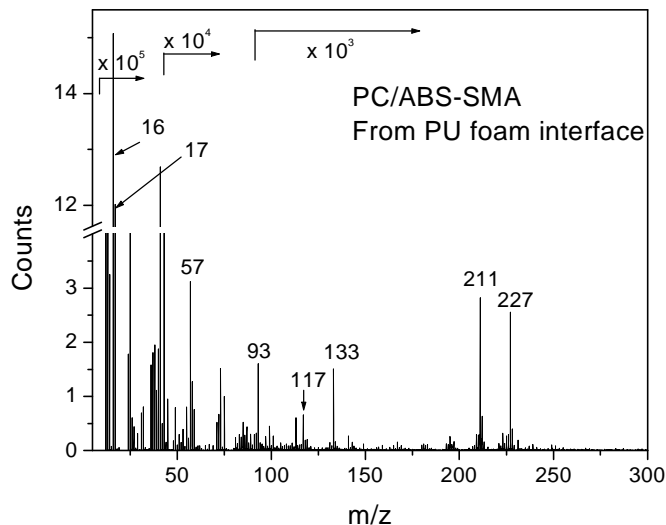


Figure 3.4.3: ToF-SIMS negative ion spectra for PC/ABS-SMA TP material from PU foam interface after climate treatment.

1. An increase in peak intensity in spectrum of PC/ABS-SMA TP material from PU foam interface for m/z 16 (O^-), 17 (OH^-) fragment ions, which indicates the surface enrichment with oxygen containing parts. It is also possible that the low surface tension component¹²² (i.e. polyether polyol in our case) from reacting foam mixture migrates to the interfacial region and forms a very thin layer. Therefore, it can be assumed that the observed high intensity for m/z 16 and 17 mass ions is due to a very thin layer of polyol component on TP material surface from PU foam interface.
2. The peak at m/z 149 is strongly reduced in PC/ABS-SMA TP material after removing from PU foam surface, an indication that the silicone oil impurities are removed from TP material.
3. The additional fragments in the spectra of PC/ABS-SMA TP material from PU foam interface at m/z 55, 56, and 57 ($C_2H_3NO^-$), are due to PU foam structures linked to the TP material surface.

Hence from the ToF-SIMS spectral data of PC/ABS-SMA from interface it can be concluded that there are some surface changes occurred on TP material surface after removing from PU foam and these changes are related to interfacial reaction of hydroxyl groups and MA from TP material with unreacted isocyanate.

The ToF-SIMS spectrum for PU foam sample from interface is depicted in Figure 3.4.4

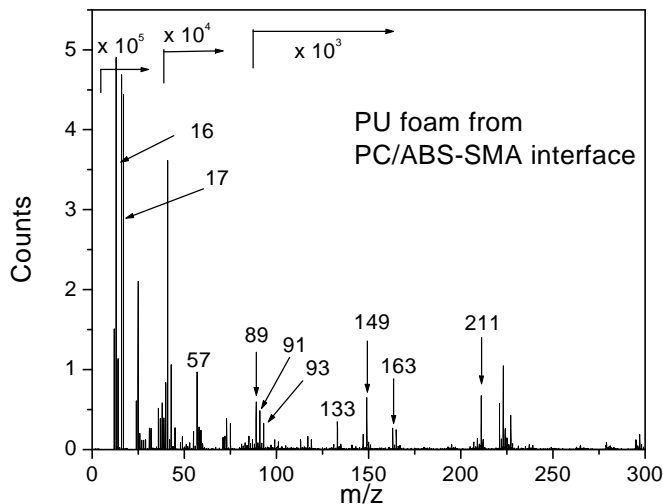
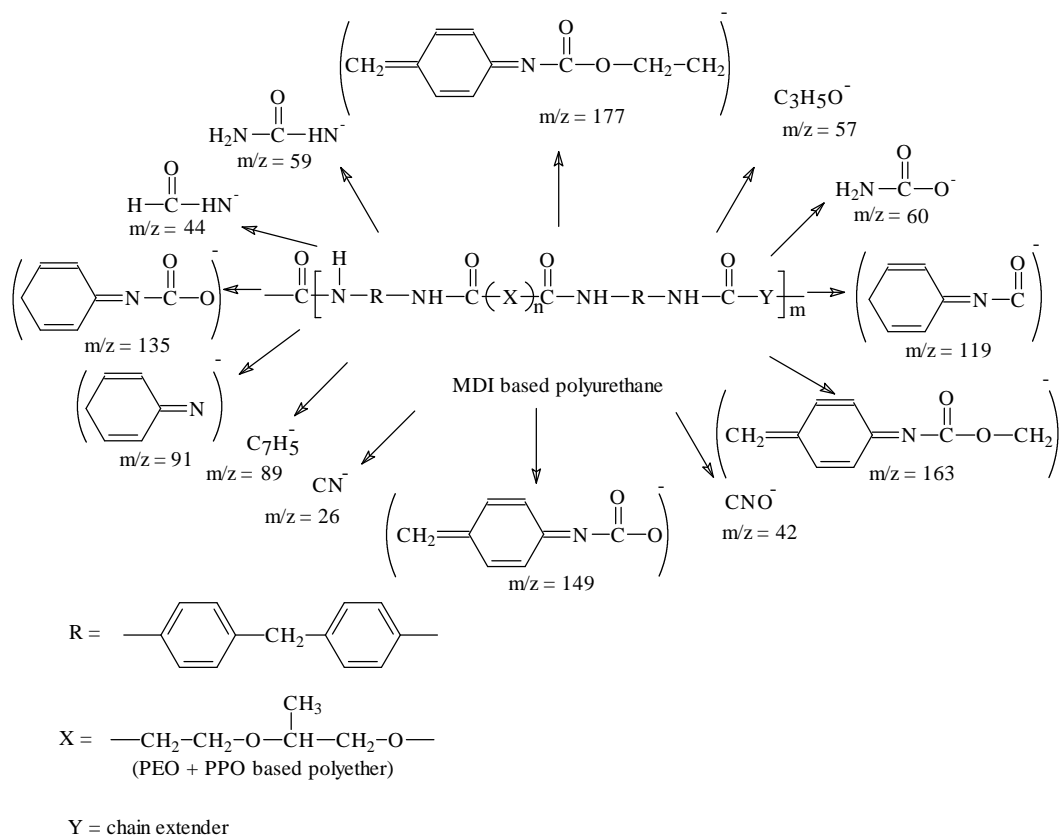


Figure 3.4.4: ToF-SIMS negative ion spectra for PU foam sample from PC/ABS-SMA interface after climate treatment.

and proposed fragmentation pattern is shown in scheme 3.4.2. The PU foam spectrum was interpreted by a series of fragment ions like $m/z = 26$ (CN^-), 42 (CNO^-), 57 ($\text{C}_3\text{H}_5\text{O}^-$), 59 ($\text{CH}_3\text{N}_2\text{O}^-$), 60 (CH_2NO_2^-), 77 (C_6H_5^-), 89 (C_7H_5^-), 91 ($\text{C}_6\text{H}_5\text{N}^-$), 92 ($\text{C}_6\text{H}_6\text{N}^-$), 119 ($\text{C}_7\text{H}_5\text{NO}^-$), 133 ($\text{C}_9\text{H}_9\text{NO}^-$), 135 ($\text{C}_7\text{H}_5\text{NO}_2^-$), 163 ($\text{C}_9\text{H}_9\text{NO}_2^-$), and 177 ($\text{C}_{10}\text{H}_{11}\text{NO}_2^-$). The 93, and 211 mass ion fragments are highly indicative about some PC related structure linked with PU foam. As in case of PU foam spectrum almost every fragment has nitrogen atom, so it can be concluded that the PU foam at interface is mainly composed of structures that contain nitrogen, i.e. urethane and urea hard segments.



Scheme 3.4.2: Proposed fragment structures for some of the characteristic ions in the negative ion spectra of MDI based polyurethane foam.

3.4.2. X-ray photoelectron spectroscopy

The surface chemical composition of neat PC/ABS-SMA TP material, PC/ABS-SMA TP material from foam surface after climate treatment and corresponding foam surface, was determined by XPS technique. The XPS results for all the samples show the presence of four elements: carbon, oxygen, nitrogen and silicone. The atomic % data for investigated samples are given in Figure 3.4.5. The detection of silicone indicates the presence of some surface contaminations like silicone oil, as discussed in ToF-SIMS results. In case of TP material from foam surface, no silicone was found and the same amount of silicone was present on foam surface separated from same TP material. It means that after skinning the PU foam from TP material the silicone oil impurities are removed. The atomic % of carbon and nitrogen are also decreased after separation from PU foam

interface, while there was an increase of oxygen content. The elemental content for oxygen and carbon atoms for TP material from PU foam interface looks nearly the same like PU foam sample.

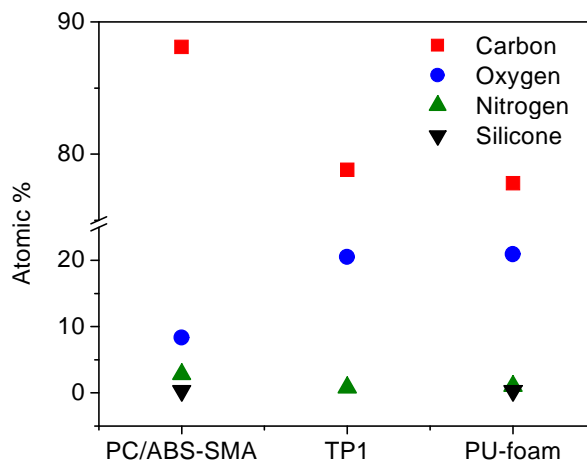


Figure 3.4.5: The elemental content from neat PC/ABS-SMA TP material, PC/ABS-SMA TP material from PU foam surface (TP1) and PU foam from PC/ABS-SMA TP material surface after climate treatment.

The results for the C 1s spectra were resolved into three peaks and the respective data for fitting are given in Figure 3.4.6. The peak resolution gave three peaks, at 284.6, 286.2 and 290.6 eV in case of neat PC/ABS-SMA, which can be assigned to like that of carbon-carbon bond, carbon linked to oxygen by single bond and carbonyl carbon respectively. Nearly at the same binding energies three peaks are present in case of TP sample from PU foam interface (Figure 3.4.6b) but the peak areas are quite different from the neat sample and it looks similar to PU foam sample (Figure 3.4.6c). The same spectral pattern for O 1s (spectra are not shown here) peak was found like the C 1s peak for the three investigated samples. From this spectral comparison it seems that some PU foam parts are remaining at TP material surface after separating from interface and the similar results were obtained from AFM measurements (section 3.3.1), where some foam particles were detected on TP material surface from interface.

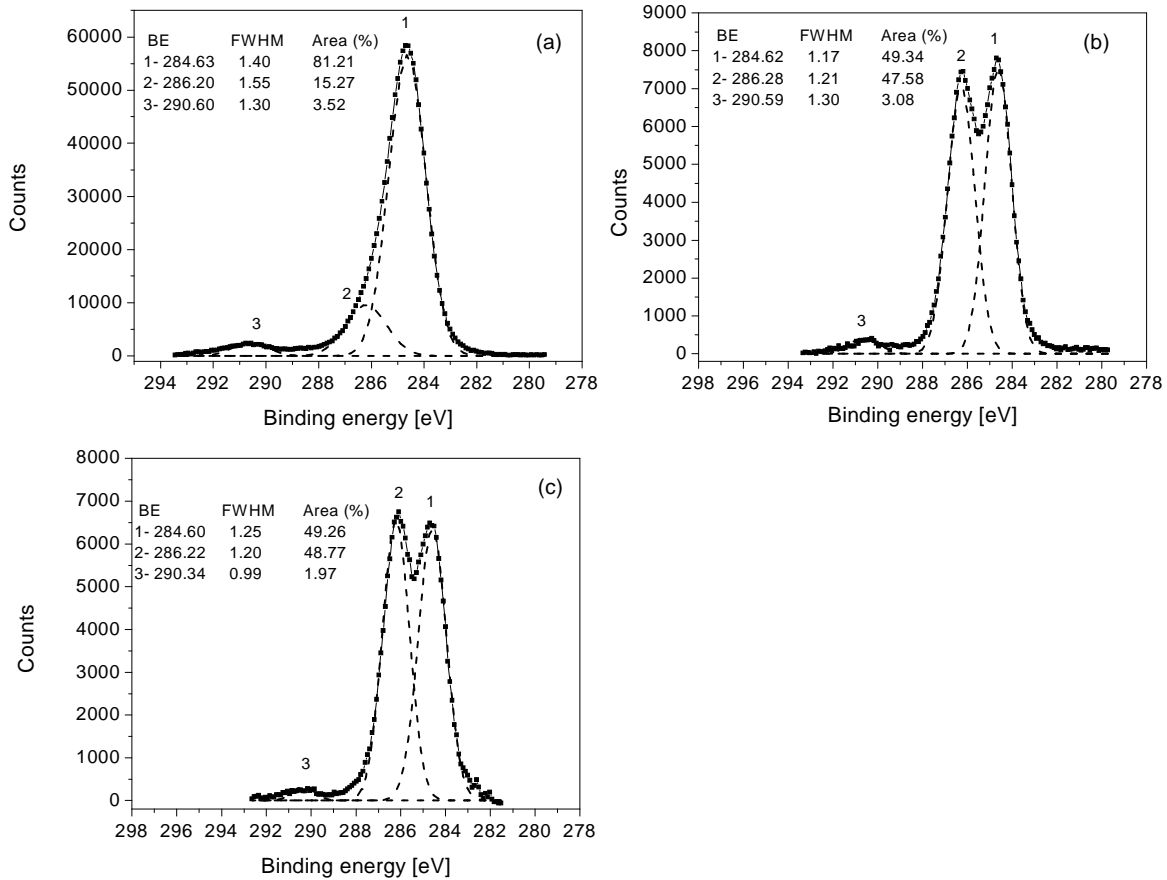


Figure 3.4.6: C1s comparison plots for: (a) neat PC/ABS-SMA, (b) PC/ABS-SMA from PU foam surface and (c) PU foam from PC/ABS-SMA surface after climate treatment. The peaks labeled 1, 2 and 3 in Figure correspond to carbon atom in C-C, C-O, and C=O groups respectively.

3.4.3. Short summary of ToF-SIMS and XPS results

The XPS and ToF-SIMS results indicate the presence of silicone oil at the TP material surface, which has effect on end use of TP material. The silicone oil impurities on TP material surface are remaining mainly on the foam surface after foaming and taking off the PU foam.

In ToF-SIMS spectrum of TP material from PU foam interface the intensities of O⁻ and OH⁻ fragment ions were strongly increased, indicating a surface modification. Also from XPS results an increase in oxygen content was observed for TP material from PU foam interface. The fragment ions at m/z 55, 56, and 57 in the spectrum of TP

material from PU foam interface have confirmed the presence of PU foam related structures on TP material surface. Furthermore, the mass ion peaks at m/z 93 and 211 in PU foam spectrum were assigned to the PC fragments. On the basis of ToF-SIMS and XPS results it can be assumed that the PU foam has an interfacial reaction with TP material.

3.5. Structure analysis in polyurethane foams at the interface

The sequence of foaming reaction has been studied by a number of investigators using FTIR spectroscopy.^{123-125,60} PU foams are prepared by the reaction of isocyanate with polyol in the presence of a blowing agent (water as indirect blowing agent), a surfactant, catalyst, etc. The reactive processing of PU foam formation from liquid monomers and oligomers involves a complex combination of both chemical and physical events. In less than 10 min, a liquid mixture of relatively low molar mass is transformed into the macromolecular architecture of solid foam. Information regarding both the reaction mechanism and structure development during reactive processing is essential, such that an objective description of the effect of individual component of reaction mixture on steps taking place and ultimately selective control of the process can be achieved.

Due to complex nature of PU foam structure and morphology development, the use of model systems has been very important for the study of the different aspects of PU foams especially at interfaces. The reactivity and concentration of the reactants in PU foam formulation has strong influence on the development of PU foam morphology. Many authors have employed FTIR spectroscopy in order to investigate both the reaction kinetics and the morphology development during the foaming process.^{126,127} The phase separation of polyurea segments can be monitored through hydrogen bonding studies during PU foam reaction process.¹²⁸ By using FTIR spectroscopy, Rossmly et al. have shown that in initial stages of reaction process, the formed urea hard segments stay in solution but at certain level of reaction they separate as second phase due to their concentration and molar mass development.^{129,130} Kim et al. showed by X-ray scattering on interface between rigid PU foam and zinc phosphated steel some crystallite structures and they found that these crystallites contribute to the interfacial strength.¹³¹ The same authors also claimed that the number of these crystalline structures is much more

important than their size.¹³² Other authors believe that the hard segments contribute to the hydrogen bonding/chemical bonding at interface depending on the nature of the substrate material.^{133,134}

In this section the results on the reaction studies of PU foams and the structure analysis in compact PU films at TP material plate interface in three different PU foam systems are presented. The FTIR-ATR technique was used to study the reaction process and morphology development in PU foam systems. SAXS, NR, and TEM techniques were employed for the structure analysis. At the interface between PU foam and TP material a $110 \pm 30 \mu\text{m}$ thick compact PU film was formed (see Figure 3.5.1). Investigating the inner structure of this PU film, a layered morphology parallel to the surface with a typical thickness between 260 and 400 nm for each layer was found.

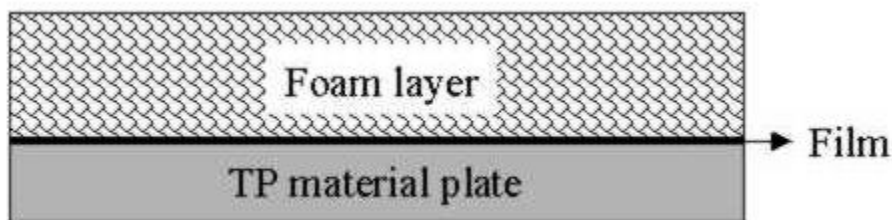


Figure 3.5.1: A schematic representation of PU foam layer on TP material surface.

3.5.1. FTIR spectroscopy

Representative infrared (IR) spectra for the reaction process of the isocyanate part of MDI with polyether polyols and water are shown in Figure 3.5.2. This region is useful to study the reaction process, as the band at 2265 cm^{-1} includes the isocyanate asymmetric stretching vibrations. The decrease in the intensity of this band was used to monitor the conversion of isocyanate functional group as a function of reaction process with polyol and water in three different PU foam systems.

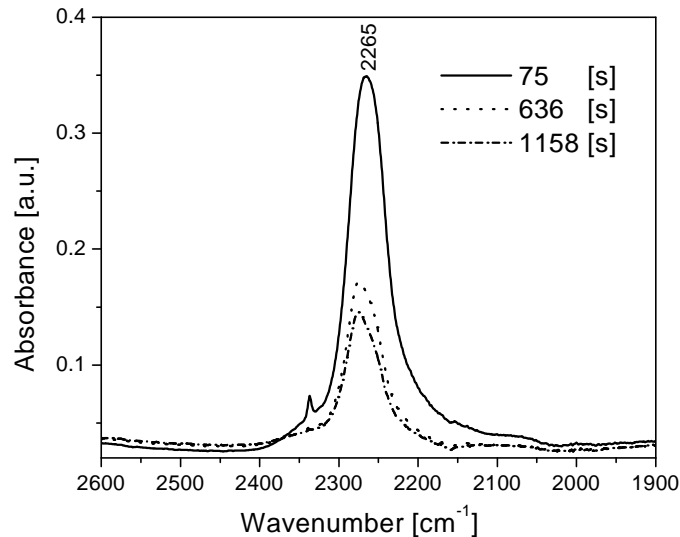


Figure 3.5.2: FTIR-ATR spectra of isocyanate absorption band (2265 cm^{-1}) during the reaction process with polyol and water in h-PU-a foam system at 40°C taken at different times after mixing the components.

The first measurement after the reaction mixture was placed on ATR cell shows for the integrated area of the 2265 cm^{-1} peak the highest value, which decreases continuously with time. Representative results on h-PU-a foam system at 40°C are shown in Figure 3.5.3. The curve depicted in Figure 3.5.3 can be fitted by bi-exponential decay functions (Equation 3.5.1) and the obtained parameters are given in Table 3.5.1.

$$y = y_0 + A_1 e^{-t/t_1} + A_2 e^{-t/t_2} \quad (3.5.1)$$

In this equation, y is the measured peak area at time t , with constant background y_0 , and decay times t_1 and t_2 .

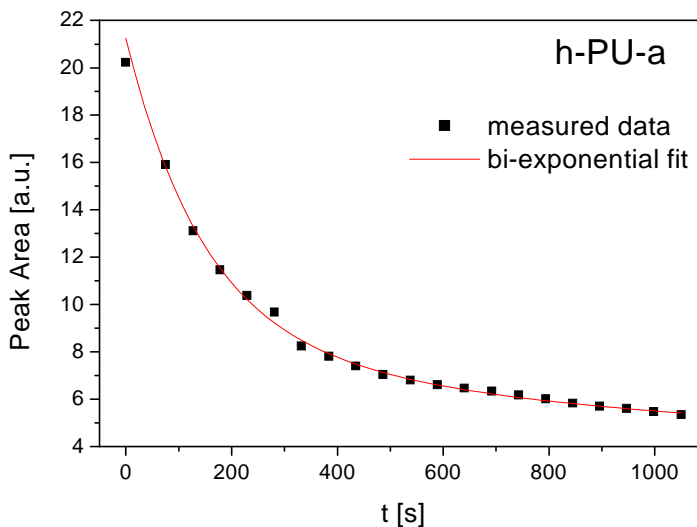


Figure 3.5.3: Integrated peak area of isocyanate absorption band (2265 cm^{-1}) as a function of time. The data are fitted to a bi-exponential decay function.

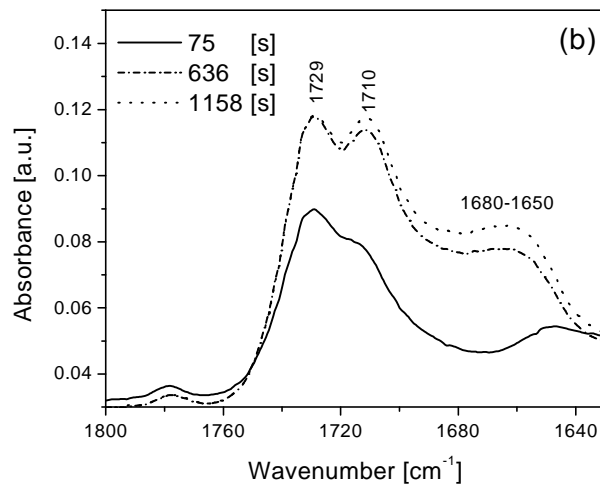
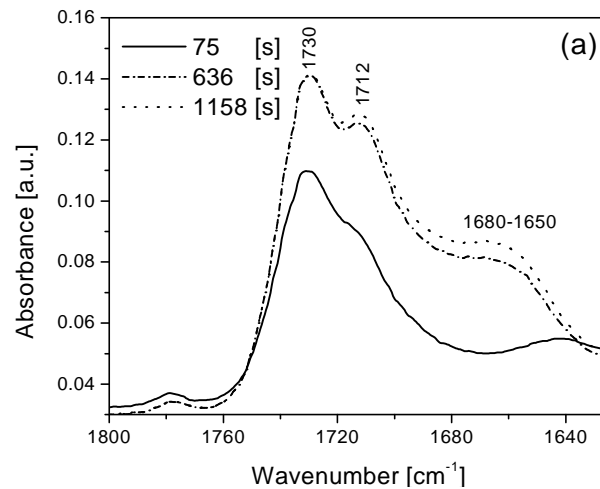
Table 3.5.1: Reaction times obtained by fitting a bi-exponential decay function to the peak area of isocyanate absorption band (2265 cm^{-1}).

Reaction time [s]	Foam Systems		
	h-PU-a	h-PU-b	h-PU-c
t_1	146 ± 10	73 ± 7	72 ± 7
t_2	850 ± 100	600 ± 70	350 ± 40

The observed time scales indicate that the isocyanate in the reaction mixture is following two different reaction kinetics, i.e. reacting with two different species. Accordingly, the t_1 and t_2 are representing a fast and slow reaction of the isocyanate, respectively. Rossmly et al.¹²⁹ reported that the water is more reactive in the PU foam formulation than the polyether polyol and aromatic amines. Therefore, t_1 should correspond to the reaction of isocyanate with water, and t_2 to the reaction of isocyanate with polyols.

The three foam formulations do not differ only in water content, but also in the additives. These additives strongly influence the isocyanate conversion. The three foam formulations can be described as slow, intermediate, and fast foams. These observed differences in the three foam systems are in well order according to the chosen additives. Finally, formulation PU-c shows the fastest reaction with water and polyol, whereas PU-a is the slowest.

Figure 3.5.4 demonstrates the influence of formulation differences and reaction rate on structure/morphology development. Observing the time dependence of the absorption bands between 1730 and 1630 cm^{-1} , the formation of urethane, hydrogen bonded urethane and urea, non bonded urea can be followed. Due to Elwell et al.¹³⁵ the non hydrogen bonded urethane (1730 cm^{-1}) and non bonded urea (1715 cm^{-1}) evolve at



Continued

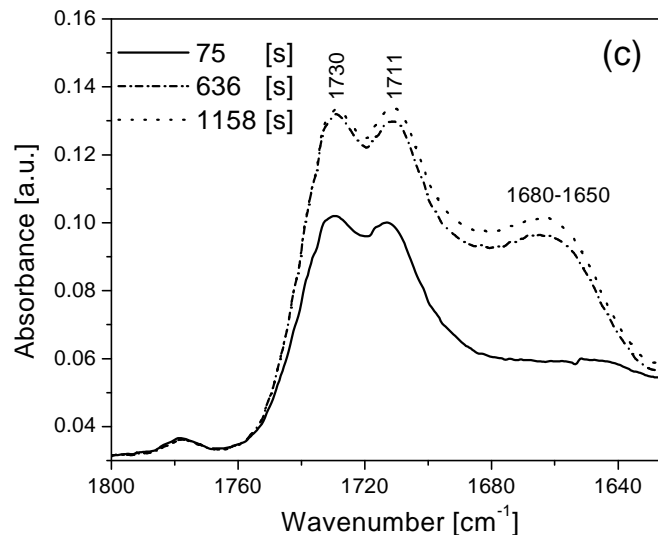


Figure 3.5.4: FTIR-ATR spectra in the carbonyl region at different times during the reaction process of isocyanate with polyol and water in three different PU foam systems at 40°C: (a) h-PU-a; (b) h-PU-b, and (c) h-PU-c. The absorbance bands associated with urethane (1730 cm^{-1}), soluble urea and hydrogen-bonded urethane ($1700 - 1715\text{ cm}^{-1}$) and hydrogen bonded urea ($1650 - 1680\text{ cm}^{-1}$) groups are labeled on respective absorption band.¹³⁶

early stage in the reaction. The bonded structures correspond to those structures that are microphase and macrophase separated aggregate structures and their formation usually takes place through hydrogen bonding process. Whereas the non bonded structures are those which are not in the form of aggregate structures.^{137,138} The IR bands related to the urethane and soluble urea (1730 and 1715 cm^{-1}) can be seen clearly in Figure 3.5.4, but the slowest foam with less amount of water (h-PU-a, Figure 3.5.4a) has weak urea signal at 1715 cm^{-1} . Foam h-PU-b (Figure 3.5.4b) with faster urea forming process has an increased urea signal whereas foam h-PU-c (Figure 3.5.4c) with highest amount of water has also the most intense urea signal. It is also apparent from Figure 3.5.4 that there is an induction time prior to the formation of hydrogen bonded urea, i.e. microphase separation of urea hard segments occurs in all the investigated foam systems (indicated by $1650 - 1680\text{ cm}^{-1}$ band). The intensity of broad band linked with hydrogen bonded urea ($1650 - 1680\text{ cm}^{-1}$) in each foam system is also related to extent of phase separation.¹³⁵

3.5.2. Small angle X-ray scattering

The SAXS measurements were carried out to study the hard segment distances¹³⁹⁻¹⁴² in compact PU film at interface. These studies were performed on deuterated and non-deuterated samples, respectively. The determined SAXS profiles for compact PU film of non-deuterated samples are shown in Figure 3.5.5. The intensities are rescaled and Lorentz corrected (Iq^2), and a Porod background ($I \sim q^{-4}$) is subtracted, where q ; the scattering vector = $(4\pi/\lambda)\sin\theta$, and the I is the scattering intensity. The bulk samples were also measured (results are not given here) and the peak was at the same position as we found for the compact film samples.

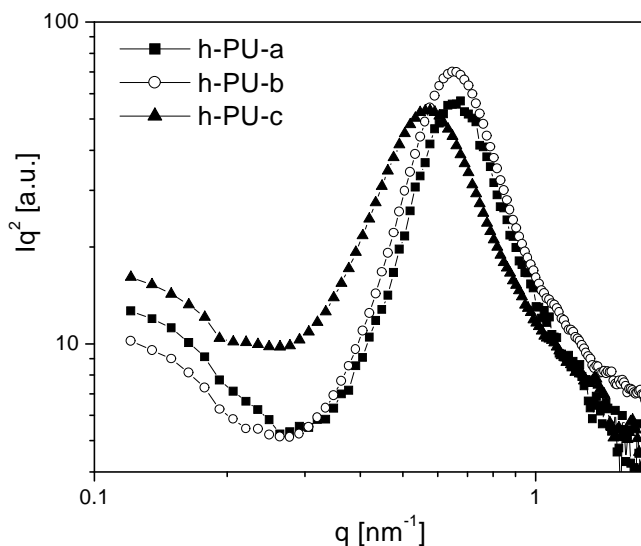


Figure 3.5.5: Lorentz and background corrected SAXS traces for powders of compact PU film as a function of scattering vector q in three different foam systems with water as indirect blowing agent. The peaks correspond to the average hard segment distance in the sample.

A significant peak was observed in each measurement, which corresponds to a typical hard segment distance in the sample. The hard domains distance was calculated using Bragg's law: $d = 2\pi/q_{\max}$. The q_{\max} is the position of the peak, estimated by subtracting a monotonic background (Porod) and then fitting with a Gaussian. The hard domain distances do not differ in h-PU-a and h-PU-b, but differences exist between h-

PU-c and the other two samples (Table 3.5.2). In low q range the curves differ from each other due to a high amount of inner surfaces i.e. all boundaries between different electron density regions, e.g. foam bubbles, hard segment, fillers, etc.

Table 3.5.2: Results of SAXS measurements with H₂O as indirect blowing agent.

Parameters	h-PU-a	h-PU-b	h-PU-c
q_{max} [nm ⁻¹]	0.65 ± 0.02	0.65 ± 0.02	0.58 ± 0.02
d [nm]	9.7 ± 0.3	9.7 ± 0.3	10.8 ± 0.3

The SAXS profiles for partially deuterated samples are shown in Figure 3.5.6 and the results for these samples are given in the Table 3.5.3. In case of d-PU-a and d-PU-b samples, the peak is nearly at the same position. However, in d-PU-c sample the peak position is shifted to low q values.

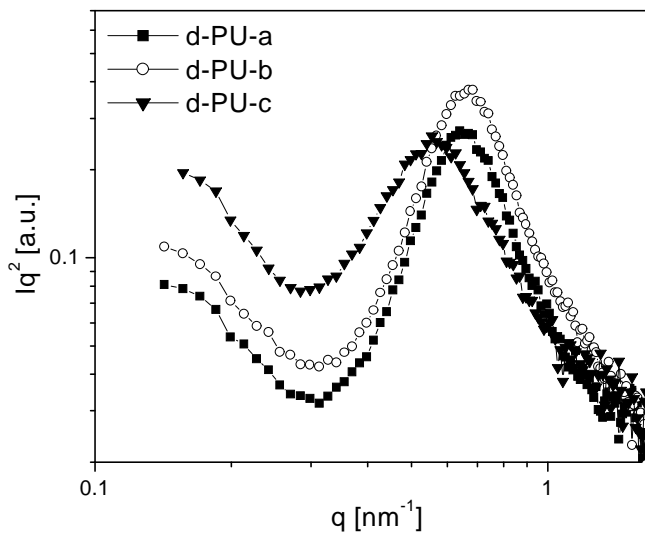


Figure 3.5.6: Lorentz and background corrected SAXS traces for powders of compact PU film as a function of scattering vector q in three different foam systems with D₂O as indirect blowing agent. The peaks correspond to the average hard segment distance in the sample.

Table 3.5.3: Results of SAXS measurements with D₂O as indirect blowing agent.

Parameters	d-PU-a	d-PU-b	d-PU-c
q_{max} [nm ⁻¹]	0.65 ± 0.02	0.66 ± 0.02	0.57 ± 0.02
d [nm]	9.7 ± 0.3	9.5 ± 0.3	11.0 ± 0.4

These SAXS measurements have shown that the hard segment distances remain nearly unchanged at the interface by exchanging the blowing agent H₂O to D₂O. These hard segments are embedded in a typical microphase segregated structure, and according to Armisted et al., their size does not change with water content in PU foam formulation.¹⁴³ So it seems that there are also secondary parameters like crosslinker that also contribute to the formation of these structures. The additives also have strong influence on formation of urea hard segments. Li et al.¹³⁶ have studied the effect of chain extenders (additives) on morphology development in flexible PU foams and they found that by using additives the onset of microphase separation was delayed and the interdomain spacing was increased. This was assumed to be due to the precipitation of chain extenders in the hard segments, change in structure and the ordering of the hydrogen bonding in hard segment, which leads to the decrease in intradomain cohesion of hard segments and increase of compatibility between the soft- and hard-segment blocks. Our results also indicate the similar behavior. Hence, the observed difference in hard segment distance in h-PU-c film sample as compared to the other two systems (h-PU-a and h-PU-b) is due to the formulation difference.

3.5.3. Transmission electron microscopy

The TEM images acquired from compact PU film formed at interface are displayed in Figures 3.5.7 and 3.5.8 for deuterated and non-deuterated samples, respectively. Elongated structures (arranged in layered form) parallel to the surface in the range of ~ 400 nm can be seen in the image of deuterated sample (Figure 3.5.7).

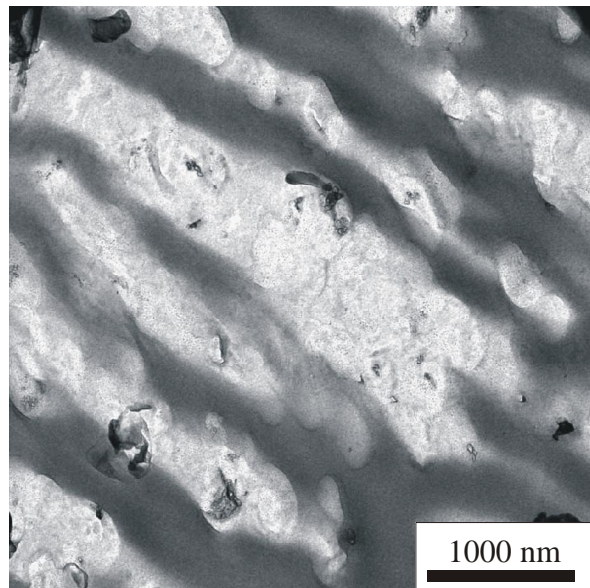


Figure 3.5.7: TEM image of compact PU film sample (d-PU-a) after staining with RuO_4 , which is sensitive for hard segments.¹⁴⁴ The elongated structures are parallel to film surface. A typical layer thickness is 400 nm.

Similar, but slightly thinner structures can be observed in a non-deuterated sample of a typical thickness in the range of 260 nm (Figure 3.5.8). The formation of these layered structures at interface in compact PU film takes place during polymerization process caused by liquid-liquid phase separation. Due to the difference in hydrophobicity of PPO and PEO parts of polyol, a phase separation between a PEO based polyol and H_2O rich phase and a PPO based polyol rich and H_2O poor phase will start. The more hydrophobic phase with PPO based polyol will preferentially cover the surface of the hydrophobic TP material at the interface. As a result of concentration gradient the process of phase separation will form a second layer consisting of a PEO based polyol and H_2O rich phase. Finally an arrangement of layers with different composition, leading to alternating regions with higher and lower hard segment density (elongated structures parallel to the surface in TEM images) is formed at the interface.

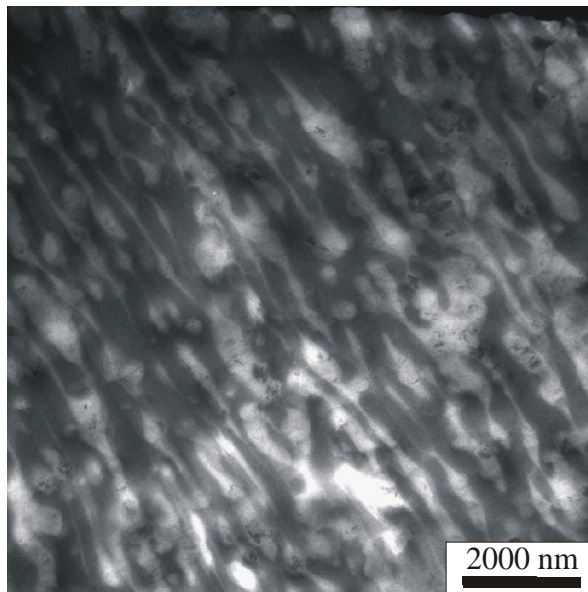


Figure 3.5.8: TEM image of compact PU film sample (h-PU-a) after staining in RuO_4 . The elongated structures are parallel to film surface. A typical layer thickness is 260 nm.

The differences in size of elongated structures in deuterated and non-deuterated samples could be due to the reaction process. Rossmly et al. showed using infrared spectroscopy of polyethers with different reactivity that the urea hard segments initially formed stay in solution, but at a certain point they separate as a second phase due to their concentration and molar mass buildup.^{129,130} Higher the reactivity, the lesser will be the time to separate the mixture into equilibrium phases.

The typical hard segment distance in the range of 10-20 nm as detected by SAXS measurements discussed above, could not be observed in these TEM images. The same effect was described by Neff et al.¹⁴⁴ Their TEM studies in bulk PU foams showed diffuse urea aggregates with a size between 50 and 200 nm, but the internal hard segment distances were only visible after degrading the soft segments.

3.5.4. Neutron reflection

After determining the specular and non-specular reflection regimes from the measured data (Figure 3.5.9), the scattering vector q was evaluated by using equation 3.5.2 and

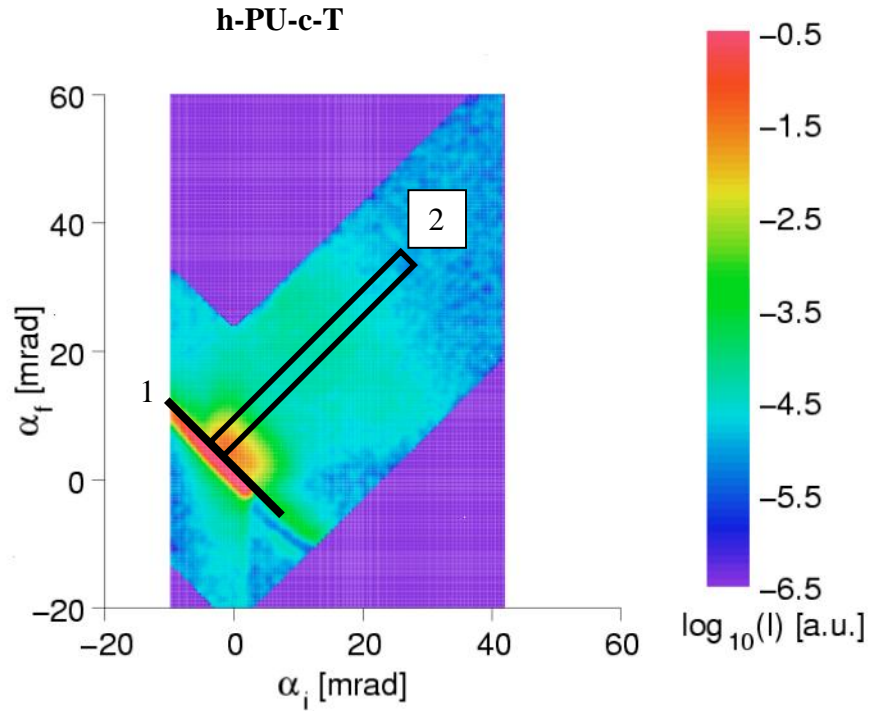


Figure 3.5.9: NR profile for h-PU-c-T sample after climate treatment (standard cycle). The specular and non-specular regions can be distinguished along the thick black line 1, and the data in frame 2 are used for calculations. α_i and α_f correspond to the initial and final angle between the sample surface and flight direction of neutrons.

the representative neutron reflection profile for one of the investigated sample (h-PU-a-T) is depicted in Figure 3.5.10.

$$q = 4\pi / \lambda * \sin((\alpha_i + \alpha_f) / 2) \quad (3.5.2)$$

Where q is the scattering vector, α_i and α_f is the initial and final angle between the sample surface and flight direction of neutrons, and λ is the used neutron wavelength.

In the q -range 0.014 - 0.04 \AA^{-1} fluctuations (‘Kiessig fringes’) in the reflection signal can be observed (indicated by vertical lines in Figure 3.5.10). These fluctuations can be fitted by a layered structure of parts with higher and lower scattering length density. From TEM results we know that two phases with nearly the same thickness and a regular elongated structural arrangement perpendicular to the surface in compact PU film exist in not well resolved form. Using the parratt32 program¹⁴⁵ for fitting the results, we obtained the thickness for both phases. The data above $q = 0.03 \text{ \AA}^{-1}$ could not be fitted

and this is due to the underlying background from the hard segment Bragg's reflection.

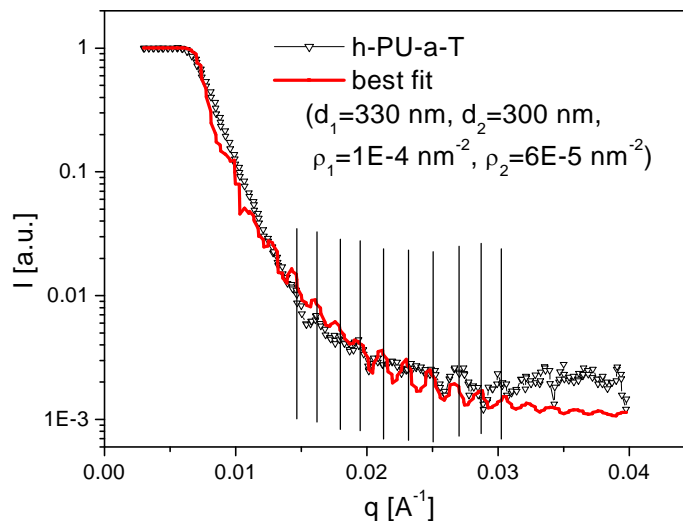


Figure 3.5.10: Neutron reflectivity as a function of the scattering vector q for PU foam sample (h-PU-a-T) after climate treatment. The differences between the fit and the data above $q = 0.03$ \AA^{-1} is due to the underlying background from the hard segment Bragg's reflection. The vertical lines indicate the significant fluctuations of the measurement.

In the case of H_2O samples, all layers are in the range of 300 nm. If the thickness of both layers is not in the same range (i.e. the thickness or the volume fraction differs more than 10%) the significance of the fluctuations decrease, which is observed in the h-PU-c-T (Figure 3.5.11) sample with $d_1 = 270$ nm and $d_2 = 360$ nm. In the q range above 0.04 \AA^{-1} , not depicted in the Figure 11, the scattering of the hard segments can be observed. The observed hard segment distances coincide with SAXS measurements discussed above.

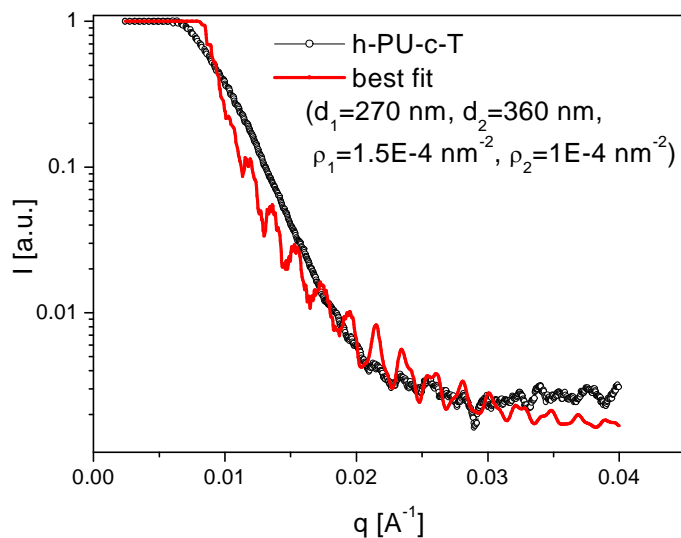


Figure 3.5.11: Neutron reflectivity as a function of the scattering vector q for PU foam sample (h-PU-c-T) after climate treatment. The differences between the fit and the data above $q = 0.03 \text{ \AA}^{-1}$ is due to the underlying background from the hard segment Bragg's reflection.

Only one of the deuterated samples (d-PU-b-T) shows significant fluctuations, which were fitted with a 400 nm thick layer system, which is at the limit of resolution of the instrument. There are several possible reasons, why the other samples will show no proper fluctuations: (a) they have thicker layers, as observed in TEM images, and are therefore above the resolution of the instrument; (b) the volume fraction of each phase is not near 50%; and (c) the layer thickness is not homogenous in the sample.

The NR measurements have shown that the compact PU film at interface is internally ordered in layered structures. On this basis, we can assign two phases with different (scattering length) densities. These phases do not correspond to hard and soft segment, as the typical hard segment distances are $\sim 10 \text{ nm}$ and the phases have $\sim 300 \text{ nm}$ thickness. As we observed different scattering length density, which can not be assigned to hard and soft segments and there is no other possibility that the material is macrophase separated,¹⁴⁶ so it can be concluded that the formation of two regions of different scattering length densities is due to the aggregation (formed through phase separation mechanism) of hard segment domains.

For more detail the difference in hard segment distances and the aggregated structures is explained schematically in Figure 3.5.12. A layer of hydrophobic component of the PU foam mixture will cover the hydrophobic TP surface, i.e. with a higher amount of PPO and less water. Depending on the reaction time the layer thickness may vary, but due to the phase separation of hydrophilic and hydrophobic parts, a second, PEO and water rich layer will be formed in next step. Depending on volume fraction and mobility of the phases this layered structure can be repeated several times. These layers were observed in TEM and NR measurements. Within each phase, the formation of urea hard segments takes place, preferentially in the PEO and water rich phase, as the water is reaction partner of MDI to form finally urea. In next step a microphase separation between hard and soft segments occur. The hard segments unite through hydrogen bonding and form big aggregates,¹⁴⁷ with a typical distance of 10 nm between them, which was detected by SAXS.

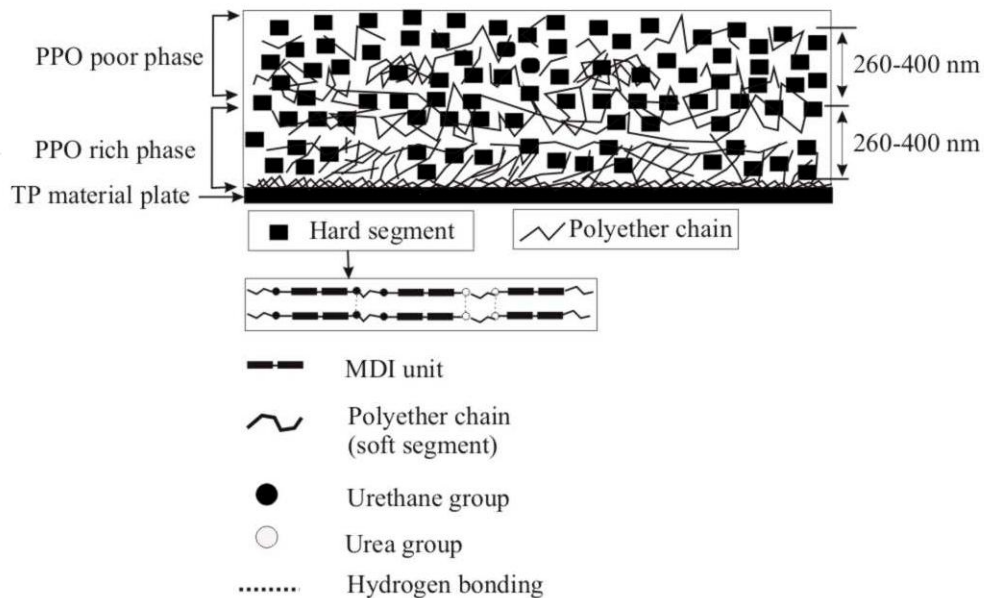


Figure 3.5.12: A schematic representation of hard segments and layered arrangement of aggregate structures in compact PU film formed at interface with TP material plate. The layered arrangement of aggregate structures (260 to 400 nm with high and low content of hard segments corresponding to PPO rich and poor phase) was observed by TEM and NR measurements.

3.5.5. Short summary of structure analysis results

From the reaction process of isocyanate, the observed reaction time t_1 and t_2 correspond to the reaction of water and polyol with isocyanate group, (NCO) respectively. The observed dependency of t_1 and t_2 is in well order according to the formulation difference among three different foam systems. The h-PU-c system shows the fastest reaction with water and polyol, whereas h-PU-a is the slowest formulation. The influence of formulation differences on morphology development (i.e., formation of urethane, hydrogen bonded urethane and urea) was observed by interpreting IR spectra in carbonyl region. The formation of non bonded urea (1715 cm^{-1}) was lowest in less reactive foam system compared to the other two.

A thin compact PU film at the interface (PU foam/TP material interface) of $110 \pm 30\text{ }\mu\text{m}$ thickness was found. From the SAXS investigations the hard segment distances were observed in PU film samples at the interface. The same segment-segment distance i.e. in the order of $d = 9.7 \pm 0.3\text{ nm}$ were observed in h(d)-PU-a and h(d)-PU-b for deuterated and non-deuterated PU film samples. But in h(d)-PU-c it was $10.9 \pm 0.4\text{ nm}$ for deuterated and non-deuterated PU film sample. These differences in hard segment distances in three foam systems are due to the different reaction rates. The reaction rate has influence on the microphase separation process of hard segments.

TEM and NR measurements showed that the PU film at the interface is internally ordered in a layered morphology. The thickness of the layers differs from 260 nm for H_2O samples upto 400 nm for D_2O samples. The origin of these layers is due to the phase separation in early stage of reaction process (i.e. reaction of isocyanate with polyol and water). On this basis, we can assign two phases with different (scattering length) density and these phases mainly correspond to the macrosegregated structures, as it is clear from TEM images.

3.6. Diffusion coefficient studies of MDI in thermoplastics

Several articles have been published¹⁴⁸⁻¹⁵¹ on diffusion studies of small molecular liquids into polymer systems. This type of diffusion process plays an important role in a wide variety of areas such as the drying of paint, adhesion, separation membrane efficiency, and solvent resistance. Basically, the diffusion theory is based on the solubility of one material into the other and that is directly related to the adhesion strength.¹⁵² When two materials of different properties are brought into contact, an interface area will be developed between them as result of interdiffusion process. The interphase area will be the mixture of A and B material (Figure 3.6.1). The model described below demonstrates the relationship between diffusion and adhesion process.¹⁵³

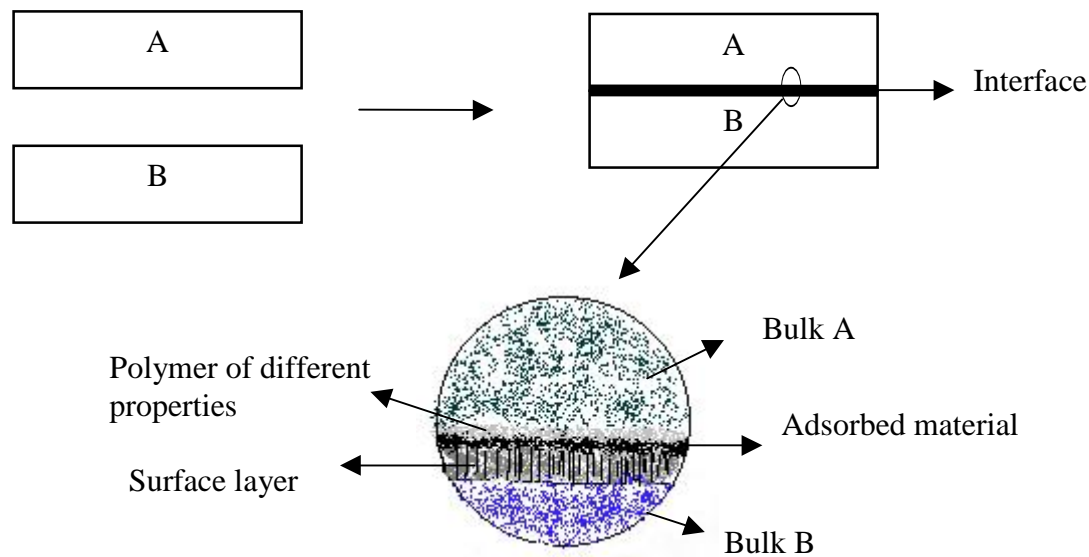


Figure 3.6.1: Schematic representation of interdiffusion process of material A and B.¹⁵⁴ The interfacial area is explained in enlarged image.

If the adhesive has the same solubility parameter like the adherend, then the formation of interphase will be favorable.^{155,156} As a result of this, a strong contact will develop between two materials. So the development of interphase between two phases can only be possible when there is diffusion process.

In this section the results on the diffusion process of liquid foam component MDI in TP material systems at 40°C are discussed. Regarding this the following TP material

systems were investigated: (a) PC/ABS-SMA (b) PC/ABS (c) PC/SAR-GF and (d) PC/ABS-GF. The mass uptake of MDI in TP materials was checked simply by gravimetry and the extent of diffused MDI layer was monitored by FTIR microscopy. The diffused layer thickness was measured from optical microscopic studies.

3.6.1. MDI mass uptake by thermoplastics

The data of MDI mass uptake at 40°C by TP materials is shown in Figure 3.6.2. The mass uptake (Δm) is the maximum amount of MDI sorbed per unit weight of TP materials and it is expressed in terms of wt.-%. The mass uptake of MDI by TP materials ranges from 0.65 ± 0.05 to 7.90 ± 0.67 wt.-%. All the TP materials show qualitative similar behavior of MDI mass uptake with time. However, quantitatively different MDI masses were sorbed into different TP material samples. The experiments were continued for long times to ensure the maximum MDI sorption. As given in Figure 3.6.2 the PC/ABS sample has shown the maximum mass uptake of MDI, while the minimum

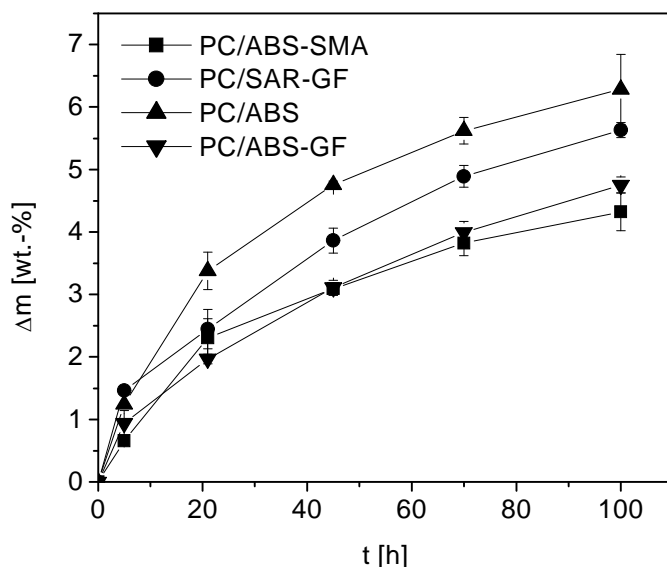


Figure 3.6.2: Mass uptake (wt.-%) curves for different TP materials in MDI at different time intervals at 40°C.

sorption was observed for PC/ABS-SMA sample. The lower sorption in PC/ABS-SMA might be due to the SMA content in the sample, as neat SMA did not show any MDI

uptake (data not shown). This shows that MDI does not diffuse into SMA component of the blend. Samples like PC/SAR-GF and PC/ABS-GF have shown the intermediate results, those were between the two samples discussed above. The data show that the sample PC/ABS-GF (70 wt.-% PC and 20 wt.-% ABS) had shown significantly lesser MDI uptake as compared to PC/ABS (60 wt.-% PC and 40 wt.-% ABS). This observation reveals that the MDI uptake is strongly enhanced by increasing the ABS content of the samples from 20 to 40 wt.-%. However, due to the different compositions of the samples, it is very difficult to explain the influence of individual content of the samples on MDI uptake.

3.6.2. Determination of type of diffusion

To gain further insight into the MDI sorption mechanism, the sorption results were fitted to equation¹⁴⁸ 3.6.1:

$$d = At^\alpha \quad (3.6.1)$$

Where

d diffusion length, or mass uptake (Δm)

A proportionality factor

t time

α diffusion exponent

The diffusion exponent (α) is a parameter related to the diffusion mechanism. The value lies between 0.5 for Fickian (Case I) and 1 for non-Fickian (Case II and anomalous) diffusion process.

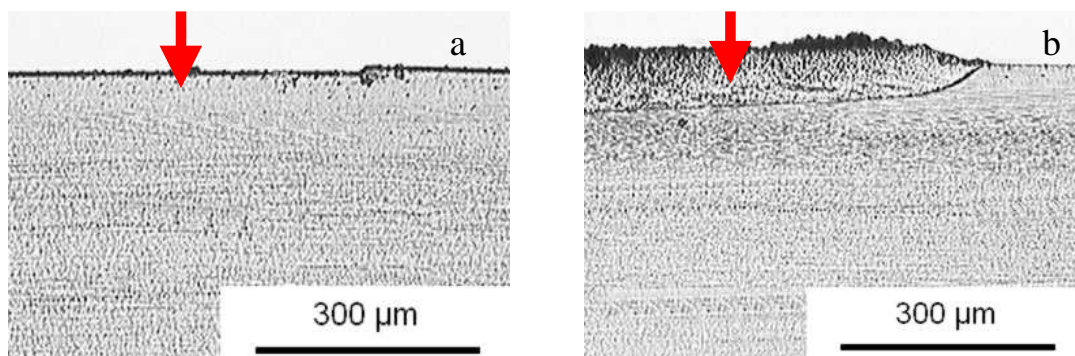
The least-squares estimation of α obtained at the >95% confidence limit is presented in Table 3.6.1 for different TP materials at 40°C. In all the TP materials the value of α lies between 0.50 and 0.65. PC/ABS-SMA and PC/ABS have higher values of α , i.e., MDI sorption mechanism deviates slightly from the Fickian mode in these two samples.

Table 3.6.1: Summary of the values for diffusion exponent α , and linear regression R obtained from equation $\Delta m = At^\alpha$ to the curves of TP material (Δm vs t) in MDI at 40°C.

Substrate	Diffusion exponent α	Linear regression R
PC/ABS-SMA	0.63 ± 0.03	0.96
PC/SAR-GF	0.50 ± 0.02	0.99
PC/ABS	0.55 ± 0.02	0.98
PC/ABS-GF	0.51 ± 0.02	0.99

3.6.3. Optical microscopy

In order to check the depth of diffused MDI layer in TP materials, light microscopic studies were conducted on samples without glass fiber. Images are acquired from TP materials at different time intervals. Representative microscopic pictures for PC/ABS-SMA and PC/ABS samples are shown in Figure 3.6.3. The depth of the diffused MDI layer was directly calculated from the images by excluding the swelling area above the surface of TP material and the quantitative data obtained from different images are presented in Table 3.6.2 after different time intervals. It is evident from the images that TP samples swell with MDI diffusion. Moreover, a sharp front of the MDI diffusing layer can be seen in images. The image acquired after 100 h shows less swelling of PC/ABS-SMA (Figure 3.6.3b) in MDI as compared to PC/ABS (Figure 3.6.3d). MDI was diffused



Continued

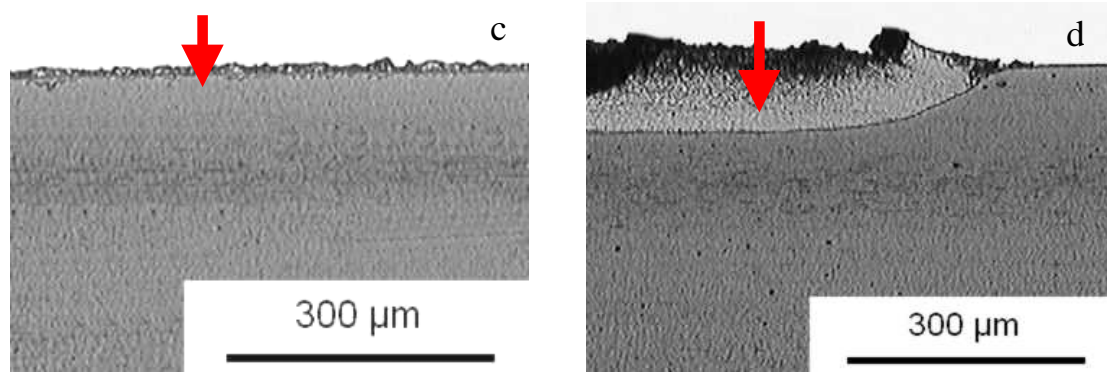


Figure 3.6.3: Light microscopic images acquired from thin sections of TP materials after MDI diffusion process at 40°C. (a) PC/ABS-SMA 5 h diffusion time, (b) PC/ABS-SMA 100 h diffusion time, (c) PC/ABS 5 h diffusion time and (d) PC/ABS 100 h diffusion time. The MDI diffusion direction and the diffused layer are indicated by arrow in each image.

to a longer distance in PC/ABS sample compared to PC/ABS-SMA. The large distance of diffused MDI profile into the TP samples can be assumed due to the higher amount of MDI diffusion. Similar trend was observed for these samples in mass uptake experiments, i.e. higher mass uptake of MDI by PC/ABS in comparison to PC/ABS-SMA sample (see Figure 3.6.2). From these results it can be assumed that MDI is not diffusing to the SMA phase of TP material.

Table 3.6.2: Summary of the diffusion length data calculated from light microscope images from TP materials after keeping in MDI at 40°C at different time intervals.

t [h]	PC/ABS- SMA		PC/ABS	
	*d [μm]	± [μm]	*d [μm]	± [μm]
5	8	1	15	2
21	36	5	38	4
45	48	8	64	5
70	63	5	70	6
100	67	9	86	12

*d = length of MDI diffused layer in TP materials

3.6.4. Determination of diffusion coefficients

The diffusion coefficients for PC/ABS-SMA and PC/ABS were calculated using the data obtained from optical micrographs in equation 3.6.2.

$$d = \sqrt{Dt} \quad (3.6.2)$$

d diffusion length

t time

D diffusion coefficient

The slope of plot of d vs $t^{1/2}$ gives diffusion coefficient D as depicted in Figure 3.6.4.

The diffusion coefficients calculated from Figure 3.6.4 for MDI in PC/ABS-SMA and PC/ABS are $1.5 \times 10^{-10} \pm 0.01 \times 10^{-10} \text{ cm}^2/\text{s}$ and $2 \times 10^{-10} \pm 0.06 \times 10^{-10} \text{ cm}^2/\text{s}$, respectively. The results show that MDI has higher value of diffusion coefficient for TP material without SMA and with high PC content (PC/ABS, 60 wt.-% PC). It shows that the MDI is not diffusing to the SMA phase of TP material and due to this MDI has smaller value of diffusion coefficient for the PC/ABS-SMA TP material.

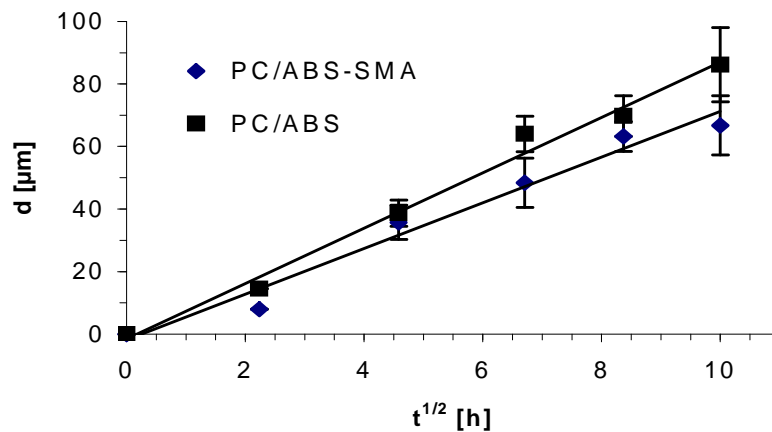


Figure 3.6.4: Plot of the diffusion distance d of MDI in TP material vs $t^{1/2}$, along with a linear fit. The result of the fitting procedure gives the diffusion coefficient.

3.6.5. FTIR microscopy

At first, the spectra of the individual materials (MDI and TP materials) were recorded in order to select the IR bands typical for a given component as given in Figure 3.6.5. The MDI band at 2240 cm^{-1} was used to follow the diffusion of MDI into the TP material

samples. The decrease in intensity of this band was related to the penetration depth of MDI in TP materials.

The intensity of selected IR band for MDI at different depth scales in TP materials after 100 h of sorption time is depicted in Figure 3.6.6a and 3.6.6b. These spectra were obtained with step width of 16.5 μm starting from neat TP material (without MDI diffused layer) to the edge of sample, followed through the area with diffused MDI layer. In Figure 3.6.6, the evaluation of the selected specific IR band of the isocyanate (2273cm^{-1}) group of MDI across the diffused layer, to which the volume concentration of MDI starting from the constant level of absorbance of this band to a decreasing value in

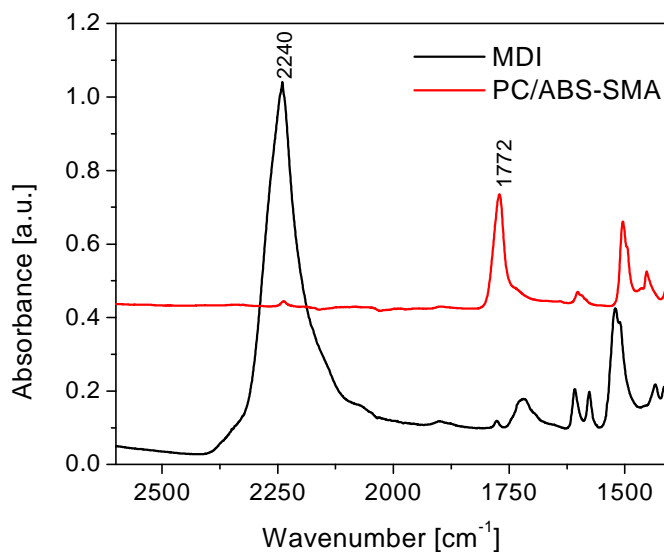


Figure 3.6.5: Comparison of FTIR spectra of neat materials (MDI and PC/ABS-SMA). The peak at 2240 cm^{-1} corresponds to isocyanate group where as 1772 cm^{-1} is for carbonyl group of polycarbonate.

the bulk of TP material is exhibited. The area of this absorption band (isocyanate band) was then used to estimate the MDI distribution in TP materials. The other FTIR scanning spectra obtained from PC/ABS-SMA and PC/ABS samples at different sorption times were quite similar to those shown in Figure 3.6.6 and therefore they are not depicted here. However, the absorption data obtained by scanning the TP material sample with diffused

MDI layer is shown in Figure 3.6.7a for PC/ABS-SMA and in 3.6.7b for PC/ABS. The

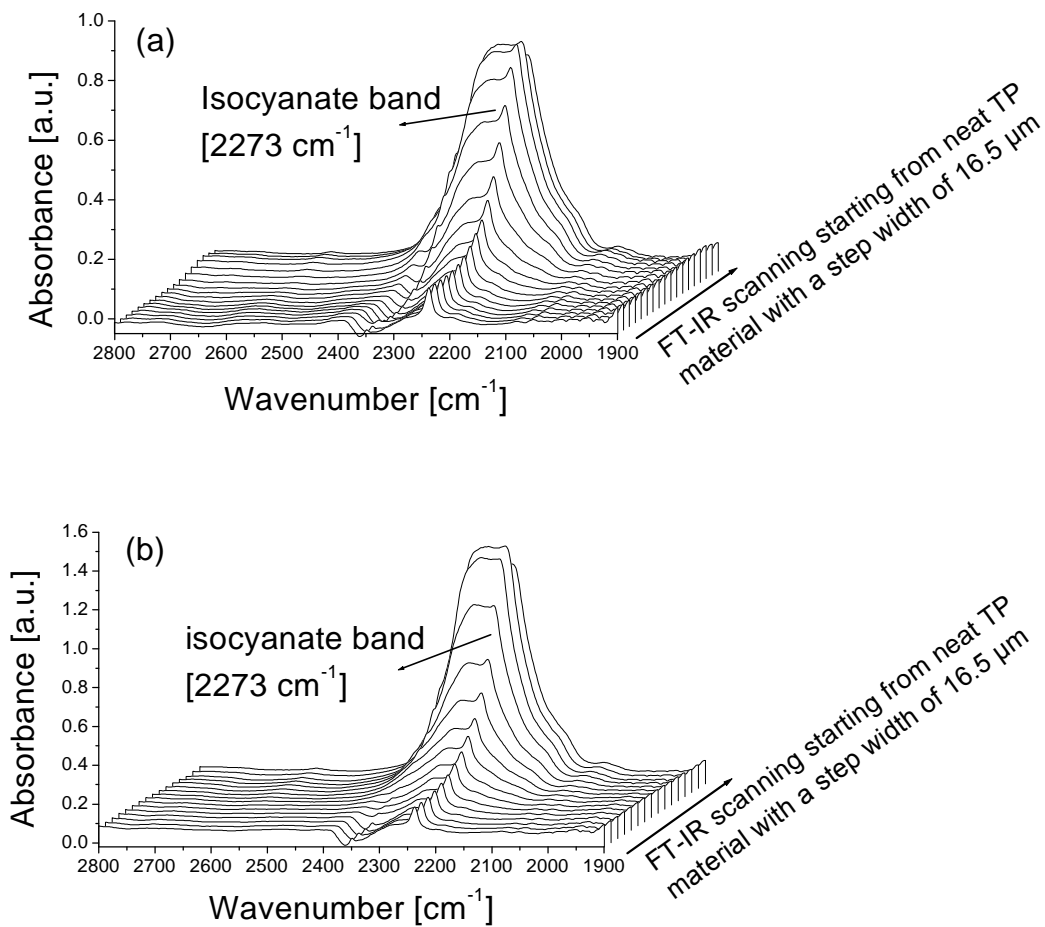


Figure 3.6.6: Evolution of the isocyanate IR band in TP materials: (a) PC/ABS-SMA in MDI at 40°C for 100 h, (b) PC/ABS in MDI at 40°C for 100 h.

data shown in Figure 3.6.7a and 3.6.7b were obtained by integrating the absorbance of isocyanate band (2273 cm⁻¹). It can be seen from the Figure that absorbance of this band is directly related to extent of diffused MDI layer in TP materials. As absorbance is directly related to the concentration of any material, so it is possible to use the intensity of isocyanate absorption band in order to calculate the diffusion coefficient. The data plotted in Figure 3.6.7 were fitted to Equation 3.6.3 to calculate the diffusion coefficient.¹⁵⁷

$$C = \operatorname{erfc} \frac{d}{2\sqrt{Dt}} \quad (3.6.3)$$

In this equation C is the concentration of diffusing substance, d diffusion length, D diffusion coefficient, and t time.

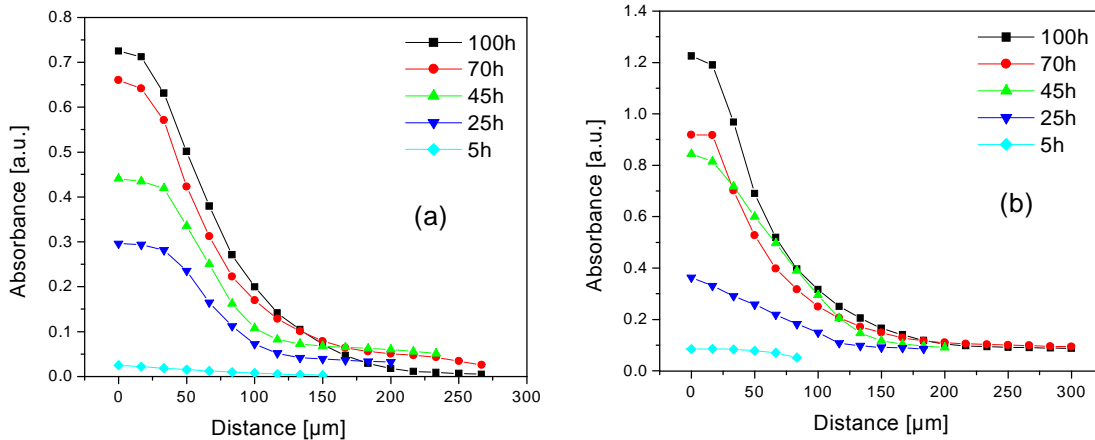


Figure 3.6.7: Plot of absorbance Vs scan width for isocyanate band (2273 cm^{-1}) after 5, 25, 45, 70, and 100 hours sorption time. (a) PC/ABS-SMA in MDI at 40°C , (b) PC/ABS in MDI at 40°C .

In order to fit the data presented in Figure 3.6.7 to Equation 3.6.3, the values of diffusion coefficient were assumed similar to those obtained from the diffusion length data (reported in Table 3.6.2) in optical micrographs. The fitted curve along with the experimental values is shown in Figure 3.6.8. It is clear from the Figure that the data obtained after 70 and 45 h of MDI diffusion times show the best fit indicating that the value of diffusion coefficient is similar to that of obtained from diffusion length data.

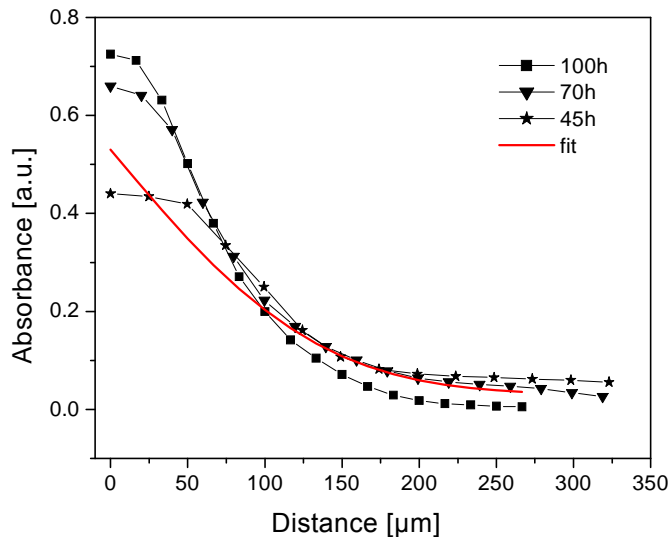


Figure 3.6.8: Plot of absorbance Vs scan width for isocyanate band (2273 cm^{-1}) after 45, 70, and 100 hours sorption time. The fitted curve is also plotted along the data.

3.6.6. Short summary of diffusion coefficient results

The mass uptake and penetration behavior of MDI in different PC containing TP materials was studied. Diffusion of MDI in all the TP materials was found to follow a Fickian process. The higher mass uptake of MDI ($6 \pm 0.6\text{ wt.-%}$) was observed for PC/ABS sample compared to the other samples. The extent of diffused MDI layer in PC/ABS sample was higher compared to the PC/ABS-SMA sample. Diffusion coefficient calculated from diffusion length data revealed higher value ($2 \times 10^{-10} \pm 0.06 \times 10^{-10}\text{ cm}^2/\text{s}$) for PC/ABS sample with high PC content compared to the PC/ABS-SMA sample with low PC content.

Chapter 4

Summary

The adhesion of PU foams on different TP material systems was investigated to understand the behavior and relative contribution of each material at interface by employing different techniques. During the course of these studies three different PU foams and five different TP materials were evaluated. The PU foams were based on MDI and poly(propylene) and poly(ethylene) oxide based polyether polyols containing poly(styrene-co-acrylonitrile) dispersions to a minor extent. While the TP materials were blends of different polymers (PC, SMA, ABS and silicone acrylate rubber). In some TP material glass fibers were used as reinforcing material.

The major outcomes of this work are summarized as follows:

1. The PU foam adhesion with TP materials was measured through peel test measurements. The PU-a and PU-b foam systems have shown the best adhesion (cohesive mode of peeling) before climate treatments. The highly reactive foam system (PU-c) did not produce good adhesive bonds with TP materials (adhesive mode of peeling). An explanation of this effect can be that the highly reactive foam system does not completely wet the surface of TP materials due to this it has weak adhesion compared to the less reactive foam systems.
2. The aging of PU foam/TP material sample joint was simulated using different climate conditions. In case of PC containing TP material the PU foam/TP material adhesion was strongly reduced in a standard climate cycle with high humidity conditions. In SMA TP material the PU foam/TP material interface remains nearly unaffected even after long climate treatments with high RH. The possible explanation of this could be the reaction process of SMA TP material with isocyanate. The neat maleic anhydride (MA) reacts with isocyanate as studied by FTIR-ATR to give imide bond (results are reported in Appendix A-2) and this is the reason why PU foam shows better adhesion results with SMA TP material even after long time climate treatments compared to the other TP materials. The relationship between the adhesion and diffusion lead to

the proposal to study the diffusion process of MDI (a liquid foam component) with TP material systems. The diffused MDI may react with TP materials that also contribute to the adhesion strength and durability. The results of these investigations indicated that the magnitude of diffusion coefficient depends on PC content in TP materials. The TP materials with the higher content of PC have the higher value of diffusion coefficient.

3. In standard climate treated samples it was noted that the relative effect of water diffusion through the interface might also influence the PU foam/TP material adhesion durability. This was evaluated by treating the samples in a climate cycle without humidity. It was observed that such type of climate treatment did not show any effect on adhesion performance, which shows that the high humidity has major contribution towards the loss of adhesion.
4. The influence of high humidity, high temperature and low temperature on PU foam/TP material adhesion was also evaluated separately. It was found that the high humidity and high temperature have the same effect like standard climate treatment but low temperature did not show any significant effect on adhesion performance. The surface roughness of TP material did not appear to show a large contribution towards adhesion strength. It was proved after climate treatment, that the samples with glass fiber and with higher surface roughness did not show good adhesion strength.

After different climate treatment experiments it was found that SMA is the best TP material for adhesion. The reason is (probably) a chemical linkage between isocyanate and MA, when imide is formed. PU-a is the best foam system for adhesion. The reason can be the slower foaming process (due to the type of polyol and H₂O content) compared to the other systems.

5. The contact angle measurements were carried to measure the surface energy of neat TP materials, TP material from PU foam interface after climate treatments and neat PU foam samples. The higher degree of surface energy was found for neat SMA TP material as compared to the PC containing TP materials. The glass fiber containing TP materials have higher surface tension compared to the sample without glass fiber. Also the TP material with high PC content, (PC/ABS-GF, with 70 wt% PC) has

shown the higher surface tension, as compared to the sample (PC/ABS, 60 wt.-% PC) with low PC content. Among PU foam samples the highly reactive PU-c system has the highest surface tension as compared to the less reactive PU-a foam system. It shows that the PU foam reactivity leads to difference in surface tension.

The surface tension of TP materials from PU foam (PU-a) interface after climate treatment has increased significantly as compared to the neat TP materials. After washing and drying the sample (PC/ABS-GF) the total surface tension remained unchanged but the polar part was decreased from 12.7 to 3.5 mN/m. The decrease in polar part of surface tension can be related to the evaporation of sorbed water (during climate treatment) from TP material. The total surface tension remained unchanged and that could be due to the non-washable PU foam parts linked to TP material.

In contact angle hysteresis studies the liquid foam components have shown more wetting compared to water on TP material surfaces. This was exemplified by their contact angles. No direct correlation of surface roughness and contact angle hysteresis was observed in samples with glass fiber. The surface tension obtained from MDI and water contact angles was higher compared to polyols.

6. The neat TP material and samples from PU foam/TP material interface after climate treatments were investigated using AFM and optical microscopic techniques. For quantitative evaluation of interaction behavior of TP material at interface, the surface roughness was measured from AFM height images. It was found that the TP material becomes rougher after removing from PU foam/TP material interface. Some PU foam parts were also detected on TP material surface as well. Some micro-deformations at the PU foam surface were also observed. The deformations on PU foam surface results from the distribution of strong and weak adhesive bonds at interface. These micro-deformations on foam surface may result from an inhomogeneous stress distribution during peel test. In areas where the adhesive bonds are weak, the interfacial load produces less or even no micro-deformations on PU foam surface. Optical microscopic investigations have shown that the formation of these micro-deformations is directly related to the adhesion strength, as it was confirmed from the optical micrographs of PU foam sample after separating from SMA TP material.

7. The neat PC/ABS-SMA TP material and samples from PU foam/TP material interface after climate treatments were also investigated using ToF-SIMS and XPS techniques. ToF-SIMS analysis indicated that TP material surface is predominantly composed of polycarbonate (one of the component of TP material). Also some silicone oil impurities were detected on TP material surface. The detached specimens were investigated using ToF-SIMS, and XPS. The results showed some indirect evidence about the interface reaction of PU foam with TP material systems. The silicone oil impurities were removed from TP material after skinning from PU foam surface.
8. The PU foam reaction process and the structure analysis was carried out using different techniques. From the reaction process of isocyanate, it was found that isocyanate is following two types of reaction processes, i.e. the reaction of isocyanate group (NCO) with water and polyol, respectively. Due to these two time scales (t_1 and t_2) were observed. The observed dependency of t_1 and t_2 was in agreement with the formulation difference among three different foam systems. The h-PU-c system shows the fastest reaction with water and polyol, whereas h-PU-a was the slowest formulation. The influence of formulation differences on morphology development (i.e., formation of urethane, hydrogen bonded urethane and urea) was observed by interpreting the IR spectra of the carbonyl region. The formation of non bonded urea (1715 cm^{-1}) was lowest in less reactive foam system compared to the other two.

At the interface (PU foam/TP material interface) a thin compact PU film of $110 \pm 30\text{ }\mu\text{m}$ thickness was found. TEM and NR measurements showed that the PU film is internally ordered in a layered morphology. The thickness of the layers differs from 260 nm for H₂O samples up to 400 nm for D₂O samples. The origin of these layers is due to phase separation in early stage of reaction process (i.e. reaction of isocyanate with polyol (PEO/PPO) and water). On this basis, one can assign two phases with different (scattering length) density and these phases mainly correspond to the macro-segregated structures, as it is clear from TEM images.

From the SAXS investigations the hard segment distances were observed in PU film samples at the interface. The same segment-segment distance i.e. in the order of $d = 9.7 \pm 0.3\text{ nm}$ were observed in PU-a and PU-b film samples. But in h(d)-PU-c it

was 10.9 ± 0.4 nm. These differences in hard segment distances in three foam systems are due to the different reaction rates. The reaction rate has influence on the microphase separation process of hard segments.

Chapter 5

Zusammenfassung

Hauptgegenstand der Untersuchungen war die Aufklärung von Adhäsionsproblemen zwischen Polyurethanschäumen auf unterschiedlichen thermoplastischen Kunststoffen sowie letztendlich die Verbesserung der Adhäsion sowohl hinsichtlich Festigkeit als auch Beständigkeit.

Drei Polyurethanschaum-Zusammensetzungen (PU-a, PU-b, PU-c) und fünf verschiedene thermoplastische Kunststoffblends bildeten die Materialbasis. Diphenylmethandiisocyanat war die Diisocyanatkomponente für alle Polyurethane. Die Polyolkomponente waren Polyetherdiole auf PEO / PPO-Basis mit Anteilen von dispergiertem Styren-Acrylnitril-Copolymer. Die Blends der thermoplastischen Kunststoffe bestanden aus Polycarbonat (PC), Styren-Maleinsäureanhydrid-Copolymeren (SMA), Acrylnitril-Butadien-Copolymeren (ABS) und Styren-Acrylnitril-Kautschuk (SAR), teilweise glasfaserverstärkt.

Es wurden das Verhalten, die Wechselwirkungen zwischen den verschiedenen Adhäsionspartnern sowie die spezifischen Beiträge der verschiedenen Materialien mit unterschiedlichen Methoden untersucht.

Die wesentlichen Ergebnisse sind:

1. Die Schaumsysteme PU-a und PU-b zeigten vor den klimatischen Beanspruchungen die besten Adhäsionsresultate. Das hochreaktive Schaumsystem PU-c versagte im Adhäsionstest. Wahrscheinlich wird der thermoplastische Kunststoff von dem hochreaktivem Schaumsystem nur ungenügend benetzt.
2. Die Alterung der Adhäsion war im Falle der PC-haltigen Thermoplaste am stärksten ausgeprägt. In SMA-PU-Systemen blieb die Grenzflächen-Wechselwirkung nahezu unbeeinflusst von den klimatischen Bedingungen. Möglicherweise reagiert das SMA-Copolymer mit dem Isocyanat. Die Reaktion zwischen monomerem Maleinsäureanhydrid und Isocyanat resultiert in der Ausbildung von Imidbindungen, wie mittels FTIR-ATR nachgewiesen werden konnte. (s. Anhang A-2)

Bei der Bestimmung des Diffusionskoeffizienten von MDI (eine flüssige Schaumkomponente) mit TP Material wurde festgestellt, dass die Größe des Diffusionskoeffizienten vom PC-Gehalt des TP abhängt. Je höher der PC-Gehalt desto höherer Diffusionskoeffizient.

3. In Standard-Klimatests wurde festgestellt, dass die Beständigkeit der Adhäsion zwischen PU-Schaum (PU-a und PU-b) und Thermoplast auch durch die Diffusion des Wassers zur Grenzfläche hin beeinträchtigt wird. Klimatests in trockener Atmosphäre zeigten keinerlei Auswirkung auf die Adhäsion.
4. Eine Verlängerung der Hochtemperaturabschnittes des Standardklimatests bei 80% relativer Luftfeuchte führte zu keiner weiteren Beeinflussung der Adhäsion. Die Adhäsion wurde in ähnlicher Weise beeinflusst wie im Standardklimatest. Eine Beschränkung der klimatischen Beanspruchung auf den Tieftemperaturbereich des Standardklimatest hatte selbst bei einer Ausdehnung der Beanspruchung auf bis zu drei Tage keinen signifikanten Einfluss auf die Adhäsion. Dieses Verhalten war unabhängig von der Rauigkeit, die z.B. durch Glasfaseranteile beeinflusst wird.

Unter dem Gesichtspunkt der Adhäsion geht aus den verschiedenen Klimatest Untersuchungen hervor, dass das SMA das beste Thermoplastmaterial und das Schaumsystem PU-a die beste Polyurethanformulierung ist.

5. Die Oberflächenenergie des SMA-Copolymeren war die höchste im Vergleich zu den anderen Thermoplasten. Glasfaseranteile führten generell zu höheren Oberflächenspannungen. Von den PU-Schaumzusammensetzungen hatte das reaktivste System (PU-c) die höchste Oberflächenspannung, die Formulierung PU-a die niedrigste. Das heisst, es gibt eine Korrelation zwischen Reaktivität des Schaumsystems und seiner Oberflächenspannung.

Die Oberflächenspannung der Thermoplastmaterialien wird durch den Kontakt mit dem PU-Schaum erhöht. An einer Materialkombination (PC/ABS-GF) konnte gezeigt werden, dass Reinigung und Trocknung der Kontaktfläche keinen Einfluss auf die Gesamtoberflächenenergie hatten. Es verschob sich jedoch die Relation von polaren zu dispersen Anteilen der Gesamtoberflächenspannung. Der polare Anteil sank von 12,7 auf 3,5 mN/m. Der niedrigere polare Anteil kann mit der Verdampfung des an der Kontaktfläche sorbierten Wassers (aufgenommen **während der**

klimatischen Tests) in Zusammenhang gebracht werden. Die konstant gebliebene Gesamtoberflächenenergie kann auf die nicht durch Waschen entfernbaren, auf der Oberfläche des Thermoplasts verbliebenen PU-Schaumanteile zurückgeführt werden.

Die Benetzbarkeit aller ausgewählten Thermoplastsysteme mit den flüssigen PU-Schaumkomponenten war in allen Fällen relativ gut. Die Benetzbarkeit, geprüft mittels Kontaktwinkel-Hysteresemessungen, war für diese Komponenten besser als die Benetzbarkeit mit Wasser. Auch hier konnte keine direkte Beeinflussung durch die Oberflächenrauigkeit gefunden werden..

6. Die Oberflächentopographie wurde durch das Abtrennen der PU-Schaumkomponente aus dem Adhäsionsverbund mit PC/ABS-SMA nach dem Klimatest untersucht. Das lieferte Aussagen zur Festigkeit der Bindung zwischen dem Thermoplast und dem PU-Schaum. Obwohl die Proben Adhäsionsversagen aufwiesen, zeigten sowohl die licht-als auch die Kraftmikroskopischen Untersuchungen eine mehr oder weniger starke Strukturierung der Thermoplastoberfläche. Die entstandenen Strukturen an der Thermoplastoberfläche sind abhängig von der Adhäsionsfestigkeit und liefern demzufolge nach dem Trennen der beiden Kontaktpartner eine indirekte Information über die vorhanden gewesene adhäsive Bindung.
7. Das PC/ABS-SMA Ausgangsmaterial und Proben aus der Grenzschicht nach dem Ablösen des PU-Schaums wurden mit ToF-SIMS und XPS untersucht. Die Zusammensetzung des reinen TP an der Oberfläche wird durch die PC Komponente dominiert, wobei zusätzlich Reste von Silikonöl nachgewiesen werden konnten. Die Proben aus der Grenzschicht zeigten Hinweise auf das Verbleiben von Schaumteilen auf der TP Oberfläche. Der Anteil von Silikonöl wurde auf der TP-Seite reduziert und konnte auf der Schaum-Seite nachgewiesen werden.
8. Bei der Schaumbildung des PU wurde für die Reaktion des Isocynats zwei verschiedene Reaktionsprozesse (mit Wasser und mit Polyol) mit verschiedenen Zeitskalen (t_1 und t_2) beobachtet werden. Die Variation dieser Zeiten für verschiedene Schaumsysteme geht mit deren Zusammensetzung einher, d.h. das reaktive System h-PU-c wies deutlich kürzere Zeiten als das System h-PU-a. Der Einfluss der Schaumzusammensetzung auf die Morphologiebildung (Entstehung von Urethan, Urea und durch Wasserstoffbrücken gebundene Bereiche) konnte aus den IR-

Spektren in der Carbonyl-Region gefolgert werden. Die Bildung von nicht-gebundenem Urea war am geringsten bei dem gering reaktiven Schaumsystem h-PU-a.

An der Grenzschicht zwischen PU-Schaum und TP bildete sich ein dünner, kompakter PU-Film von $110 \pm 30 \mu\text{m}$ Dicke. Bei TEM und NR Untersuchungen wurde eine lamellar geordnete Morphologie im Inneren des Filmes gefunden. Die Dicke der einzelnen Schichten lag zwischen 260 nm für H₂O Proben und 400 nm für D₂O Proben. Die Bildung dieser Schichten geht auf eine Phasenseparation im frühen Reaktionsstadium zwischen hydrophobem PPO und hydrophilem PEO zurück.

Typische Hartsegment-Abstände konnten aus SAXS-Messungen bestimmt werden. Dabei ergab sich für die Proben PU-a und PU-b mit $d = 9.7 \pm 0.3 \text{ nm}$ ein geringerer Abstand als bei der reaktiven Probe PU-c mit $d = 10.9 \pm 0.4 \text{ nm}$.

Chapter 6

Future perspectives

The adhesion test results (PU foam and TP materials adhesion results) presented in this thesis can currently be applied in a qualitative manner. From the adhesion test results of three different PU foams on SMA containing TP material, it can be proposed to develop such a material, which has high degree of surface reactive functional groups. The reactive functional groups on TP material surface are important to produce the chemical bonding at the interface especially when used in a climate with high humidity and high temperature conditions. Some more sophisticated analytical methods are required to study the affect of climate treaments on adhesion of PU foam with TP materials

Some additional experimental work is also required to study the topographic and chemical composition of PU foam and TP material from interface. ToF-SIMS will be the best method to study the chemical composition of interface materials. The NR and TEM investigations has given a new insight in this study, that can also be extended to further investigations, e.g. the selective degradation of PU foam chains (soft segment) on TP material surface at interface region and investigations of remaining PU foam parts by using TEM technique. Such type of investigations will provide the information which PU foam structures are linked with TP material at interface.

Chapter 7

Literature

1. Kinloch, A. J. *Adhesion and Adhesives Science and Technology*, Chapman and Hall London 1990 Chapter 1.
2. Suh, K. W.; Park, C. P.; Maurer, M. J.; Tusim, M. H.; De Genova, R.; Broos, R.; Sophiea, D. P. *Adv. Mater.* **2000**, 12(23), 1779.
3. Leenslag, J. W.; Huygens, E.; Tan, A. *Cell. Polym.* **1997**, 16(6), 411.
4. Van Eetvelde, E.; Banner, C.; Cenens, J.; Chin, S. J. *Cell. Plast.* **2002**, 38(1), 31.
5. Saunders, J.; Frisch, K. *Polyurethane Chemistry and Technology*, Part 1: Interscience, New York, 1963.
6. DeBell, J. M.; Goggin, W. C.; Gloor W. E. *German Plastic practice*, DeBell and Richardson, Cambridge, Mass. 1946.
7. Dennis, G. L.; Paul, C. In *Hand Book of Adhesive Technology* Pizzi, A.; Mittal, K. L. ed. Marcel Dekker: New York, 1994, Chapter. 24.
8. Comyn, J. in *Durability of Structural Adhesives* Kinloch, A. J., ed. Applied Science, London, 1983, p.85.
9. Schliekelmann, R. J. *Bonded Joints and Preparation for Bonding* AGARD Lecture Series 1979, 102, p. 1.
10. Annual Book of ASTM Standards 1992, Section 15, Vol. 15.06, Adhesives.
11. Arnott, D. R. in *Adhesively Bonded Joints for Fiber Composite and Metal Structures* CRC-AS, Workshop, AMRL, Melbourne, 20th Feb. 1996.
12. Engel, J. H.; Fitzwater, R. N. in *Adhesion and Cohesion*, P. Weiss, ed. Elsevier, Amsterdam, 1962, p. 89.
13. Schultz, J.; Nardin, M. in *Handbook of Adhesive Technology* Pizzi, A.; Mittal, K. L. ed. Marcel Dekker: New York, 1994, Chapter 2.
14. Packham, D. E. *J. Adhes.* **1992**, 39, 137.
15. McBain, J. W.; Hopkins, D. G. *J. Phys. Chem.* **1925**, 29, 188.

16. Reinhart, F. W. in *Adhesion and Adhesives, Fundamentals and Practice* Society of Chemical Industry London, 1954, p. 9.
17. Bright, K.; Malpass, B. W.; Packham, D. E. *Nature* **1969**, 223, 1360.
18. Arrowsmith, D. J. *Trans. Instit. Met. Finish.* **1970**, 48, 88.
19. Venables, J. D. *J. Mater. Sci.* **1985**, 19, 2431.
20. Evans, J. R.; Packham, D. E. *J. Adhes.* **1979**, 10, 177.
21. Wang, T. T.; Vazirani, H. N. *J. Adhes.* **1972**, 4, 353.
22. Kieffer, A.; Schmidt-Naake, G.; Krueger, G.; Hennemann, O.-D. *Proceedings of the Annual Meeting of the Adhesion Society* 1997, 20th, 589.
23. Voyutskii, S. S. *Adhes. Age* **1960**, 5(4), 30.
24. Anand, J. N. *J. Adhes.* **1973**, 5, 265.
25. De Gennes P. G. *J. Chem. Phys.* **1971**, 55, 572.
26. Doi, M.; Edwards, S. F. *J. Chem. Soc. Fara. Trans 2: Mol. Chem. Phys.* **1978**, 74(10), 1789, 1802, 1818.
27. Graessley, W. W. *Adv. Polymer Sci.* **1982**, 47, 76.
28. Jud, K.; Kausch, H. H.; Williams, J. G. *J. Mater. Sci.* **1981**, 16, 204.
29. De Gennes, P. G. *C. R. Acad. Sci. Paris Ser.* **1981**, B291, 219 1980, 292, 1505, 1981.
30. Prager, S.; Tirrell, M. *J. Chem. Phys.* **1981**, 75, 5194.
31. Deryaguin, B. V. *Research* **1955**, 8, 70.
32. Weaver, C. *Farad. Special Discussions* **1975**, 2, 18.
33. Skinner, S. M.; Savage, R. L.; Rutzler, J. E. *J. Appl. Phys.* **1953**, 24, 439.
34. Chapman, B. N. in *Aspects of Adhesion* Alner, D. J. ed. University of London Press, London 1970, p. 43.
35. Krupp, J.; Schnabel, W. *J. Adhes.* **1973**, 5, 296.
36. Schmidt, R. G.; Bell, J. P. *Adv. Polym. Sci.* **1986**, 15, 33.
37. Comyn, J. *Int. J. Adhes. Adhes.* **1992**, 12(3), 145.
38. Carre, A.; Schultz, J. *J. Adhes.* **1983**, 15, 151.
39. Gutowski, W. *Int. J. Adhes. Adhes.* **1987**, 7(4), 189.
40. Allen, K. W. *Int. J. Adhes. Adhes.* **1993**, 13(2), 67.
41. Allen, K. W. *J. Adhes.* **1987**, 21, 261.

42. Andrews, E. H.; Kinloch, A. J. *Proc. Roy. Soc.* **1973**, A332, 385.
43. Gent, A. N.; Kinloch, A. J. *J Polym. Sci.* **1971**, A2, 659.
44. Cherry, B. W.; Hakeen, M. I. Adhesion-10, ed. Allen, K. W., Chapter 4, p.42. Elsevier, Applied Science Publishers, London, 1986.
45. Mittal, K. L. *Polymer Science and Technology*, 9A, p. 129, Plenum Press, New York, 1975.
46. Fowkes, F. M. *Ind Eng. Chem.* **1964**, 56, 40.
47. Owens, D. K.; Wendt, R. C. *J. Appl. Polym. Sci.* **1969**,13, 1741.
48. Bolger, J. C. *in Adhesion Aspects of Polymeric Coatings*, ed. Mittal, K. L., Plenum Press, New York, 1983, p. 3.
49. Watts, J. F.; Chehimi, M. M.; Gibson, E. M. *J. Adhes.* **1992**, 39, 145.
50. Bayer, O. *Angew. Chem.* **1947**, A59, 275.
51. Hoechtlen, A. *Kunststoffe* **1952**, 42, 303.
52. Modesti. M.; Adriani, V.; Simioni. F. *Polym. Eng. Sci.* **2000**, 40(9), 2046.
53. Kaushiva. B. D.; McCartney. S. R.; Rossmly. G. R.; Wilkes. G. L. *Polymer.* **2000**, 41, 285.
54. Rossmly. G. R.; Kollmeier H. J.; Lidy. W.; Schator. H.; Wiemann. M. *J. Cell. Plast.* **1981**, 17, 319.
55. Katsamberis. D. J. *Appl. Polym. Sci.*, **1990**, 41, 2059.
56. Dabi. S.; Zilka. A. *Eur. Polym. J.* **1980**, 16(1), 95.
57. Zygmunt, W. *Polyurethanes Chemistry, Technology and Applications*, 1993, p. 86.
58. Blakwell. J.; Nagarajan. N. R. *Polymer* **1981**, 22(2), 202.
59. Wu. W.; Simpson. P. G.; Black. W. B. *J. Polym. Sci. Part B: Polym. Phys.* **1980**, 18(4), 751.
60. Elwell, M. J.; Ryan A. J.; Grünbauer H. J. M.; Lieshout, H. C. V. *Macromolecules* **1996**, 29, 2960.
61. http://www.bpf.co.uk/bpfindustry/plastics_materials_Polycarbonate_PC.cfm.
62. Fraser, R. A. W.; Ward, I. M. *J. Mater. Sci.* **1977**, 12, 459.
63. Pitman, G. L.; Ward, I. M. *Polymer* **1979**, 20, 895.
64. Chang, F. C.; Hsu, H. C. *J. Appl. Polym. Sci.* **1994**, 52, 1891.

65. Chang, F. C.; Chu, L. H. *J. Appl. Polym. Sci.* **1992**, 44, 1615.
66. Inberg, J. P. F.; Gaymans, R. J. *Polymer* **2002**, 43, 4197.
67. Grabowski, T. S.; Va, V. W. United States Patent, 3130177, 1964.
68. Chao, H. Shin-I.; Fasoldt, C. L.; Safieddine, A. M.; Lietzau, C. United States Patent, 5688837, 1997.
69. Schreiber, H. P.; Tocheff, E.; Sengupta, A. *Polyurethanes World Congr. Proc.* 1993, 323.
70. Pisanova, E.; Zhandraov, S.; Dutschk, V.; Mader, E. *Adhes. 99, Int. Conf. Adhes. Adhes.* **1999**, 7, 357, IOM Communications Ltd., London, UK.
71. Patel, S.; Makadia, C.; Guan, Q.; Metha, S.; McCarthy, S. P. *Annu. Tech. Conf. Soc. Plast. Eng.* **2000**, 58(3), 2658.
72. Schreiber, H. P.; Renyan, Q.; Sengupta, A. *J. Adhes.* **1998**, 68(1-2), 31.
73. Stroem, G.; Fredriksson, M.; Stenius, P. *J. Coll. Inter. Sci.* **1987**, 119, 352.
74. Gebhard, K. F. *Grundlagen der physikalischen Chemie von Grenzflächen und Methoden zur Bestimmung geometrischer Grössen*; FGH IGB Stuttgart, 1982.
75. Janczuk, B.; Bialopiotrowicz, T.; Wojcik, W. *J. Coll. Inter. Sci.* **1989**, 127(1), 59.
76. Lander, L. M.; Siewierski, L. M.; Brittain, W. J.; Volger, E. A. *Langmuir* **1993**, 9, 2237.
77. Rabel, W. *Farbe und Lack* **1971**, 77, 997.
78. Strobl, G. R. *Acta Crystallogr.* **1970**, A26, 367.
79. Keisler, C.; Lataillade, J. L. *J. Adhe. Sci. Technol.* **1995**, 9(4), 395.
80. Boucher, E.; Folkers, J. P.; Hervet, H.; Léger, L. *Macromolecules* **1996**, 29, 774.
81. Gong, L.; Friend, A. D.; Wool, R. P. *Macromolecules* **1998**, 31, 3706.
82. Brown, R. H. *Material Forum* **2000**, 24, 49.
83. Lee, I.; Wool, R. P. *Macromolecules* **2000**, 33, 2680.
84. Goldberg, H. D.; Cha, G. S.; Brown, R. B. *J. Appl. Polym. Sci.* **1991**, 43, 1287.
85. Gardon, J. L. *J. Appl. Polym. Sci.* **1963**, 7, 625.
86. Sancaktar, E.; Gomatam, R. *J. Adhes. Sci. Technol.* **2001**, 15(1), 97.
87. Liao, C. D.; Hsieh, H. K. *J. Polym. Sci. Part A: Polym. Chem.* **1994**, 32, 1665.
88. Krol, P.; Krol, B.; Pilch-P, B. *Pol. J. Chem. Technol.* **2003**, 5(3), 84.
89. Brewis, D. M.; Critchlow, G. W. *Int. J. Adhes. Adhes.* **1997**, 17(1), 33.

90. John, M.; Arjona, M. C.; Dechent, W. L.; Stoffer, J. O. Proceedings of the International Waterborne, High-Solids, and Powder Coatings Symposium, 1996, 23, 397.
91. Broos, R.; Herrington, R. M.; Casati, F. M. *Cell. Polym.* **2000**, 19(3), 169.
92. Brewis, D. M.; Comyn, J.; Raval, A. K.; Kinloch, A. J. *Int. J. Adhes. Adhes.* **1990**, 10(4), 247.
93. Packham, D. E. *Int. J. Adhes. Adhes.* **2003**, 23, 437.
94. Extrand, C. W. *Langmuir* **2003**, 19, 3793.
95. Bico, J.; Tordeux, C.; Quéré, D. *Europhys. Lett.* **2001**, 55(2), 214.
96. Scharnowski, D. *Diplomarbeit*, Martin- Luther-Universität Halle-Wittenberg, 1999.
97. Chibowski, E. in *Contact Angle Wettability and Adhesion*, Mital, K. L. ed. 2, 2002, VSP, Utrecht.
98. Chibowski, E.; Ontiveros-Ortega, A.; Perea-Carpio, R. *J. Adhes. Sci. Technol.* **2002**, 16(10), 1367.
99. Bain, C. D.; Evall, J.; Whitesides, G. M. *J. Am. Chem. Soc.* **1989**, 111, 7155.
100. Möglinger, B.; Michler, G. H.; Ludwigs, H.-C. *Deformation and Fracture Behavior of Polymers* ed. Grellmann, W.; Seidler, S. Springer Verlag 2001, p. 335.
101. Kieffer, A.; Hartwig, A.; Schmidt-Naake, G.; Hennemann, O.-D. *Acta. Polym.* **1998**, 49(12), 720.
102. Kieffer, A.; Hartwig, A. *Macromol. Mater. Eng.* **2001**, 286, 254.
103. Gutman, L.; Chakraborty, A. K. *J. Chem. Phys.* **1994**, 101, 10074.
104. Gutman, L.; Chakraborty, A. K. *J. Chem. Phys.* **1995**, 103, 10733.
105. Brown, H. R.; Russell, T. P. *Macromolecules* **1996**, 29, 798.
106. Scott-S, J. *Macromolecules* **1995**, 28, 7447.
107. Dillingham, R. G.; Moriarty, C. J. *Proc Ann. Meet. Adhes. Soc.* **2002**, 25th, 316.
108. Ilsoon, L.; Richard, P. W. *Macromolecules* **2000**, 33, 2680.
109. Dillingham, R. G.; Moriarty, C. J. *J. Adhes.* **2003**, 79, 269.
110. Pisanova, E.; Zhandarov, S.; Dutschk, V.; Mader, E., *Int. Conf. Adhes. Adhes.* 7th, Cambridge, United Kingdom, **1999**, 357.

111. Vallat, M. F.; Bessaha, N.; Schultz, J.; Maucourt, J.; Combette, C. *J. Appl. Polym. Sci.* **2000**, 76(5), 665.
112. Petrie, E. M. *Handbook of Adhesives and Sealants*, McGraw-Hill, 2000, Chapter 10.
113. Lopez Manchado, M. A.; Arroyo, M.; Biagiotti, J.; Kenny, M. J. *J. Appl. Polym. Sci.* **2003**, 90, 2170.
114. Chilkotic, A.; Ratner, B. D.; Briggs, D. *Chem. Mater.* **1991**, 3, 51.
115. Chan, C. M. *Polymer Surface Modification and Characterization*, Hanser: New York, 1994.
116. Briggs, D.; Fletcher, I. W.; Reichlmaier, S.; Sanchez, J. L. A.; Short, R. D. *Surf. Interface Anal.* **1996**, 24, 419.
117. Briggs, D. *Surface Analysis of Polymers by XPS and Static SIMS* Cambridge University Press: New York, 1998.
118. Galuska, A. A. *Surf. Interface Anal.* **1997**, 25, 1.
119. Affrossman, S.; Bertrand, P.; Hartshorne, M.; Kiff, T.; Leonard, D.; Pethrick, R. A.; Richards, R. W. *Macromolecules* **1996**, 29, 5432.
120. Lianos, L.; Quet, C.; Due, T. M. *Surf. Interface Anal.* **1994**, 21, 14.
121. Briggs, D. *Surf. Interface Anal.* **1986**, 9(1-6), 391.
122. Brant, P.; Karim, A.; Douglas, J. F.; Bates, F. S. *Macromolecules* **1996**, 29, 5628.
123. Armistead, J. P.; Wilkes, G. L. *J. Appl. Polym. Sci.* **1988**, 35, 601.
124. Bailey-Jr., F. E.; Gritchfield, F. E. *J. Cell. Plast.* **1981**, 17(6), 333.
125. Elwell, M. J.; Ryan, A. J.; Grünbauer, H. J. M.; Lieshout, H. C. V. *Polymer* **1996**, 37(8), 1353.
126. McClusky, J. V.; Priester, R. D.; O'Neill, R. E.; Willkomm, W. R.; Heaney, M. D.; Capel, M. A. *J. Cell. Plast.* **1994**, 30, 338.
127. Priester, R. D.; McClusky, J. V.; O'Neill, R. E.; Turner, R. B.; Harthcock, M. A.; Davis, B. L. *J. Cell. Plast.* **1990**, 26, 346.
128. Brunette, C. M.; Hsu, S. L.; MacKnight, W. J. *Macromolecules* **1982**, 15, 71.
129. Rossmly, G. R.; Kollmeier, H. J.; Lidy, W.; Schator, H.; Wiemann, M. *J. Cell. Plast.* **1977**, 13, 26.

130. Rossmly, G. R.; Kollmeier, H. J.; Lidy, W.; Schator, H.; Wiemann, M. *J. Cell. Plast.* **1981**, 17(6), 319.
131. Kim, J.; Ryba, E.; Miller, J. W.; Bai, J. *J. Adhes. Sci. Technol.* **2003**, 17(10), 1351.
132. Kim, J.; Ryba, E. *J. Adhes. Sci. Technol.* **2001**, 15, 1747.
133. Sugama, T.; Kukacka, L. E.; Carciello, N.; Warren, J. B. *J. Mater. Sci.* **1988**, 23, 101.
134. Kalpana, S. K.; Marek, W. U. *J. Coat. Technol.* **2000**, 72(903), 35.
135. Elwell, M. J.; Mortimer, S.; Ryan, A. J. *Macromolecules* **1994**, 27, 5428.
136. Li, W.; Ryan, A. J.; Meier, I. K. *Macromolecules* **2002**, 35, 6306.
137. Bailey, F. E.; Critchfield, F. E. *J. Cell. Plast.* **1981**, 17, 333.
138. Merten, R.; Lauerer, D.; Dahm, M. *J. Cell. Plast.* **1968**, 4, 262.
139. Raymond, N.; Adeyinka, A.; Christopher, W. M.; Anthony, J. R. *J. Polym. Sci. Part B: Polym. Phys.* **1998**, 36, 573.
140. Dimitrios, V. D.; Garth, L. W. *J. Appl. Polym. Sci.* **1997**, 66, 2395.
141. Benjamin, C.; Benjamin, S. H. *Chem. Rev.* **2001**, 101, 1727.
142. James, P.A.; Garth, L. W. *J. Appl. Polym. Sci.* **1998**, 35, 601.
143. Armisted, J. P.; Wilkes, G. L.; Turner, R. B. *J. Appl. Polym. Sci.* **1988**, 35, 601.
144. Neff, R.; Adedeji, A.; Macosko, C. W.; Ryan, A. J. *J. Polym. Sci. Part B: Polym. Phys.* **1998**, 36(4), 573.
145. http://www.hmi.de/bensc/instrumentation/instrumente/v6/refl/parratt_en.htm
146. Rightor, E. G.; Urquhart, G. S.; Hitchcock, A. P.; Ade, H.; Smith, A. P.; Mitchell, G. E.; Priester, R. D.; Aneja, A.; Appel, G.; Wilkes, G.; Lidy, W. E. *Macromolecules* **2002**, 35, 5873.
147. Shinichi, S.; Yoshihiro, O.; Harunori, S.; Takeshi, N.; Lameck, B.; Shunji, N. *J. Polym. Sci. Part B: Polym. Phys.* **2000**, 38, 1716.
148. Snively, M. C.; Koenig, L. J. *J. Polym. Sci. Part B: Polym. Phys.* **1999**, 37, 2261.
149. Masaro, L.; Zhu, X. X. *Prog. Polym. Sci.* **1999**, 24, 731.
150. Richard, P.; Chartoff, Tai Woo Chiu. *Polym. Eng. Sci.* **1980**, 20(4), 244.
151. Charles, M. H. *Polym. Eng. Sci.* **1980**, 20(4), 252.

152. Schreiber, H. P.; Ouhlal, A. *J. Adhes.* **2003**, 79(2), 141.
153. Yang, F.; Pitchumani, R. *Macromolecules* **2002**, 35(8), 3213.
154. <http://www.umaine.edu/adhesion/gardner/5402002/theories%20of%20adhesion.pdf>.
155. Iyenger, Y.; Ericken, D. E. *J. Appl. Polym. Sci.* **1967**, 11, 2311.
156. Aradian, A.; Raphael, E.; de Genes, P. G. *Macromolecules* **2000**, 33, 9444.
157. Crank, J. *The mathematics of diffusion*, 2nd ed. Oxford Clarendon Press 1979.
158. Young, T. *Trans. R. Soc. London* **1805**, 95, 65.
159. Good, R. J. *S. C. T. Monogr.* **1967**, 25, 328.
160. Girifalco, L. A.; Good, R. J. *J. Phys. Chem.* **1957**, 61, 904.
161. Good, R. J. *J. Adhes. Sci. Technol.* **1992**, 6, 1269.
162. Padday, J. F. in *Handbook of adhesion* Packham, D. E. ed. New York, Longman., 1992, p. 82.
163. Sulman, L. H. *Trans. Inst. Min. Metall.* **1919**, 19, 44.
164. Van Oss, C. J.; Good, R. J.; Chaudhury, K. M. *J. Chromatogr.* **1987**, 391, 53.
165. Van Oss, C. J.; Good, R. J. *J. Macromol. Sci. Chem.* **1989**, A26, 1183.
166. Good, R. J.; Van Oss C. J.; in *Modern Approaches to Wettability: Theory and Application* Loeb, G. ed. Plenum, New York, 1992.
167. Adamson, A. W.; Gast, A. P. *Physical Chemistry of Surfaces*, 6th ed. Wiley, New York, 1997.
168. Bikiris, D.; Matzinos, P.; Larena, A.; Flaris, V.; Panayiotou, C. *J. Appl. Polym. Sci.* **2001**, 81, 701.

Appendixes

A-1. Contact angle data analysis

The contact angle results were obtained from the sessile drop measurements using the geometric mean method of Owens, Wendt, and Rabel.^{46,76} They applied the Young's Equation.¹⁵⁸

$$\gamma_{sl} = \gamma_{sv} - \gamma_{lv} \cos \theta \quad (\text{A-1.1})$$

where γ refers to surface tension or surface energy, the subscripts sv , sl , and lv , refer to the solid-vapor, solid-liquid, and liquid-vapor interfaces respectively, and θ is the contact angle formed between a pure liquid and the surface of the solid as shown schematically in Figure A-1.1.

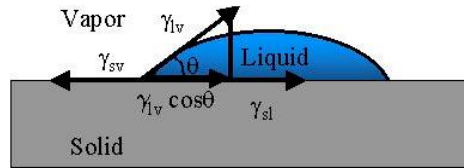


Figure A-1.1: Schematic illustration of the Young's Equation (A-1.1) at the three phase boundary of a sessile drop on a solid surface.

Together with geometric mean method the γ_{sl} value defined by Good and Girifalco in Equation A-1.2.¹⁵⁹⁻¹⁶¹

$$\gamma_{sl} = \gamma_{lv} + \gamma_{sv} - 2\sqrt{\gamma_{lv}^d + \gamma_{sv}^d} - 2\sqrt{\gamma_{lv}^p + \gamma_{sv}^p} \quad (\text{A-1.2})$$

Where d and p refer to the disperse and polar parts of the surface tension, respectively. By combining equation A-1.1 and A-1.2 leads to Equation A-1.3:

$$\frac{(1 + \cos \theta)\gamma_{lv}}{2\sqrt{\gamma_{lv}^d}} = \sqrt{\gamma_{sv}^p} \cdot \sqrt{\frac{\gamma_{lv}^p}{\gamma_{lv}^d}} + \sqrt{\gamma_{sv}^d} \quad (\text{A-1.3})$$

In Equation A-1.3 the polar (γ_{lv}^p) and the disperse part (γ_{lv}^d) of surface tension of the test liquid can be determined by using Equations A-1.4 and A-1.5.

$$\gamma_{lv}^p = \gamma_{lv} \cdot \text{polarity} \quad (\text{A-1.4})$$

$$\gamma_{lv}^d = \gamma_{lv} - \gamma_{lv}^p \quad (\text{A-1.5})$$

The square root of the ratio of the polar and disperse parts of the surface tension is used in the Owens, Wendt, and Rabel graphical data evaluation and this generates the intersection value of the x -axis. Whereas the intersection value of y -axis can be obtained by solving the left hand side of Equation A-1.3. After plotting and fitting the data by linear regression, the square of the slope ($(\gamma_{sv}^p)^{1/2}$) gives the polar part of the surface tension of the solid surface and the intercept ($(\gamma_{sv}^d)^{1/2}$) gives the disperse part of surface tension. The explanation of this calculation method is demonstrated in Figure A-1.2.

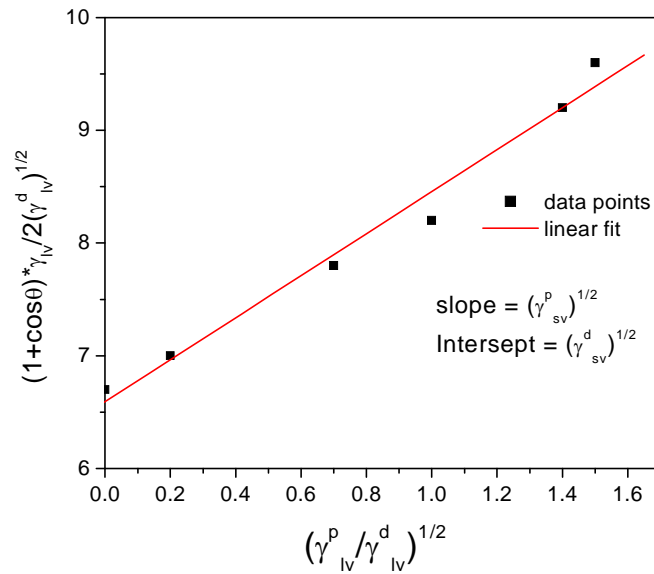


Figure A-1.2: A graphic representation of Owens, Wendt, and Rabel approach for calculation of surface tension.

The surface energies are also linked with the failure of adhesive bond. Adhesion failure involves the creation of new surfaces and hence surface energies. The surface

energy term may be the work of adhesion (W_a) or work of cohesion (W_c) depending on whether the failure is adhesive or cohesive. These are defined as.¹⁶²

$$W_a = \gamma_{sv} + \gamma_{lv} - \gamma_{sl} \quad (\text{A-1.6})$$

$$W_c = 2\gamma_{lv} \quad (\text{A-1.7})$$

In terms of wetting behavior of solid surface one would expect only one value of contact angle i.e. solid/liquid, liquid/air. However, by experimental means, it is possible to measure at least two different contact angles on the same solid surface and for the same liquid, which are termed as advancing (θ_a) and receding (θ_r) contact angles. The difference between θ_a and θ_r is called the contact angle hysteresis $\Delta\theta$ (Equation A-1.8).¹⁶³

$$\Delta\theta = \theta_a - \theta_r \quad (\text{A-1.8})$$

In terms of contact angle hysteresis the surface energies can be estimated by using Equation A-1.9.^{96,97}

$$\gamma_{sl} = \gamma_{lv} (\cos\theta_r - \cos\theta_a) \frac{(1 + \cos\theta_a)^2}{(1 + \cos\theta_r)^2 - (1 + \cos\theta_a)^2} \quad (\text{A-1.9})$$

The required parameters in this Equation are:

- a) the liquid vapour surface tension (γ_{lv})
- b) advancing contact angle (θ_a)
- c) receding contact angle (θ_r).

This equation is based on the assumption that no precursor film left behind, during the receding mode of drop.

The contact angle hysteresis can be related to the work of spreading W_s of liquid on solid surface. Which can be easily calculated from the work of adhesion W_a and the work of cohesion W_c :

$$W_s = W_a - W_c \quad (\text{A-1.10})$$

In the following equation the work of adhesion can be determined from the advancing and receding contact angles.¹⁶⁴⁻¹⁶⁷

$$W_a = \gamma_{lv}(1 + \cos\theta_a), \text{ and } W_r = \gamma_{lv}(1 + \cos\theta_r) \quad (\text{A-1.11})$$

$$W_c = 2\gamma_{sv} \quad (\text{A-1.12})$$

Table A-1.1: Advancing and receding contact angles on PC/ABS-SMA plate for probe liquids measured by the tilted plate method, and the total surface free energy of the PC/ABS-SMA surface obtained from Equation A-1.9.

Liquid	Liquid surface tension [mN/m]	Advancing contact angle θ_a [°]	Receding contact angle θ_r [°]	Contact angle Hysteresis $\Delta\theta$ [°]	Total surface energy [mJ/m ²]
Water	72.8	89.5 ± 4.4	30.4 ± 4.6	59.0 ± 1.7	27.6
MDI	47.6	45.0 ± 1.0	7.7 ± 2.3	37.2 ± 1.5	37.6
PO-a	34.3	35.5 ± 1.3	10.3 ± 1.3	25.2 ± 0.1	29.7
PO-b	34.9	35.4 ± 1.1	17.7 ± 1.7	21.7 ± 1.5	30.4
PO-c	34.9	36.8 ± 2.4	12.4 ± 2.2	24.4 ± 0.5	30

Table A-1.2: Advancing and receding contact angles on SMA plate for probe liquids measured by the tilted plate method, and the total surface free energy of the SMA surface obtained from Equation A-1.9.

Liquid	Liquid surface tension [mN/m]	Advancing contact angle θ_a [°]	Receding contact angle θ_r [°]	Contact angle Hysteresis $\Delta\theta$ [°]	Total surface energy [mJ/m ²]
Water	72.8	79.2 ± 3.5	20.5 ± 3.1	58.8 ± 4.3	32.6
MDI	47.6	36.2 ± 1.2	13.2 ± 1.9	22.9 ± 0.8	41
PO-a	34.3	27.5 ± 1.5	8.9 ± 1.5	18.6 ± 1.3	31.5
PO-b	34.9	29.4 ± 1.7	10 ± 1.7	19.4 ± 1.8	31.7
PO-c	34.9	32.9 ± 3.9	11.2 ± 2.4	21.7 ± 3.1	30.9

Table A-1.3: Advancing and receding contact angles on PC/SAR-GF plate for probe liquids measured by the tilted plate method, and the total surface free energy of the PC/SAR-GF surface obtained from Equation A-1.9.

Liquid	Liquid surface tension [mN/m]	Advancing contact angle θ_a [°]	Receding contact angle θ_r [°]	Contact angle Hysteresis $\Delta\theta$ [°]	Total surface energy [mJ/m²]
Water	72.8	88.5 ± 2.0	35.3 ± 3.0	53.2 ± 3.1	27
MDI	47.6	45.9 ± 0.9	18.4 ± 1.2	27.5 ± 0.5	37.5
PO-a	34.3	42.3 ± 1.0	15.6 ± 2.7	26.7 ± 1.6	28
PO-b	34.9	41.5 ± 5.7	15.2 ± 5.5	26.3 ± 1.3	28.7
PO-c	34.9	43.1 ± 4.2	16.0 ± 1.7	27.1 ± 2.5	28.3

Table A-1.4: Advancing and receding contact angles on PC/ABS plate for probe liquids measured by the tilted plate method, and the total surface free energy of the PC/ABS surface obtained from Equation A-1.9.

Liquid	Liquid surface tension [mN/m]	Advancing contact angle θ_a [°]	Receding contact angle θ_r [°]	Contact angle Hysteresis $\Delta\theta$ [°]	Total surface energy [mJ/m²]
Water	72.8	90.2 ± 2.9	32.2 ± 7.1	58.0 ± 5.4	26.5
MDI	47.6	39.9 ± 1.5	10.9 ± 2.0	29.0 ± 0.7	39.6
PO-a	34.3	36.7 ± 1.9	14.7 ± 2.0	21.9 ± 1.2	29.5
PO-b	34.9	35.5 ± 1.3	15.4 ± 2.6	20.1 ± 1.4	30.4
PO-c	34.9	35.8 ± 1.9	15.7 ± 1.9	20.1 ± 0	30.3

Table A-1.5: Advancing and receding contact angles on PC/ABS-GF plate for probe liquids measured by the tilted plate method, and the total surface free energy of the PC/ABS-GF surface obtained from Equation A-1.9.

Liquid	Liquid surface tension [mN/m]	Advancing contact angle θ_a [°]	Receding contact angle θ_r [°]	Contact angle Hysteresis $\Delta\theta$ [°]	Total surface energy [mJ/m ²]
Water	72.8	78 ± 4	21.3 ± 4.6	56.8 ± 5.5	33.8
MDI	47.6	30 ± 4	6.8 ± 4	22.8 ± 0.6	42.9
PO-a	34.3	31.4 ± 1.7	10.5 ± 1.2	20.9 ± 0.9	30.7
PO-b	34.9	31.9 ± 2.5	12.4 ± 2.8	20.2 ± 0.9	31.2
PO-c	34.9	31.2 ± 3	11.9 ± 2.7	20.1 ± 0.9	31.3

A-2. Investigations on the reaction of isocyanate (MDI) with maleic anhydride

The idea behind this experiment was to use maleic anhydride (MA) as adhesion promoter.¹⁶⁸ In order to follow the reaction process of isocyanate with MA first the FTIR spectra of both pure reactants (MDI and MA) were recorded and are shown in Figure A-2.1. The MA spectrum (Figure A-2.1a) shows the two distinct carbonyl peaks at 1855

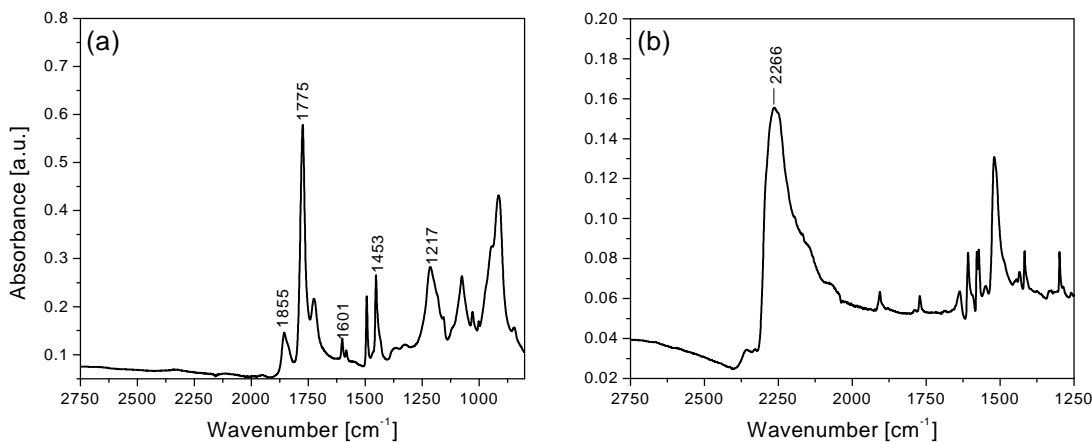


Figure A-2.1: FTIR-ATR spectra of (a) pure maleic anhydride and (b) pure MDI. The isocyanate (2266 cm⁻¹) and acid anhydride bands (1855 and 1775 cm⁻¹) are labeled in the Figure respectively.

and 1775 cm^{-1} (both peaks are linked to the MA carbonyl groups). The MDI spectrum (Figure A-2.1b) shows a very prominent isocyanate peak at 2266 cm^{-1} . The other peaks in the spectrum of both materials were not of much interest. Therefore, they are not interpreted here.

The reaction of isocyanate with MA was monitored by the disappearance of the characteristic peaks (Figure A-2.2) of isocyanate group at 2266 cm^{-1} and acid anhydride carbonyl at 1848 cm^{-1} . The spectra at 70°C show the initial spectra before the imide formation has occurred. The spectra taken after 110 min at 70°C did not show any observable change in the IR bands of MDI and MA. Then the temperature was increased to 90°C and the spectra were recorded at regular intervals, there was an indication of appearance of imide formation after 160 min of reaction time. After 210 min the IR bands for isocyanate and MA groups disappeared and new band at 1713 cm^{-1} appeared that could be assigned to the imide formation. The disappearance of strong -NCO absorption peak at 2268 cm^{-1} and C=O stretching vibration peak of acid anhydride at 1848 cm^{-1} in the IR spectra is an evidence that the reaction has taken place between isocyanate and MA.

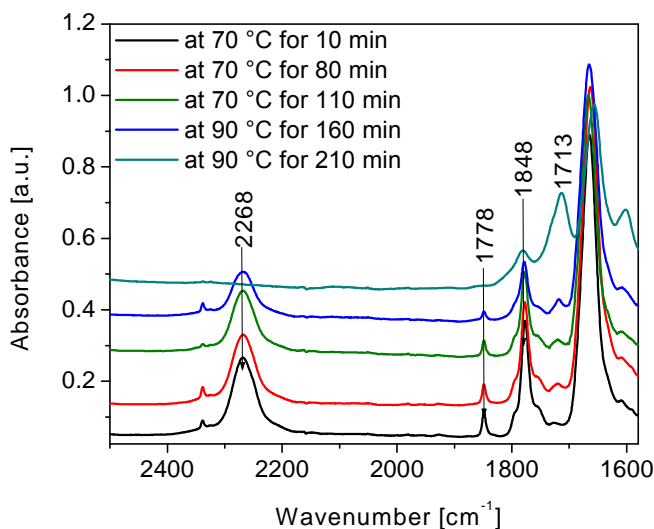


Figure A-2.2: FTIR-ATR spectra taken during the reaction of MDI and MA. The spectrum taken after 10 min is the beginning of the reaction and the spectrum taken after 210 min is the end of reaction. The IR bands linked with isocyanate (2268 cm^{-1}), acid anhydride (1848 and 1778 cm^{-1}) and imide (1713 cm^{-1}) are labeled on the respective peak for each functional group.

In order to calculate the imide content from reaction product of isocyanate and MA a calibration curve was constructed. Concerning this, different concentrations of bismaleimide (BMI) were prepared in dimethyl sulphoxide (DMSO) and then FTIR spectra were recorded for each concentration. The obtained FTIR data for imide peak at 1713 cm^{-1} were used in the calibration curve as shown in Figure A-2.3. The evaluated imide content from the reaction product was 0.147 [mol %]. These studies have shown that MA reacts with isocyanate and give a reasonable amount of the reaction product (imide formation).

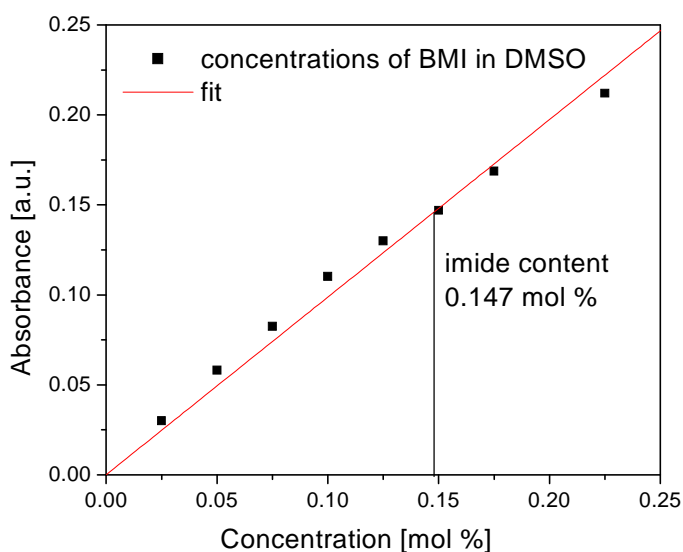


Figure A-2.3: Calibration curve for the calculation of imide content. The absorbance of imide band at 1713 cm^{-1} is plotted against different concentrations of BMI in DMSO. A linear fit of data was used to calculate the imide content from the reaction of MA and isocyanate.

Acknowledgement

The work in this thesis is the result of three years whereby I have been accompanied and supported by many people. It is great opportunity for me that I can express my thanks to all of them.

First, I would like to sincerely acknowledge my supervisor Prof. Dr. rer. nat. habil. Joerg Kressler for his continuous guidance, inspiration and enthusiasm throughout my work and providing me an opportunity to work in his group. I have been in his research group since July 2001. During these years I have known my Prof. as sympathetic and person of principles.

I would like to thank Dr. K. Busse, Dr. J. Vogel, Dr. H. Kausche, Dr. Z. Funke, Dr. H. Hussain, Mr. Kaiser, Mr. C. Peetla and the other members of my group who monitored my work.

I am also obliged to Dr. R. Adhikari (Merseburg), Dr. A. Wutzler (Merseburg), Dr. E. Dayss (Merseburg), Frau Sachse (Merseburg), Dr. R. Thomann (Freiburg), and Dr. U. Rücker (Jülich) for their help and cooperation over the course of my work in their laboratories. Diverse help from groups of Prof. Dr. rer. nat. habil. W. Grellmann, Prof. Dr. rer. nat. habil. G. Ieps, Prof. Dr.-Ing. Habil. H.-J. Radusch, and Prof. Dr. rer. nat. habil. G. H. Michler is gratefully acknowledged.

I feel a deep sense of gratitude for my father (late) and mother who formed part of my vision and taught me the good things that really matter in life. I wish to give a very special thank to my wife Sadaf Bashir Nasir, for moral support, and unlimited patience; it would have been impossible for me to successfully finish this work without her understanding and help. Finally I am grateful to my brothers and sister, for rendering me the sense and the value of brotherhood. I am glad to be one of them.

M.Phil. Nasir Mahmood

Resume

1. Personal Information

Full Name: Nasir Mahmood
Date of Birth: 7th May 1974
Place of Birth: Bahawalpur/Pakistan
Nationality: Pakistani

2. Academic Qualification

Since July 2001: PhD Student, Martin-Luther University of Halle-Wittenberg,
Department of Engineering Sciences, Institute of Bioengineering,
Halle (Saale), Germany.

1998-2000: Master of Philosophy in Organic Chemistry Department of Chemistry
Quaid-I-Azam University Islamabad, Pakistan.

1996-1998: Master of Science in Chemistry Department of Chemistry Quaid-I-
Azam University Islamabad, Pakistan.

Statement

I certify that this thesis is based on my own work. I also certify that to the best of my knowledge any help received in preparing this work, and all sources used, have been acknowledged in this Thesis.

M.Phil. Nasir Mahmood